μSR studies of the vortex state in type-II superconductors

Jeff E. Sonier

Los Alamos National Laboratory, Los Alamos, New Mexico 87545

Jess H. Brewer and Robert F. Kiefl

Department of Physics and Astronomy, University of British Columbia, Vancouver, Canada V6T 1Z1
and Canadian Institute for Advanced Research, Toronto, Ontario, Canada M5G 1Z8

The authors present a review of recent muon spin rotation (μSR) studies of the vortex state in type-II superconductors. There are significant gaps in our understanding of this unusual phase of matter, especially in unconventional superconductors, for which the description of the vortex structure is a subject of great controversy. The μSR technique provides a sensitive local probe of the spatially inhomogeneous magnetic field associated with the vortex state. For the case of a regular vortex lattice, the magnetic penetration depth λ and the coherence length ξ can be simultaneously extracted from the measured internal field distribution. The penetration depth is directly related to the density of superconducting carriers in the material, and measurements of its variation with temperature, magnetic field, and impurities can provide essential information on the symmetry of the order parameter. The coherence length measured with μSR is the length scale for spatial variations of the order parameter within a vortex core. A primary goal of this review article is to show that measurements of these fundamental length scales are fairly robust with respect to the details of how the field distribution is modeled. The reliability of the results is demonstrated by a comparison of the μSR experiments with relevant theories and with other experimental techniques. The authors also review μSR measurements that have focused on the study of pinning-induced spatial disorder and vortex fluctuation phenomena. The μSR technique has proven to be a powerful tool for investigating exotic vortex phases, where vortex transitions are directly observable from changes in the μSR line shape. Particular emphasis is given to μSR experiments performed on high-temperature superconductors since high-quality single crystals have become available.

CONTENTS

I. INTRODUCTION

The vortex state of a type-II superconductor constitutes the response of the material to an applied magnetic field greater than the lower critical field H_{c1} and less than the upper critical field H_{c2}. Recent experimental and theoretical studies of the high-temperature cuprate superconductors have focused attention on this unique phase of matter. This resurgence of interest stems from numerous findings that seem inconsistent with predictions based on the established pairing-state symmetry of these materials. Studies aimed at characterizing the nature of the vortex state have the potential to yield new information essential to developing a detailed understanding of the microscopic pairing mechanism in unconventional superconductors.

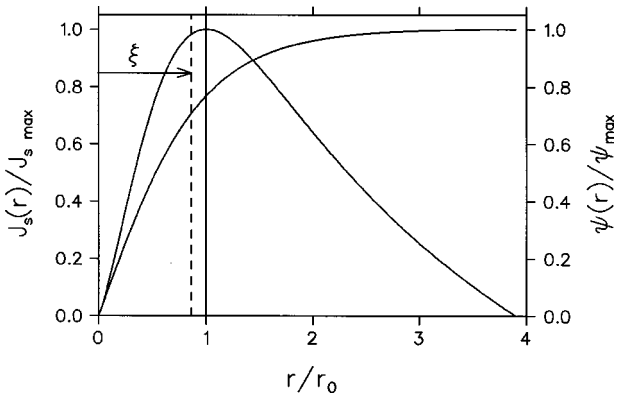

FIG. 1. Conventional vortex core, showing dependence of the supercurrent density $J_s(r)$ and the order parameter $\psi(r)$ on the distance r from the center of a vortex line. $J_s(r)$ is normalized to its maximum value $J_{s_{\max}}$ at a distance $r=r_0$, whereas $\psi(r)$ is normalized to its maximum value $\psi_{\max}$ far from the vortex core.

In the presence of an applied static magnetic field H, a type-II superconductor responds by forming supercurrents that screen the field. For $H<H_{c1}$ (the so-called Meissner state), these supercurrents flow around the perimeter of the sample in such a way as to shield the interior of the superconductor from the magnetic field (Meissner and Ochsenfeld, 1933). Near the surface, where the supercurrents are greatest, there is penetration of the field. In particular, the interior magnetic-field component parallel to the surface falls off exponentially with distance from the surface over a characteristic length scale, the *magnetic penetration depth* λ. Measurements of λ are one way of probing low-energy electronic excitations, as λ^{-2} is proportional to the density of superconducting carriers n_s (London and London, 1935).

For larger applied magnetic fields $H_{c1}<H<H_{c2}$ (the so-called vortex or mixed state), the supercurrent response is such that the field penetrates the sample in the form of quantized flux lines, called *vortices* (Abrikosov, 1957). Each vortex contains one quantum of flux ($\Phi_0 = hc/2e$). In a conventional s-wave superconductor, the shielding currents circulate around the individual vortices. As in the Meissner state, the screening is not perfect, so that the field decays outside the core region of a vortex over the length scale λ. Within the core region, the superfluid density $n_s(r)$, the superconducting order parameter $\psi(r)$, and the supercurrent density $J_s(r)$ are all strongly suppressed (see Fig. 1). The order parameter rises from zero at the vortex axis ($r=0$) to its maximum value outside the vortex core over a length scale called the *coherence length* ξ. Thus, in the vortex state, ξ is the characteristic length scale for spatial variations of the order parameter and is closely related to the size of the vortex cores.

Experiments that probe the vortex state can be divided into three categories, those that measure (i) thermal and transport properties, (ii) electronic structure, and (iii) the inhomogeneous magnetic field. Thermal conductivity, resistivity, and specific-heat measurements are included in (i) and (ii), scanning tunneling spectroscopy (STS) in (ii), and small-angle neutron scattering and magnetic imaging with superconducting quantum interference devices (SQUIDs) in (iii). Nuclear magnetic resonance (NMR) and muon spin rotation (μSR) spectroscopy probe both (ii) and (iii). For example, measurements of the Knight shift and T_1 with NMR or μSR are sensitive to the electronic structure of vortices, whereas T_2 measurements locally probe magnetic-field variations in the bulk. It is μSR measurements of the latter kind that are the main focus of this review. The μSR technique accurately measures the internal magnetic-field distribution associated with the vortex lattice, which is in general a function of both space and time. For a regular Abrikosov lattice (Abrikosov, 1957) consisting of a periodic arrangement of vortices, the characteristic length scales λ and ξ can be simultaneously determined.

There are many other important applications of μSR to the study of superconductivity that do not involve measurements in the vortex state, such as studies of the antiferromagnetic or spin-glass phases (see, for example, Nishida *et al.*, 1987; Brewer *et al.*, 1988, Budnick *et al.*, 1988), measurement of relaxation rates associated with phase transitions (see, for example, Kiefl *et al.*, 1993), and detection of spontaneous internal magnetic fields in unconventional superconductors (Heffner *et al.*, 1990; Kiefl *et al.*, 1990; Luke *et al.*, 1993, 1998). Some of these other topics are treated in a recent article by Amato (1997), which reviews μSR studies of heavy-fermion superconductors.

II. THE μSR TECHNIQUE

The μSR experiments reviewed in this article utilized the so-called *transverse-field technique*. In a transverse field μSR experiment, one measures the internal magnetic-field distribution in the vortex state with a resolution of about 0.1 mT—which is of the order of the magnetic fields caused by nuclear dipoles. A nearly 100% spin-polarized beam of low-energy positive muons is produced from pion decay (i.e., $\pi^+ \rightarrow \mu^+ + \nu_\mu$) at rest in the surface layer of a primary production target (C or Be). The muons from pion decay have a kinetic energy of 4.119 MeV and are polarized opposite to their momentum direction. They are implanted one at a time into the bulk of the superconductor (with a mean stopping range of about 120 mg/cm^2 in carbon) with their initial spin polarization perpendicular to the applied magnetic field. For strong applied fields this requires use of a Wien filter (consisting of crossed electric and magnetic fields) upstream of the sample to rotate the muon spin from its natural orientation (antiparallel to the beam momentum) by 90° with respect to the beam momentum and applied field (Beveridge *et al.*, 1985). In almost all known cases, the positive muon stops at interstitial sites due to electrostatic repulsion by atomic nuclei. In the high-temperature superconductors there is good evidence that the muon binds to a negatively charged oxygen ion, which may or may not belong to the CuO_2 plane (see, for example, Brewer *et al.*, 1990;

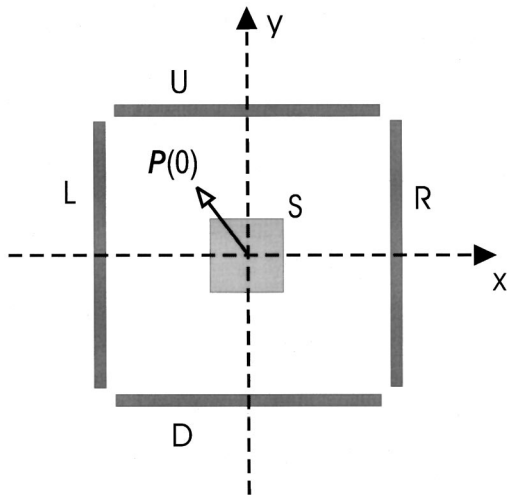

FIG. 2. Four positron counters, L, R, U, and D, surrounding the sample S. The initial muon spin polarization is denoted as $\mathbf{P}(0)$ and the applied magnetic field is directed out of the page.

Nishida and Miyatake, 1990). However, the precise location of the muon is unimportant since the vortex lattice spacing in magnetic fields typical for a transverse-field μSR experiment ($\mu_0 H < 8$ T) is much larger than the dimensions of the crystallographic unit cell ($\sim 10^2$–10^3 times). Consequently the muon stops at random on the length scale of the vortex lattice.

Since the muon is a spin-1/2 particle with no quadrupole moment, there are no splittings due to quadrupolar interactions—thus giving μSR a distinct advantage over most NMR techniques. Also, the electric charge of the muon is $+1$, so the Knight-shift contribution is greatly reduced compared to NMR. Consequently the spectrum for μSR is easier to relate to the distribution of local magnetic field in the sample. Another advantage of μSR is that it is easily performed on single crystals, whereas conventional NMR is generally limited to polycrystalline samples, due to the finite penetration depth of the rf field.

The implanted muon precesses about the local magnetic field $\mathbf{B}(\mathbf{r})$ with a Larmor frequency

$$\omega_\mu = \gamma_\mu B(\mathbf{r}), \tag{1}$$

where $\gamma_\mu/2\pi = 135.5342$ MHz/T is the muon gyromagnetic ratio. After a mean lifetime $\tau_\mu = 2.197\,\mu$s, the muon decays into a positron and two neutrinos (i.e., $\mu^+ \rightarrow e^+ + \nu_e + \overline{\nu}_\mu$). The distribution of decay positrons is asymmetric with respect to the spin-polarization vector $\mathbf{P}(t)$ of the muon, where the highest probability of emission is along the direction of the muon spin. Consequently the time evolution of the muon spin polarization $\mathbf{P}(t)$ can be monitored, since an ensemble of muons reveals its spin direction at the times of the decays. Scintillation detectors placed around the sample are used to detect the positrons emitted from the μ^+ decay.

Figure 2 shows a simple four-counter arrangement. The number of decay positrons recorded per time bin Δt in the ith counter is given by

$$N_i(t) = N_i^\circ e^{-t/\tau_\mu}[1 + A_i^\circ P_i(t)] + B_i^\circ, \tag{2}$$

where N_i° is a normalization constant, A_i° is the maximum precession amplitude, B_i° is the time-independent random background, and $P_i(t)$ is the time evolution of the muon spin-polarization component in the ith direction. For the case in which all muons see the same field B and therefore precess at the same frequency ω_μ, $P_i(t)$ is given by

$$P_i(t) = \cos(\omega_\mu t + \theta_i), \tag{3}$$

where θ_i is the initial phase of the muon spin-polarization vector relative to the ith direction. In general θ_i is nonzero, since the initial muon polarization $\mathbf{P}(0)$ will rarely be perfectly aligned with any counter's acceptance, even in zero field, and an arriving muon will have precessed during its flight through the magnetic field to the sample. The muon rapidly thermalizes on time scales of order 10^{-10} s through interaction with the lattice (Cox, 1987). This has no effect on the muon polarization.

A. Asymmetry spectra

Equation (2) can be written

$$N_i(t) = N_i^\circ e^{-t/\tau_\mu}[1 + A_i(t)] + B_i^\circ, \tag{4}$$

where $A_i(t) = A_i^\circ P_i(t)$ is the *single-counter asymmetry function* for the ith raw histogram. Rearranging Eq. (4) gives

$$A_i(t) = e^{t/\tau_\mu}\left[\frac{N_i(t) - B_i^\circ}{N_i^\circ}\right] - 1. \tag{5}$$

$A_i(t)$ is introduced to eliminate the muon lifetime (a well-known quantity) and the overall normalization N_i° and the random background B_i°, which have no physical significance.

As long as the muon precession period is very short compared to the muon lifetime, N_i° and B_i° can be obtained numerically by the following procedure: If one treats $N_i(t)$ as a continuous function (the actual discrete sums can easily be deduced from the integrals below) then (Riseman, 1993; Brewer, 1994)

$$N_i^\circ = \frac{S_i \tau_\mu E_i^+ - R_i T_i}{\tau_\mu^2 E_i^+ E_i^- - T_i^2}$$

$$\text{and} \quad B_i^\circ = \frac{R_i \tau_\mu E_i^- - S_i T_i}{\tau_\mu^2 E_i^+ E_i^- - T_i^2}, \tag{6}$$

where

$$S_i \equiv \int_{t_i}^{t_f} N_i(t)\,dt,$$

$$R_i \equiv \int_{t_i}^{t_f} N_i(t)\exp(t/\tau_\mu)\,dt,$$

$$E_i^\pm \equiv \pm[\exp(\pm t_f/\tau_\mu) - \exp(\pm t_i/\tau_\mu)],$$

$$\text{and} \quad T_i \equiv t_f - t_i, \tag{7}$$

the time interval over which the integrals are evaluated.

This numerical procedure becomes increasingly unreliable in weaker magnetic fields (below about 0.05 T), for which asymmetry spectra can be extracted from the raw histograms for *opposing pairs* of counters (the so-called two-counter asymmetry), as described by Brewer (1994).

B. The depolarization function

In the vortex state, muons experience a spatially varying magnetic field due to the periodic arrangement of the vortices. The field is assumed to be in the $\hat{z}$ direction everywhere. In this case, the time evolution of the x component of the total muon polarization is

$$P_x(t)=\frac{1}{N}\sum_{i=1}^{N}\cos[\gamma_\mu B(\mathbf{r}_i)t+\theta], \tag{8}$$

where the sum extends over all muon sites and $B(\mathbf{r}_i)$ is the magnitude of the local field at site i. Ideally, the sum is replaced by an integral, so that

$$P_x(t)=\int_0^\infty n(B)\cos(\gamma_\mu Bt+\theta)dB, \tag{9}$$

where $n(B)$ is the μSR line shape—i.e., $n(B)dB$ is the probability that the muon experiences a local magnetic field between B and $B+dB$ and precesses at the frequency $\omega_\mu=2\pi\nu_\mu=\gamma_\mu B$. The envelope of the oscillating muon spin polarization $P_x(t)$ decays or dephases with increasing time according to the width of $n(B)$.

In a real material, there are perturbations of the periodic vortex lattice caused by random pinning of the vortices and fluctuations in temperature or applied magnetic field. These additional sources of field inhomogeneity can often be accounted for by multiplying the muon polarization function by a *depolarization function* $G(t)$, so that

$$P_x(t)=G(t)\int_0^\infty n(B)\cos(\gamma_\mu Bt+\theta)dB. \tag{10}$$

According to Brandt (1988a), a Gaussian function

$$G(t)=\exp\left(-\frac{1}{2}\sigma_{\rm VL}^2t^2\right) \tag{11}$$

is a good approximation, where $\sigma_{\rm VL}$ is the muon spin-depolarization rate due to these perturbations of the vortex lattice.

The vortex lattice is also distorted by demagnetization effects associated with the geometrical shape of the sample. For a plate-shaped crystal with the field applied perpendicular to the flat face, the average internal field (vortex density) is reduced near the sample edges, resulting in a domelike field profile over the width of the sample (Indenbom *et al.*, 1994). The field variation due to the sample geometry will usually be minor relative to the large field inhomogeneity of the vortex lattice—especially at fields well above the lower critical field H_{c1} (Forgan *et al.*, 1997). However, if the vortex lattice is highly disordered or in the melted phase, the sample geometry can dominate the field variation of the μSR line shape (see Sec. III.D.3).

There are other contributions to the local field B_μ at the muon site besides those associated with the vortex lattice. For example, fields from electronic and nuclear dipolar moments, as well as the spin polarization of the conduction electrons at the muon site, will result in a shift of the average field and/or broaden the μSR line shape. The Knight shift [defined as $K=(B_\mu-B_{\rm ext})/B_{\rm ext}$, where $B_{\rm ext}$ is the external field] originating from the magnetic-field-induced polarization of the conduction electrons, is typically on the order of the experimental resolution ($\sim$100 ppm). Local electronic moments can also contribute to the frequency shift by producing an effective dipolar field and an additional hyperfine contact field at the muon site. The latter may arise in f-electron compounds from an indirect RKKY (Ruderman-Kittel-Kasaya-Yosida) interaction, which enhances the spin polarization of the conduction electrons (see, for example, Amato, 1997).

A distribution of dipolar fields can increase the depolarization rate of the muon spin precession signal. The muon depolarization function due to a dense system of nuclear dipolar fields is well described by a Gaussian function (Schenck, 1985),

$$G(t)=\exp\left(-\frac{1}{2}\sigma_{\rm dip}^2t^2\right). \tag{12}$$

In general,

$$\sigma_{\rm dip}^2=\gamma_\mu^2\langle(\Delta B_{\rm dip})^2\rangle, \tag{13}$$

where $\langle(\Delta B_{\rm dip})^2\rangle=\langle(B_{\rm dip}-\langle B_{\rm dip}\rangle)^2\rangle$ is the second moment of the distribution of nuclear dipole fields at the muon site. Typically $\sigma_{\rm dip}$ is on the order of $0.1\,\mu{\rm s}^{-1}$. A more precise expression for $\sigma_{\rm dip}$ can be obtained by taking into account the orientation of the applied magnetic field, the location of the muon in the crystal lattice, and the electric quadrupole interaction with nearby atomic nuclei.

Electronic dipolar fields, which are in general not randomly oriented, can also strongly influence the muon spin-depolarization rate. For example, in the electron-doped high-temperature superconductor $Nd_{1.85}Ce_{0.15}CuO_{4-\delta}$, the large magnetic moments of the Nd^{3+} ions produce an additional line broadening, which makes it difficult to separate out the field distribution associated with the vortex lattice (Luke *et al.*, 1997). The depolarization function that contains both the effects of the dipolar moments ($\sigma_{\rm dip}$) and the perturbations of the vortex lattice ($\sigma_{\rm VL}$) is generally assumed to be

$$G(t)=\exp\left[-\frac{1}{2}(\sigma_{\rm dip}^2+\sigma_{\rm VL}^2)t^2\right]=\exp\left(-\frac{1}{2}\sigma_f^2t^2\right), \tag{14}$$

where σ_f is the net effective depolarization rate due to sources other than the ideal vortex lattice.

If a muon diffuses rapidly in the sample within its lifetime, it will experience the local magnetic field at many locations in the vortex lattice—which is equivalent

to a time-varying magnetic field at the muon site. If the muon diffuses fast enough, these fields are averaged out, resulting in a reduction of the depolarization rate associated with the dephasing effect of the spatially varying magnetic field (Schenck, 1985). This ''motional averaging'' effect is analogous to the ''motional narrowing'' phenomenon in NMR (Abragam, 1970). Increasing mobility of the muon first leads to a suppression of the van Hove singularity produced by the field at the vortex centers. Contrary to naive expectations of motional narrowing, a further increase in the muon diffusion rate results in an increase in the damping rate of the muon precession signal (Brandt and Seeger, 1986). Only with still faster diffusion, whereby the muon explores several unit cells of the vortex lattice, does the damping rate decrease as expected (Brandt and Seeger, 1986). Generally speaking, muon diffusion rates in the vortex state of a superconductor are very small below ~100 K. Even in high-purity Nb single crystals, only a slight smearing of the van Hove singularities of the μSR line shape can be attributed to muon diffusion (Schwarz *et al.*, 1986; Herlach *et al.*, 1990).

C. Four-counter complex muon polarization

Now consider the complete set of four positron counters in Fig. 2. Ignoring geometric misalignments and differences in counter efficiency, the x component of the muon polarization $P_x(t)$, monitored by the L and R counters, differs from the y component of the muon polarization $P_y(t)$, monitored by the U and D counters, by a phase of 90°. The two components of the muon polarization can be combined to form a *complex* polarization function

$$\tilde{P}(t)=P_x(t)+iP_y(t), \tag{15}$$

where

$$P_x(t)=G(t)\int_0^\infty n(B)\cos(\gamma_\mu Bt+\theta)dB, \tag{16}$$

and

$$P_y(t)=G(t)\int_0^\infty n(B)\cos(\gamma_\mu Bt+\theta-\pi/2)dB$$

$$=G(t)\int_0^\infty n(B)\sin(\gamma_\mu Bt+\theta)dB. \tag{17}$$

The complex asymmetry for the four-counter setup is defined as

$$\tilde{A}(t)=A^\circ\tilde{P}(t)=A^\circ P_x(t)+iA^\circ P_y(t)$$

$$=A_x(t)+iA_y(t), \tag{18}$$

where $A_x(t)$ and $A_y(t)$ are the real and imaginary parts of the complex asymmetry, respectively. Equations (5) and (6) show how to extract the asymmetry function $A_i(t)$ numerically from each raw time histogram $N_i(t)$. In terms of the individual counters, the real asymmetry $A_x(t)$ and the imaginary asymmetry $A_y(t)$ are

$$A_x(t)=\frac{1}{2}[A_R(t)-A_L(t)] \text{ and} \tag{19}$$

$$A_y(t)=\frac{1}{2}[A_U(t)-A_D(t)]. \tag{20}$$

One can then fit the real and imaginary parts of the asymmetry simultaneously.

D. The rotating reference frame

In magnetic fields in which the frequency of the muon spin precession is high, it is convenient to fit the measured asymmetry spectrum in a *rotating reference frame*. To do this, one multiplies the complex muon polarization $\tilde{P}(t)$ by the function $\exp(i\omega_{\rm RRF}t)$. The rotating-reference-frame frequency $\omega_{\rm RRF}$ is chosen so that $|\overline{\omega}_\mu-\omega_{\rm RRF}|$ is small enough to produce a reasonable number of oscillations over the fitted time interval (here $\overline{\omega}_\mu$ is the average muon spin precession frequency in the laboratory frame). There are two primary benefits of performing such a transformation. The first is that the quality of the fit can be visually inspected. More importantly, it allows the data to be packed into fewer bins, which greatly enhances the fitting speed.

Figure 3 shows a typical muon spin precession signal in the normal and vortex states of $YBa_2Cu_3O_{6.95}$ for a magnetic field $\mu_0H=0.5$ T applied parallel to the $\hat{\boldsymbol{c}}$ axis. The signals are displayed in a reference frame rotating at about 3 MHz below the Larmor precession frequency of a free muon. Dephasing of the signal arises from an inhomogeneous distribution of magnetic fields in the sample. Above the superconducting transition temperature T_c, at which the applied field penetrates the entire sample, the small relaxation is mainly due to nuclear dipolar moments. The nonrelaxing signals arising from individual muons precessing in different local fields combine to give a relaxing signal. On the other hand, below T_c the relaxation is considerably larger due to the inhomogeneous field distribution associated with the vortex lattice. Note that the error bars in Fig. 3 grow as a function of time. Because of the finite muon lifetime, there are fewer counts in the bins at later times, resulting in an exponential increase in the statistical error bars. For this reason, μSR spectra rarely extend beyond 10–15 μs.

E. The fast Fourier transform

The muon time spectrum itself is not very revealing to the eye, so a *fast Fourier transform* (FFT) is often performed to display the distribution of frequencies (or local fields) in the sample. The FFT is an algorithm developed by Cooley and Tukey (1965) for efficiently computing the Fourier transform of a discrete spectrum. A Fourier transform of the complex muon polarization $\tilde{P}(t)$ yields a good approximation of the actual internal field distribution, i.e.,

$$n(B)=\int_0^\infty \tilde{P}(t)e^{-i(\gamma_\mu Bt+\theta)}dt. \tag{21}$$

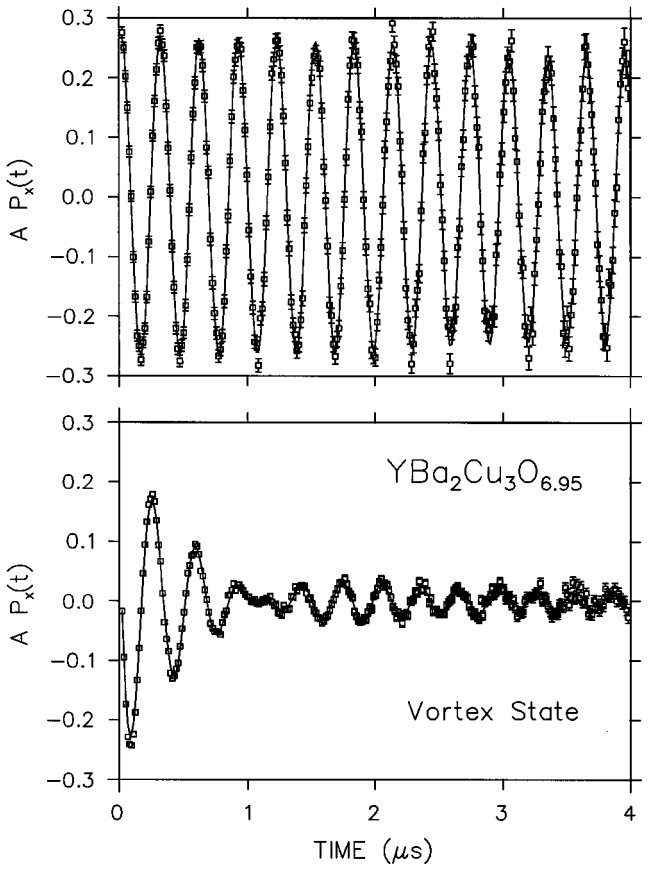

FIG. 3. The muon spin precession signal in $YBa_2Cu_3O_{6.95}$ [T_c = 93.2(0.25) K] at $\mu_0 H = 0.5$ T, displayed in a rotating-reference-frame frequency of 3 MHz. Top panel: in the normal state at $T = 120$ K. Bottom panel: in the vortex state at $T = 2.4$ K. The solid curves are fits that are described later in this article.

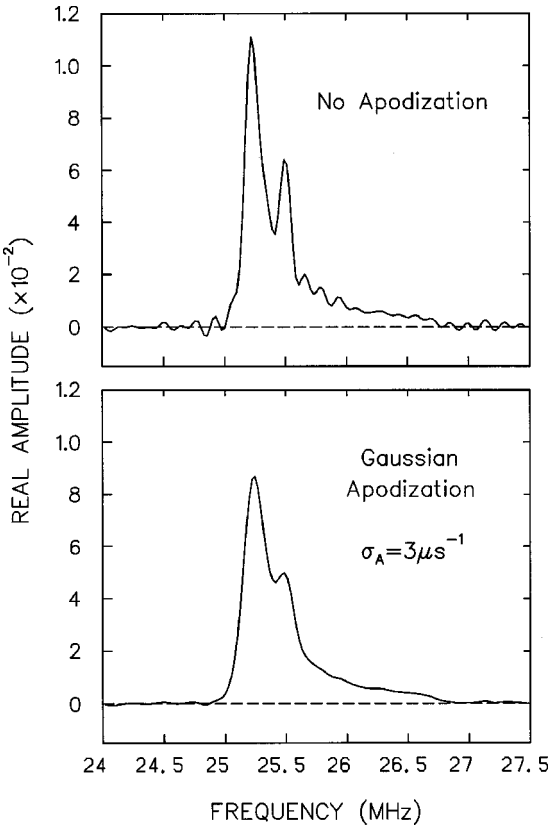

FIG. 4. Fourier transform of the muon precession signal in the vortex state of $YBa_2Cu_3O_{6.95}$: top panel, with apodization; lower panel, without apodization.

Unfortunately, there are several problems with the FFT that confine its usefulness to visual illustrations and even limit its effectiveness there. First, the reduced number of counts at later times introduces noise into the frequency spectrum. Second, the finite time range of the μSR spectrum produces a "ringing" effect in the FFT. These unwanted distortions are minimized through an apodization procedure in which the asymmetry spectrum is multiplied by a weighting function varying smoothly between one and zero (Riseman *et al.*, 1995). For example, the Fourier transform can be apodized with a Gaussian function so that

$$n_A(B) = \int_0^\infty \tilde{P}(t) e^{-i(\gamma_\mu B t + \theta)} e^{-\sigma_A^2 t^2/2}\, dt. \tag{22}$$

However, this apodization procedure also broadens the output frequency spectrum of the Fourier transform, smearing out sharp features of interest. This is clearly seen in Fig. 4, which shows an example of a FFT with and without apodization. The apodization parameter σ_A is chosen to provide a compromise between the statistical noise in the spectrum and the additional broadening of the spectrum that such a procedure introduces. This inherent problem with FFT's makes fitting in the frequency domain much more difficult than in the time domain, where such problems are more easily avoided. Fast Fourier transforms are nevertheless very useful in assessing how well the theoretical field distribution fits certain features in the spectra. This can be done by performing an FFT on both the data and the best-fit theory function.

Figure 5 shows the real part of the FFT for the time spectra in Fig. 3 (which we shall often refer to as the μSR line shape). Above T_c, the μSR line shape is symmetric with some broadening due to the nuclear dipolar moments. Below T_c, the observed line shape is primarily due to the vortex lattice. The latter approximately resembles the theoretical field distribution expected for a hexagonal Abrikosov vortex lattice (shown in Fig. 6) but with an additional peak at 67.3 MHz due to a small residual background signal, which is explained in the next section. The sharp cutoff at low fields in Fig. 6 is due to the minimum of the field distribution, which occurs at the center of the triangle formed by three adjacent vortices. The peak is due to the van Hove singularity produced by the saddle point midway between nearest-neighbor vortices. The long tail is due to the region around the vortex core, and the high-field cutoff is due to the maximum field at the center of the core. The sharp features in Fig. 6 are smeared out in the FFT, primarily from the apodization procedure, but also from the broadening effects discussed in Sec. II.B.

Another way to display frequency spectra is the

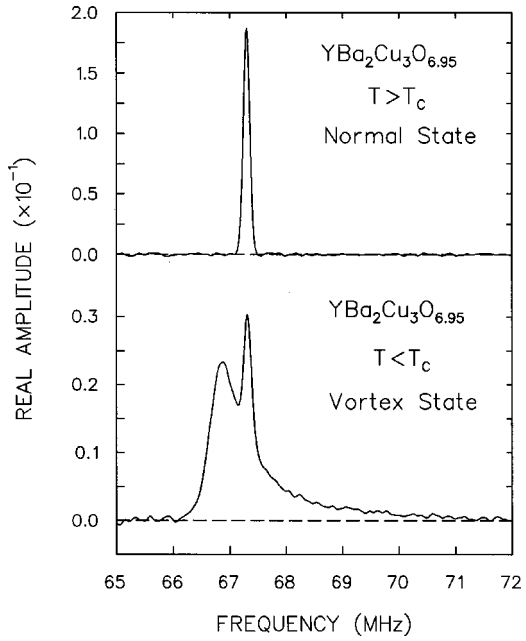

FIG. 5. Fourier transform of the precession signals in Fig. 3 using a Gaussian apodization with $\sigma_A = 3\ \mu s^{-1}$.

maximum-entropy method (Rainford and Daniell, 1994) used extensively for analyzing μSR spectra. The maximum-entropy algorithm produces a frequency spectrum that fits the data within the noise level and has maximum entropy. The entropy S, in analogy with the entropy in thermodynamics, is defined as

$$S = -\sum_{i=1}^{N} n(\omega_i) \ln\left(\frac{n(\omega_i)}{b(\omega_i)}\right), \tag{23}$$

where N is the number of frequency bins, the set of values $n(\omega_i)$ is the output frequency spectrum, and $b(\omega_i)$ is a set of default values taken to be a "flat" frequency distribution—since the frequency spectrum with maximum entropy is uniform. The entropy S is maximized subject to a constraint on the fit χ^2. This technique suppresses unwanted statistical noise and has important applications in the detection of qualitative changes in μSR line shapes with external magnetic field or temperature. However, it shares with apodization the flaw of subtly modifying the output frequency spectrum in ways that depend on the "judgment calls" of the user, altering precisely those subtle features that are the object of investigation in studies of field distributions of vortex lattices. For these reasons, analysis of μSR spectra are best performed in the time domain, where all the statistical and systematic uncertainties are better understood.

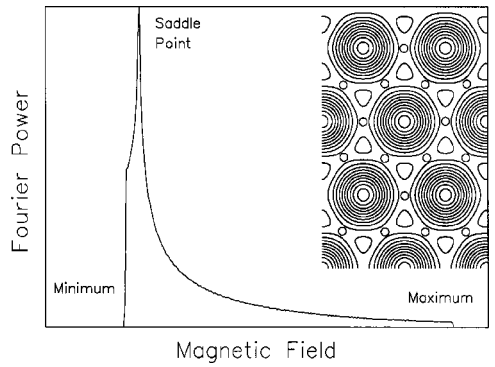

FIG. 6. Theoretical magnetic field distribution for a hexagonal vortex lattice. The inset is a contour plot of the field variation.

F. Low-background apparatus

Early transverse-field μSR studies of superconductors were plagued by a large background signal contributing significant spectral weight to the measured line shape. The background signal arose from muons that missed the sample but were registered as "good" muon-decay events. Studies of very small or thin samples require that the decay events originating from these muons be "vetoed" (i.e., not recorded). High-quality crystals of the high-temperature cuprate superconductors (i.e., those with a high degree of chemical purity and homogeneity) generally fall into this category.

To reject the unwanted muons, a "low-background" apparatus (see Fig. 7) was developed at the Tri-University Meson Facility (TRIUMF), Vancouver, Canada (Schneider *et al.*, 1993). A similar apparatus is now used at the Paul Scherrer Institut (PSI), Villigen, Switzerland. The sample is mounted on a thin sheet of aluminized Mylar that is stretched over a hollow cylindrical aluminum sample holder held in a horizontal gas-flow cryostat. A small amount of low-temperature vacuum grease is generally used to attach the crystals to the Mylar film (with their flat faces perpendicular to both the applied magnetic field **H** and the muon beam directions). The incoming muons are detected by a thin scintillation detector (M) placed before the sample and are implanted with their initial spin polarization $\mathbf{P}(t=0)$ perpendicular to **H**. The signal arising from a muon that triggers the M counter is fed through a constant-fraction discriminator, creating a logical timing pulse used to start a time-to-digital converter (TDC). The TDC stops when the decay positron from the muon is detected. The time interval for this event is digitized by the clock and a count is added to the corresponding time bin in the positron detector's histogramming memory.

The unique feature of this apparatus is the placement of a cup-shaped *veto counter* (V) behind the sample to suppress the unwanted background signal from muons that miss the sample. The decay positrons from muons stopping in the sample are detected by overlapping cylindrical forward (F) and backward (B) counters, which are mounted outside of the cryostat. As shown in Fig. 7, the F and B counters consist of four individual counters F_1, F_2, F_3, F_4 and B_1, B_2, B_3, B_4, respectively. Overlapping counters F and B subtend the solid angle denoted by the dashed lines in Fig. 7. A valid muon stop is defined as $M \cdot \overline{V}$ and a valid positron event is defined as $F_i \cdot B_i \cdot \overline{V}$, where $i = 1$, 2, 3, or 4. The arrangement of the F, B, and V counters is such that decay positrons origi-

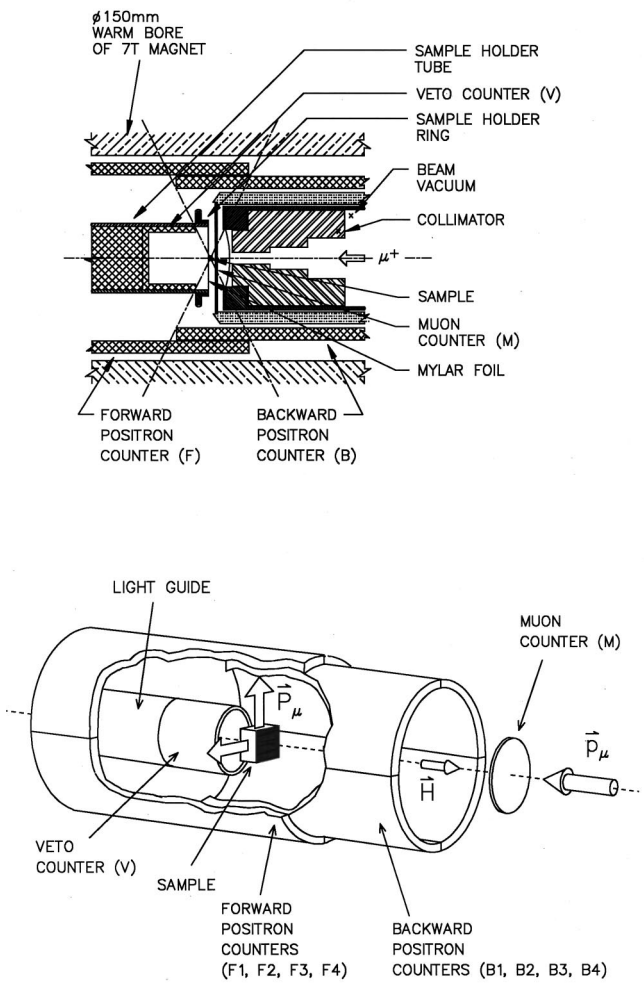

FIG. 7. The low-background μSR apparatus. The sample and veto counter (V) are contained within a cryostat, which is not shown for clarity. The lower figure shows the arrangement of the positron and muon counters described in the text.

nating from muons that miss the sample and stop in back of the V counter are rejected. Since these "bad" muons register neither a valid muon stop nor a valid decay positron, they are logically excluded from the experiment.

To ensure sufficient accuracy, measured spectra typically require 15 to 30 million muon-decay events. To clearly resolve features in the high-field tail of the μSR line shape, more events are needed when the contribution from muons stopping in the vicinity of the vortex cores is small—as is the case at low magnetic fields. Since the signal-to-noise ratio scales with $\sqrt{N}$ (where N is the number of counts) and typical counting rates are 2 to 5 thousand counts/sec (depending mainly on the sample size), it often takes an impractical amount of additional counting time to make further improvements to the quality of the measured spectra.

Further details of the μSR technique may be found elsewhere (see, for example, Schenck, 1985; Cox, 1987; Brewer, 1994; Riseman *et al.*, 1995). The essential point is that transverse-field μSR accurately probes the local distribution of magnetic field in the bulk of a superconductor. From the measured field distribution one can extract the important parameters λ and ξ and determine the nature of the vortex lattice structure.

III. MODELING THE INTERNAL MAGNETIC-FIELD DISTRIBUTION

In general, the assumptions involved in generating the theoretical muon polarization function represent the largest source of uncertainty in a μSR experiment. Studies of the vortex state require a comprehensive understanding of how the modeling procedure influences the results. The main complication is that an accurate description of the vortex state is still being developed. Below we summarize the important theoretical advances made in modeling the spatially inhomogeneous magnetic field associated with the vortex state. Later we show that many μSR measurements are fairly robust with respect to the theory chosen to model the magnetic-field distribution. However, in certain circumstances an approximate model is insufficient to reveal the underlying physics of interest.

A. Gaussian field distribution

Traditionally, the behavior of the magnetic penetration depth in the vortex state has been related to the variation of the second moment $\langle(\Delta B)^2\rangle=\langle(B-\langle B\rangle)^2\rangle$ of the μSR line shape. In an isotropic extreme type-II superconductor ($\lambda\gg\xi$) with a hexagonal Abrikosov vortex lattice (Brandt, 1988b),

$$\langle(\Delta B)^2\rangle=0.00371\Phi_0^2\lambda^{-4}, \tag{24}$$

where $\Phi_0=hc/2e=2.07\times10^{-15}$ T-m^2 is the flux quantum. To estimate $\langle(\Delta B)^2\rangle$ one often assumes a Gaussian distribution of local fields, where the time dependence of the muon spin polarization is proportional to $\exp(-\sigma^2t^2/2)$, such that (Aeppli *et al.*, 1987)

$$\sigma\propto1/\lambda^2\propto n_s, \tag{25}$$

where σ is the muon depolarization rate. This type of analysis seemed reasonable in the early days, when only sintered powders of the high-temperature superconductors were available—since, in general, the μSR line shape for a randomly aligned powder is nearly Gaussian. However, this is usually not the case for high-purity single crystals. For example, Fig. 8(a) shows a fit of the early time portion of the muon spin precession signal in a single crystal of $NbSe_2$ to a Gausssian function. The spectrum was obtained by field cooling the sample to $T=2.4$ K in a magnetic field $\mu_0H=0.35$ T applied parallel to the $\hat{c}$ axis. The quality of the fit is obviously poor. The FFT of the measured time spectrum and the Gaussian fit are shown in Fig. 8(b). The small peak at 47.46 MHz is due to muons that miss the sample and avoid the background suppression system. The background signal is typically fit to a separate Gaussian function. Clearly the asymmetric line shape associated with the sample signal does not fit well to a Gaussian function. It is men-

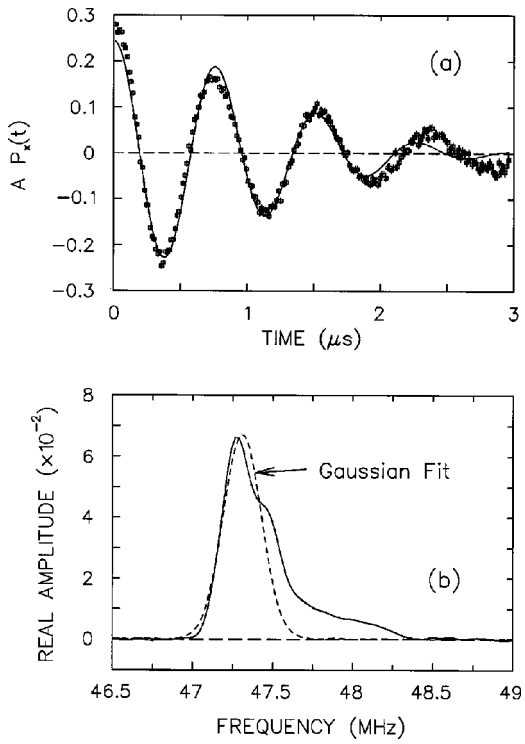

FIG. 8. Title (a) The muon spin precession signal in a crystal of $NbSe_2$ after cooling in a field $\mu_0 H = 0.35$ T to $T = 2.4$ K. The solid line is a fit to a Gaussian function $\exp(-\sigma^2 t^2/2)$. (b) Fourier transform of (solid line) the measured precession signal and (dashed line) the fit from (a).

tioned here for two reasons. First, many of the early μSR experiments reached false conclusions regarding the symmetry of the pairing state in the high-temperature cuprate superconductors using this type of analysis (see, for example, Harshman *et al.*, 1987; Kiefl *et al.*, 1988; Uemura *et al.*, 1988; Harshman *et al.*, 1989; Pümpin *et al.*, 1990a)—although, as will be discussed later (see Sec. IV.A.2), other factors may have played a more important role in the outcome of these studies. Second, fits to a simple Gaussian function are useful during the experiment, since this often yields a fair qualitative picture of the variation of λ with temperature. On the other hand, this type of analysis is grossly inaccurate if there are other sizeable contributions to the μSR linewidth that vary in a manner different from λ. As an example we note that this method is inappropriate for determining the field dependence of λ, since there is a superimposed contribution due to the changing density of vortices. In particular, the decrease of the intervortex spacing L with increasing field reduces the μSR linewidth in a manner not accounted for by Eq. (24).

In recent years it has become apparent that the μSR technique has a wider application to the study of type-II superconductors when the complete line shape is taken into account. In particular, the high-field tail of the measured internal field distribution (which is ignored in a simple Gaussian analysis) contains information related to the structure of the vortex cores. Furthermore, accounting for the full μSR line shape enables one to investigate changes in the spatial arrangement of vortices.

B. Vortex lattice in a conventional *s*-wave superconductor

1. London model

The London theory (London and London, 1935) provides the simplest approach to modeling the vortex lattice. The London model applies exclusively to extreme type-II superconductors (i.e., $\lambda \gg \xi$) and is independent of the detailed mechanism responsible for superconductivity. Furthermore, the London picture is valid at all temperatures below T_c and for internal magnetic fields $B \ll B_{c2}$. Both of these conditions are usually satisfied in a μSR experiment. For a magnetic field $\mathbf{H}$ applied in the $\hat{z}$ direction parallel to the crystallographic $\hat{c}$ axis, the London equation for the internal field profile $\mathbf{B}(\mathbf{r})$ resulting from vortices positioned at sites $\mathbf{r}_n$ is

$$\mathbf{B}(\mathbf{r}) + \lambda_{ab}^2 [\nabla \times \nabla \times \mathbf{B}(\mathbf{r})] = \Phi_0 \sum_n \delta(\mathbf{r} - \mathbf{r}_n)\hat{z}, \tag{26}$$

where $\lambda_{ab} = (\lambda_a \lambda_b)^{1/2}$ is the in-plane magnetic penetration depth and $\delta(\mathbf{r})$ is a two-dimensional delta function. We restrict all further discussion to the above-mentioned orientation of the crystal lattice in the applied field. The points $\mathbf{r}_n$ form a two-dimensional periodic lattice in the $\hat{a}$-$\hat{b}$ plane, so that $\mathbf{B}(\mathbf{r})$ may be expanded in a Fourier series. The Fourier transform $\mathbf{B}_\mathbf{K}$ is

$$\mathbf{B}_\mathbf{K} = n_f \int_{\text{cell}} \mathbf{B}(\mathbf{r}) e^{-i\mathbf{K}\cdot\mathbf{r}} d^2\mathbf{r}, \tag{27}$$

where n_f is the number of vortices per unit area and $\mathbf{K}$ are the reciprocal-lattice vectors of the unit cell. Combining with Eq. (26), the Fourier components are

$$\mathbf{B}_\mathbf{K} = \frac{B_0}{1 + K^2 \lambda_{ab}^2} \hat{z}, \tag{28}$$

where $B_0 = n_f \Phi_0$ is the average internal field. Thus the total field at the point $\mathbf{r}$ is given by

$$\mathbf{B}(\mathbf{r}) = \sum_\mathbf{K} \mathbf{B}_\mathbf{K} e^{-i\mathbf{K}\cdot\mathbf{r}} = B_0 \sum_\mathbf{K} \frac{e^{-i\mathbf{K}\cdot\mathbf{r}}}{1 + K^2 \lambda_{ab}^2} \hat{z}. \tag{29}$$

The use of a delta function as the source term in Eq. (26) means that Eq. (29) does not account for the finite size of the vortex cores. As a result, Eq. (29) has the unphysical property that $\mathbf{B}(\mathbf{r})$ diverges on the axis of the vortex line at $\mathbf{r}_n$. To correct for this, each term in Eq. (29) can be multiplied by a cutoff factor that suppresses the higher Fourier components and produces a smooth increase in the field to a finite maximum value at the center of the vortex core. A sharp cutoff at $K = 2\pi/\xi_{ab}$ is generally inappropriate because it introduces an oscillatory cutoff in real space (Forgan and Lee, 1995). A smooth cutoff may be obtained by solving the Ginzburg-Landau equations (Ginzburg and Landau, 1950). At reduced fields $b = B/B_{c_2} < 0.25$, Brandt (1972) derived the Gaussian cutoff factor $\exp(-K^2\xi^2/2)$ from the isotropic Ginzburg-Landau theory for the case $\lambda \gg \xi$. Brandt's full modification of Eq. (29) is given by (Brandt, 1977a, 1988a, 1988b)

$$\mathbf{B}(\mathbf{r}) = B_0 \sum_{\mathbf{K}} \frac{e^{-i\mathbf{K}\cdot\mathbf{r}} e^{-K^2\xi_{ab}^2/2(1-b)}}{1+K^2\lambda_{ab}^2/(1-b)}\hat{z}, \tag{30}$$

where λ_{ab} and ξ_{ab} are divided by $\sqrt{1-b}$ to account for the field dependence of the Ginzburg-Landau order parameter. When $b \ll 1$, the cutoff factor is better approximated by the Lorentzian function $\exp(-\sqrt{2}K\xi_{ab}/\sqrt{1-b})$ (Yaouanc, de Réotier, and Brandt, 1997). Later we shall show that Eq. (30) is a good approximation of $\mathbf{B}(\mathbf{r})$ in a real superconductor. However, this procedure is not completely satisfactory since the analytical cutoff factors have a limited range of validity. For most values of b, the cutoff factor derived from the Ginzburg-Landau equations is numerical.

2. Vortex core structure

As shown in Fig. 1, the order parameter $\psi(r)$ is strongly suppressed in the vicinity of a vortex line. Bardeen and Stephen (1965) described a vortex as having a core of radius $r_0 \sim \xi$ that is occupied by normal electrons. This simple picture is really only justified in dirty superconductors, where the mean free path l is much smaller than the coherence length ξ. In a clean s-wave superconductor, Caroli, de Gennes, and Matricon (1964) showed that quasiparticle states whose energy E is smaller than the bulk energy gap Δ_0 become localized in the core. Using the Bogoliubov–de Gennes equations they calculated the low-energy spectrum of quasiparticle bound states in an isolated core. The model is conceptually similar to the quantum-mechanical picture of a particle in a cylindrical potential well of radius $\xi \simeq \hbar v_F/\pi\Delta_0$ and depth Δ_0. The eigenvalues of the low-lying quasiparticle states may be written as $E_\mu \simeq \mu\Delta_0^2/E_F \sim \mu\Delta_0/k_F\xi$, where $\mu = m + 1/2$ (m is an odd integer) are the angular momentum quantum numbers and E_F is the Fermi energy. When the thermal energy $k_B T$ is much greater than the energy-level spacing, the vortex core resembles the Bardeen-Stephen model. In a dirty superconductor, the bound-state energy levels are also broadened by impurity scattering of the quasiparticles between the levels.

The quasiparticle states bound to the core are somewhat different from a simple particle in a potential well. The localized core states are superpositions of electron and hole states that are trapped in the vortex by continuous Andreev scattering from the spatially varying order parameter. Unlike particle states bound in a potential well, the Andreev core states can participate in charge transport by transferring charge to the supercurrents flowing outside of the vortex core (Rainer, Sauls, and Waxman, 1996).

A series of scanning tunneling spectroscopy (STS) measurements on the conventional superconductor $NbSe_2$ have revealed the existence of localized quasiparticle core states (Hess *et al.*, 1989; Hess, Robinson, and Waszczak, 1990; Hess, 1991; Hess, Murray, and Waszczak, 1992). Well outside the vortex cores, the voltage dependence of the differential conductance dI/dV resembled the density of states predicted in Bardeen-Cooper-Schrieffer (BCS) theory (Bardeen, Cooper, and Schrieffer, 1957). However, within the vortex core the STS spectrum showed a pronounced peak centered at $V = 0$. Theoretical calculations showed that the peak reflects the local density of states for bound quasiparticles (Shore *et al.*, 1989; Gygi and Schlüter, 1990, 1991; Klein, 1990; Ullah, Dorsey, and Buchholtz, 1990). The discrete quasiparticle energy levels have not yet been observed experimentally. In the STS experiments on $NbSe_2$, the experimental resolution of ~ 0.1 meV was greater than the expected energy-level spacing of ~ 0.001 meV.

3. Temperature dependence of the vortex core size

To determine the vortex structure for arbitrary temperature, magnetic field, and impurity concentrations, many efforts were made to solve numerically the quasiclassical Eilenberger equations (Eilenberger, 1968)—which are a reformulation of the microscopic Gor'kov theory (Gor'kov, 1958, 1959). The Eilenberger equations are valid at temperatures well above T_c^2/E_F and for spatial variations of the Green's functions that are slow over atomic distances (Serene and Rainer, 1983). In the dirty limit, the transportlike Eilenberger equations reduce to the simpler diffusionlike Usadel equations (Usadel, 1970, 1971). Kramer, Pesch, and Watts-Tobin (1974) determined the local structure of a vortex near H_{c1} by numerically solving the Usadel equations. They found that, with decreasing temperature, the pair potential $\Delta(r)$, i.e., the order parameter, rises more steeply and the magnetic field decays more rapidly as a function of distance from the center of the vortex.

Numerical solutions of the Eilenberger equations for nearly isolated vortices in the clean limit were later obtained (Pesch and Kramer, 1974; Kramer and Pesch, 1974). The size of the vortex core region was found to shrink more drastically with decreasing T than in the dirty limit. In particular, Kramer and Pesch (1974) showed that the pair potential $\Delta(r)$ and the supercurrent density $J_s(r)$ increased with radial distance r from the core center over a temperature-dependent length scale given by

$$\xi_1 \sim \xi_0 \frac{T}{T_c} \quad \text{for} \quad T_c^2/E_F \ll T \ll T_c, \tag{31}$$

where

$$\xi_1 = \Delta_0 / \lim_{r\to 0} \frac{\Delta(r)}{r}, \tag{32}$$

Δ_0 is the BCS energy gap, and ξ_0 is the BCS coherence length pertaining to the spatial extent of the Cooper pairs. The increase in the slope of $\Delta(r)$ near the vortex center with decreasing T is commonly referred to as the "Kramer-Pesch effect." Kramer and Pesch (1974) were able to reproduce these results with the Bogoliubov–de Gennes equations (which are valid over the entire temperature range), closely following the method of Caroli, de Gennes, and Matricon (1964). Since only the bound quasiparticle core states with $\mu = m + 1/2$ (m is an odd integer) contribute via the self-consistency equations to

the slope of $\Delta(r)$ [and $J_s(r)$] near the vortex center, the reduction of the core size is due to the thermal depopulation of the bound quasiparticle energy levels. Consequently the shrinking of the vortex core terminates at low temperature, where only the lowest energy level is populated (i.e., the quantum limit). From the Bogoliubov–de Gennes equations Kramer and Pesch (1974) estimated that $\xi \sim k_F^{-1}$ for $T \lesssim T_c^2/E_F$. Recently, Hayashi *et al.* (1998) performed a more rigorous numerical calculation of the quantum regime of a single vortex in a clean *s*-wave superconductor from the Bogoliubov–de Gennes equations. The temperature dependence of ξ_1 was found to decrease almost linearly with T and smoothly cross over to the saturated regime where $\xi_1 \sim k_F^{-1}$. The shrinking of the core region leads to a reduction in the number of bound-quasiparticle-state energy levels.

It is customary to approximate the spatial dependence of the pair potential within a vortex by an expression of the form

$$\Delta(r) = \Delta_0 \tanh\left(\frac{r}{\xi}\right). \tag{33}$$

However, at low temperature the numerical solutions of the Bogoliubov–de Gennes or Eilenberger equations for the spatial dependence of $\Delta(r)$ are not described by this analytical expression (see, for example, Gygi and Schlüter, 1991). The reason is that the slope of $\Delta(r)$ at the vortex center becomes very steep. Consequently the definition of ξ_1 is often used to quantify the changes in the spatial dependence of the order parameter with temperature. Although the slope of $\Delta(r)$ near the core center increases with decreasing temperature on the length scale ξ_1, $\Delta(r)$ reaches its asymptotic value Δ_0 over a distance of the order ξ_0. At high temperature, the values of ξ_1 and ξ_0 are nearly equivalent. However, ξ_0 has a weak temperature dependence at low T, where the isotropic energy gap Δ_0 exponentially cuts off the "breaking apart" of Cooper pairs as $T \to 0$ K. In an *s*-wave superconductor, Volovik (1993) showed that there is actually a singularity in the order parameter within the vortex (see Fig. 9), which becomes more pronounced with decreasing temperature. In unconventional superconductors the kink can smooth out, but according to Volovik it survives in layered systems. Throughout this review article, "vortex core" refers to the spatial region governed by ξ_1.

In a μSR experiment one is interested in how the spatial variation of the supercurrent density $J_s(r)$ changes as a function of temperature. Theoretical studies show that $|J_s(r)|$ rises to its maximum value over a distance of the order ξ_1 (Gygi and Schlüter, 1991; Hayashi *et al.*, 1998). It will be shown later that the distance from the center of the vortex core at which $|J_s(r)|$ reaches its maximum value can be extracted from the μSR spectrum. In this way, μSR can be used as a probe of the Kramer-Pesch effect.

4. Field dependence of the vortex core size

From numerical solutions of the Usadel equations, Golubov and Hartmann (1994) showed that the vortex core radius of an *s*-wave superconductor in the dirty limit expands with decreasing magnetic field. The radius of the vortex core was estimated from the half-width of the calculated spatial dependence of the order parameter within the core. These calculations were extended by Sonier, Kiefl, *et al.* (1997b) to determine the field dependence of the corresponding supercurrent density profile $J_s(r)$, which could be related to the field distribution measured with μSR. The core radius r_0, defined as the radius where $|J_s(r)|$ reaches its maximum value, showed a similar increase with decreasing magnetic field.

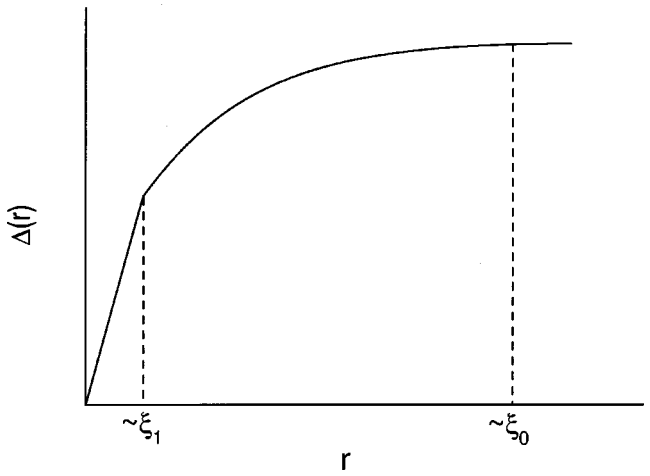

FIG. 9. The order parameter within the vortex core of an *s*-wave superconductor. The length scale ξ_1 increases as a linear function of T. From Volovik, 1993.

More recently, the Eilenberger equations were numerically solved to determine the vortex core radius in a clean *s*-wave superconductor (Ichioka, Hasegawa, and Machida, 1999a, 1999b). The core radius determined from the spatial dependence of the order parameter and the supercurrent density is found to increase with decreasing magnetic field.

5. Vortex core symmetry

The symmetry of the vortices in $NbSe_2$ was investigated by Hess, Robinson, and Waszczak (1990) using STS. In a conventional *s*-wave superconductor with an isotropic energy gap, the local density of states around an isolated vortex core is expected to exhibit circular symmetry. However, in the STS experiment, a sixfold star pattern was observed for the local density of states around a single vortex. The origin of the sixfold symmetry has been attributed to nearest-neighbor vortex interactions (Ichioka, Hayashi, and Machida, 1997), anisotropy of the density of states at the Fermi surface (Hayashi, Ichioka, and Machida, 1996), anisotropy of the *s*-wave energy gap (Hayashi, Ichioka, and Machida, 1997), and a combination of these effects. The precise form of $\mathbf{B}(\mathbf{r})$ in the vortex core region will depend on which of these interpretations is correct. For instance, if vortex-vortex interactions are the dominant source of this symmetry, $\mathbf{B}(\mathbf{r})$ will possess circular symmetry near

the vortex center and develop a sixfold symmetry with increasing radial distance. At low fields where the vortex-vortex interactions are weak, the region of circular symmetry will extend further out from the vortex center. On the other hand, if the observed sixfold symmetry is due to an anisotropic s-wave energy gap, $\mathbf{B}(\mathbf{r})$ will possess sixfold symmetry even in the vortex core region.

6. Ginzburg-Landau model

The Ginzburg-Landau theory has the spatial dependence of the order parameter built in and thus provides a phenomenological description of the magnetic-field profile in the vortex core region. Abrikosov (1957) predicted the vortex state from a periodic solution of the Ginzburg-Landau equations near H_{c2}, and provided an approximate analytical solution of these equations for an isolated vortex near H_{c1}. For intermediate fields the Ginzburg-Landau equations must be solved numerically. The magnetic-field distribution obtained from the exact numerical solutions of the Ginzburg-Landau equations coincides with that from the modified London model [Eq. (30)] at low fields and arbitrary κ (Fesenko *et al.*, 1993). Clem (1975) proposed a variational model to solve the Ginzburg-Landau equations based upon a trial function for the order parameter: $f=r/(r^2+\xi_v^2)^{1/2}$, where ξ_v is a variational core radius parameter. This model solves the Ginzburg-Landau equations approximately at low magnetic fields (i.e., for isolated vortices), yielding an analytical expression for the magnetic-field distribution

$$\mathbf{B}(\mathbf{r})=B_0\sum_{\mathbf{K}}\frac{K_1(\xi_v\sqrt{K^2+\lambda_{ab}^{-2}})e^{-i\mathbf{K}\cdot\mathbf{r}}}{K_1(\xi_v/\lambda_{ab})\lambda_{ab}K}\hat{z}, \tag{34}$$

where $K_1(x)$ is a modified Bessel function. For extreme type-II superconductors ($\lambda\gg\xi$), $\xi_v\approx\sqrt{2}\xi_{ab}$, where ξ_{ab} is the Ginzburg-Landau coherence length.

Hao *et al.* (1991) extended the Clem model to larger magnetic fields through the linear superposition of the field profiles of the individual vortices. This included multiplying the trial function for the order parameter by a second variational parameter f_∞ to take into account the suppression of the order parameter due to the overlapping of vortices. The behavior of this parameter is such that $f_\infty\to 1$ as $B\to 0$, and $f_\infty\to 0$ as $B\to B_{c2}$. Yaouanc, de Réotier, and Brandt (1997) simplified Hao's analytical model exclusively for the case of $\lambda^2K^2_{\min}\gg 1$, where $\mathbf{K}_{\min}$ is the smallest nonzero reciprocal-lattice vector. This condition is generally satisfied even at low fields for extreme type-II superconductors, such as the high-temperature cuprate superconductors. The result is that the local field at any point in the $\hat{a}$-$\hat{b}$ plane due to an applied field along the $\hat{c}$ axis is

$$\mathbf{B}(\mathbf{r})=B_0(1-b^4)\sum_{\mathbf{K}}\frac{e^{-i\mathbf{K}\cdot\mathbf{r}}uK_1(u)}{\lambda_{ab}^2K^2}\hat{z}, \tag{35}$$

where $K_1(u)$ is a modified Bessel function and

$$u^2=2\xi_{ab}^2K^2(1+b^4)[1-2b(1-b)^2]. \tag{36}$$

Brandt (1997) later developed an iteration method for solving the Ginzburg-Landau equations to compute the field profile $\mathbf{B}(\mathbf{r})$ of a vortex lattice of arbitrary symmetry, valid for any value of the magnetic field. Equation (35) agrees extremely well with these exact numerical solutions of the Ginzburg-Landau equations at low reduced fields b.

7. Vortex lattice geometry

In employing Eq. (30) or Eq. (35), one must assume an appropriate geometry for the vortex lattice. Theoretically, the equilibrium structure of the vortex lattice can be found by minimizing the Gibbs free energy

$$G_L=F_L-\frac{BH}{4\pi}, \tag{37}$$

where for instance, in the London theory, the free energy per unit volume associated with the vortices is (Campbell, Doria, and Kogan, 1988)

$$F_L=\int[\mathbf{h}^2+\lambda^2(\boldsymbol{\nabla}\times\mathbf{h})^2]d^2\mathbf{r}/8\pi A, \tag{38}$$

where A is the area of the sample. With the field applied along the $\hat{c}$ axis of the crystal, the lowest-energy configuration for an isotropic conventional s-wave superconductor was calculated to be a hexagonal vortex lattice (Kleiner, Roth, and Autler, 1964). Numerous experiments have confirmed this prediction. For instance, STS and small-angle neutron-scattering measurements on $NbSe_2$ and Nb show a nearly perfect hexagonal vortex lattice with long-range order (Hess *et al.*, 1989; Hess, Murray, and Waszczak, 1992; Gammel *et al.*, 1994; Rosov, Lynn, and Grigereit, 1994).

However, recently Yethiraj *et al.* (1999) have shown, using small-angle neutron scattering, that the vortex lattice in the conventional cubic superconductor V_3Si well below the superconducting transition temperature T_c transforms from triangular to square symmetry at a field $\mu_0H\approx 1$ T. According to the London and Ginzburg-Landau theories, the vortex lattice should be hexagonal in a cubic crystal for all field orientations. To explain the appearance of a nonhexagonal vortex lattice in V_3Si, Kogan *et al.* (Kogan, Bullock, *et al.*, 1997; Kogan, Miranović, *et al.*, 1997) introduced nonlocal corrections into the London model. In Fourier space, the relation between the supercurrent density $\mathbf{J}$ and the vector potential $\mathbf{A}$ is of the form

$$\mathbf{J}(\mathbf{K})=\hat{Q}(\mathbf{K})\mathbf{A}(\mathbf{K}), \tag{39}$$

where $\hat{Q}$ is the electromagnetic response kernel. In the London model, $\hat{Q}(\mathbf{K})=\lambda^{-2}$, so that at a given point in real space $\mathbf{J}$ depends only on $\mathbf{A}$ at that point. However, as accounted for in the microscopic theory, the response of a superconductor to an applied field is generally nonlocal, in the sense that $\mathbf{J}(\mathbf{r})$ is determined by $\mathbf{A}(\mathbf{r})$ over a surrounding volume of radius $\sim\xi_0$. The first nonlocal correction term has fourfold symmetry in the magnetic-

field distribution for a field applied parallel to the $\hat{c}$ axis, which coincides with the symmetry of the underlying crystal lattice. For other orientations of the field with respect to the lattice, higher-order terms in the nonlocal correction must be included to account for the symmetry of the experimentally observed vortex lattice. The model has also been used to describe vortex lattice symmetry changes in the borocarbide superconductors $R\mathrm{Ni}_2\mathrm{Bi}_2\mathrm{C}$ (R=Er, Lu, Y), where the vortex lattice transforms from hexagonal to square at high field (de Wilde *et al.*, 1997; Eskildsem *et al.*, 1997; Paul *et al.*, 1998). Since the finite size of the vortex cores is not included, this model is strictly valid only at low fields, for which the vortex spacing is much larger than the vortex core size. This limits its applicability to fitting μSR spectra to cases in which the vortex cores contribute very little spectral weight to the measured line shape.

To describe the square vortex lattice that forms in the unconventional superconductor $\mathrm{Sr}_2\mathrm{RuO}_4$ as a consequence of a broken-time-reversal state at low T, a Ginzburg-Landau model for a two-component odd-parity order parameter with p-wave symmetry was developed (Agterberg, 1998; Heeb and Agterberg, 1999). The field distribution determined from this model self-consistently extends the fourfold symmetry into the vortex core region. The precise vortex lattice symmetry, the shape of the individual vortices, and the orientation of the vortex lattice with respect to the underlying crystal lattice all depend on the value of the applied field H and the shape of the Fermi surface. For the case of $\mathrm{Sr}_2\mathrm{RuO}_4$, a continuous hexagonal-to-square vortex lattice transition with increasing field is predicted.

As noted by Kogan, Miranović, *et al.* (1997), it is difficult to establish a simple relation between the symmetry of the order parameter and the vortex lattice structure, since even in s-wave superconductors the latter is sensitive to temperature, magnetic field, and orientation with respect to the underlying crystal lattice. We next summarize efforts to develop a model, relevant to high-temperature superconductors, for the vortex lattice in a $d_{x^2-y^2}$-wave superconductor.

C. Vortex lattice in a $d_{x^2-y^2}$-wave superconductor

Theoretical efforts to develop a model for vortex structure in the high-temperature cuprate superconductors, assuming a dominant $d_{x^2-y^2}$-wave order parameter, form a vast body of literature. In the following we outline some of the key advances using various theoretical formalisms. The details of these and related theories could very easily form the basis of a separate review article, so a complete discussion of all the work in this field is not possible here.

1. Two-component Ginzburg-Landau models

The problem of an isolated vortex line in a $d_{x^2-y^2}$-wave superconductor was first seriously considered by Soininen, Kallin, and Berlinsky (1994), using a simple microscopic model for electrons on a lattice in the Bogoliubov–de Gennes formalism. In calculating the spatial distribution of the order parameter for a single vortex, they found that an s-wave component is induced near the vortex core with opposite winding of phase relative to the $d_{x^2-y^2}$-wave component. Several theoretical studies (Berlinsky *et al.*, 1995; Ren, Xu, and Ting, 1995; Xu, Ren, and Ting, 1995, 1996; Franz *et al.*, 1996) have considered the effect of this induced s-wave component on both an isolated vortex and the vortex lattice, in terms of Ginzburg-Landau equations containing both s-wave and $d_{x^2-y^2}$-wave order parameters. In these equations the s-wave component couples to the $d_{x^2-y^2}$-wave component through mixed gradient terms. Because of this coupling, the s-wave component is induced by spatial variations in the $d_{x^2-y^2}$-wave order parameter that occur in the vicinity of a vortex. In a tetragonal superconductor, the induced s-wave component around the vortex reflects the fourfold symmetry of the $d_{x^2-y^2}$-wave order parameter, whereas far from the core the bare $d_{x^2-y^2}$-wave component exhibits circular symmetry. Thus, in the core region of an isolated vortex, the magnetic-field distribution is predicted to be fourfold symmetric, whereas outside the core region, where the s-wave component vanishes, the field distribution has circular symmetry.

Xu, Ren, and Ting (1996) have extended the two-component Ginzburg-Landau theory to include the effects of anisotropy for an orthorhombic crystal structure—which is applicable to the $\mathrm{YBa}_2\mathrm{Cu}_3\mathrm{O}_{7-\delta}$ system. For a field applied parallel to the $\hat{c}$ axis, both the s-wave and $d_{x^2-y^2}$-wave order parameters exhibit twofold symmetry when $\gamma=(m_a/m_b)^{1/2}=\lambda_a/\lambda_b=\xi_b/\xi_a>1$ (where m_i is the effective mass tensor). Heeb *et al.* (1996) arrived at a similar orthorhombic reduction in symmetry.

Near H_{c2}, where the vortices are close together and strongly interacting, the symmetry of the vortex cores is expected to play a prevalent role in the vortex lattice geometry. Thus at high fields the two-component Ginzburg-Landau theory predicts that the s-wave component near the cores induces a fourfold-symmetric vortex lattice in a tetragonal superconductor, and a twofold-symmetric vortex lattice in an orthorhombic superconductor. However, near T_c the theory predicts that the s-wave component becomes negligible, resulting in a hexagonal vortex lattice.

It is important to realize that the conventional Ginzburg-Landau equations for a $d_{x^2-y^2}$-wave superconductor are the same as those for an isotropic s-wave superconductor, and thus also predict a hexagonal vortex lattice geometry and circular symmetric vortex cores (Ichioka, Enomoto, and Machida, 1997). It is the inclusion of an induced s-wave component that leads to the fourfold symmetry. On the other hand, Ichioka, Enomoto, and Machida (1997) have argued that since the conventional Ginzburg-Landau theory is valid only near T_c, correction terms derived from the Gor'kov equations must be added to extend the theory to lower temperatures. They found that these correction terms alone lead to a hexagonal-to-square vortex lattice tran-

sition in a $d_{x^2-y^2}$-wave superconductor in the absence of an induced s-wave component. Strictly speaking, the Ginzburg-Landau theory is valid only near the superconducting-to-normal phase boundary. For fields further below H_{c2}, additional higher-order correction terms must be added. Alternatively, the quasiclassical Eilenberger equations may be used, since they naturally contain all of these additional contributions and are valid well below the phase boundary (Ichioka, Hasegawa, and Machida, 1999b).

2. Quasiclassical predictions

Calculations from the quasiclassical Eilenberger theory show that an isolated vortex in a pure $d_{x^2-y^2}$-wave superconductor has a fourfold-symmetric core (Schopohl and Maki, 1995; Ichioka, Hayashi, *et al.*, 1996b). The calculated local density of states indicates that the low-energy quasiparticle excitations are strongly peaked in the core but have tails extending along the nodal directions of the $d_{x^2-y^2}$-wave order parameter. Unlike the bound quasiparticle states in the core of an s-wave superconductor, these states are *not localized*, since the tails do not decay to zero far outside the core region. The extended states allow for the transfer of quasiparticles between vortices, referred to as the ''vortex lattice effect.'' Above the quantum limit, the slope of the order parameter near the core center is predicted to decrease almost linearly with temperature (Ichioka, Hayashi, *et al.*, 1996b), analogous to the Kramer-Pesch effect in s-wave superconductors.

More recently, the full structure of the vortex lattice in a $d_{x^2-y^2}$-wave superconductor has been studied in the framework of the quasiclassical Eilenberger theory (Ichioka, Hasegawa, and Machida, 1999a, 1999b). Assuming the fourfold-symmetric vortex core structure of a pure $d_{x^2-y^2}$-wave superconductor, it was determined that the vortices form a square vortex lattice, except at low fields $H/H_{c2}<0.15$, where the lower-energy configuration is a hexagonal vortex lattice. At these low fields, the vortex lattice symmetry does not reflect the full symmetry of the vortex cores, since the core region occupies only a small fraction of the vortex lattice unit cell. Consequently the theoretical μSR line shape $n(B)$ for a $d_{x^2-y^2}$-wave superconductor is nearly identical to that for an s-wave superconductor at low fields. In the same studies Ichioka, Hasegawa, and Machida found that the vortex core size increases with decreasing field in a clean $d_{x^2-y^2}$-wave superconductor—as predicted for an s-wave superconductor.

The Eilenberger theory has also been employed to investigate pairing interactions, which include, in addition to the $d_{x^2-y^2}$-wave component, a component such as s or d_{xy}, as was first investigated with the two-component Ginzburg-Landau theory. The second component, which is induced by the spatial variation of the $d_{x^2-y^2}$-wave component, results in fourfold- and eightfold-symmetric vortex cores for the additional s-wave and d_{xy}-wave components, respectively (Ichioka, Enomoto, *et al.*, 1996a; Ichioka, Hasegawa, and Machida, 1999b).

3. Bogoliubov–de Gennes calculations

The vortex structure for a $d_{x^2-y^2}$-wave superconductor has been studied by a number of authors by numerically solving the Bogoliubov–de Gennes equations. Wang and MacDonald (1995) diagonalized the Bogoliubov–de Gennes Hamiltonian for a specific lattice model and determined that, unlike in the s-wave case, the energy levels of the low-energy quasiparticle excitations form a continuum. Later, Franz and Tešanović (1998) self-consistently solved the Bogoliubov–de Gennes theory for a single isolated vortex, concluding that these quasiparticle states are not localized in the core, but are extended along the nodal directions of the $d_{x^2-y^2}$-wave order parameter with a continuous energy spectrum. The result confirmed the earlier quasiclassical calculation by Ichioka, Hayashi, *et al.* (1996b), which first suggested the absence of bound core states in a $d_{x^2-y^2}$-wave superconductor.

4. London models

Unfortunately, the above theories for a $d_{x^2-y^2}$-wave superconductor generally contain too many independent or unknown parameters to be used as theoretical models for fitting μSR spectra. Affleck, Franz, and Amin (1996) attempted to resolve this issue by generalizing the London model to include fourfold anisotropies that could arise from $d_{x^2-y^2}$-wave pairing in a tetragonal superconductor. Starting from a Ginzburg-Landau free-energy density with s- and $d_{x^2-y^2}$-wave order parameters, they derived the corresponding London equation. For a magnetic field applied along the $\hat{c}$ axis, the field profile was found to be

$$\mathbf{B}(\mathbf{r}) = B_0 \sum_{\mathbf{K}} \frac{e^{-i\mathbf{K}\cdot\mathbf{r}} e^{-K^2\xi_{ab}^2/2}}{1 + K^2\lambda_{ab}^2 + 4\epsilon\lambda_{ab}^2\xi_{ab}^2(K_xK_y)^2}\hat{z}, \qquad (40)$$

where ϵ is a dimensionless parameter that controls the strength of the coupling between the s and $d_{x^2-y^2}$-wave components. For $\epsilon=0$, Eq. (40) reduces to Eq. (30). Unfortunately, the vortex lattice structure obtained by minimizing the Gibbs free energy of Eq. (37) depends on the choice of ϵ, which cannot be independently determined. Furthermore, the Gaussian cutoff factor added to the London model to account for the finite size of the vortex cores is strictly valid only at high fields.

Franz, Affleck, and Amin (1997) developed a generalized London model derived from a simple microscopic model that takes into account nonlocal electrodynamics in a $d_{x^2-y^2}$-wave superconductor. The energy-gap function for this pairing-state symmetry is

$$\Delta_{\hat{\boldsymbol{k}}} = \Delta_0(\hat{k}_{\mathbf{x}}^2 - \hat{k}_{\mathbf{y}}^2), \qquad (41)$$

where Δ_0 is the maximum value of the anisotropic gap. In a tetragonal or orthorhombic system like a high-temperature superconductor, the energy gap vanishes along *line nodes* in momentum space. The nonlocal effects discussed in Sec. III.B.7 are particularly important in a $d_{x^2-y^2}$-wave superconductor near the nodes (Kosz-

tin and Leggett, 1997), since in general the coherence length has an angular dependence such that

$$\xi_0(\hat{k}) = \frac{\hbar v_f}{\pi \Delta_{\hat{k}}}. \tag{42}$$

The divergence of ξ_0 along the nodal directions $|\hat{k}_{\mathbf{x}}| = |\hat{k}_{\mathbf{y}}|$ means that the response of quasiparticles in the vicinity of the nodes is highly nonlocal. The inclusion of nonlocal effects in the $d_{x^2-y^2}$-wave London model was shown to produce novel changes in the vortex lattice symmetry. However, this prediction also suffers from the use of an approximate source term, so that the influence of the vortex-core symmetry on the vortex lattice geometry is not accounted for self-consistently.

5. Experimental observations

Experiments on the high-temperature superconductors have not provided a picture of the vortex lattice that is entirely consistent with the theoretical models for a $d_{x^2-y^2}$-wave superconductor. In many of these experiments it has been difficult to determine how much of the observed vortex structure is directly attributable to the symmetry of the pairing state and how much is due to deformations of the vortex lattice caused by extrinsic effects. Establishing agreement with theory has also suffered from the limitation that experimental techniques used to investigate vortex structure can only probe the low-field end of the vortex phase diagram, due to the large values of H_{c2} in the high-temperature superconductors. In the $YBa_2Cu_3O_{7-\delta}$ system there is the added complication of a sizable $\hat{a}$-$\hat{b}$ plane mass anisotropy, due to the presence of CuO chains along the crystallographic $\hat{b}$ direction. Due to the orthorhombic crystal structure, twin boundaries form along the {110} directions during the cooldown stage of crystal growth, which separate domains of interchanged $\hat{a}$ and $\hat{b}$ axes. We now proceed to discuss experiments on the high-temperature cuprate superconductors performed at *low temperatures* with the magnetic field applied parallel to the crystallographic $\hat{c}$ axis.

Bitter decoration experiments[1] that image the vortex lattice at the sample surface in fields of $\sim 10^{-3}$–10^{-2} T have shown that the vortices form a hexagonal lattice in $YBa_2Cu_3O_{7-\delta}$ (Gammel *et al.*, 1987; Dolan *et al.*, 1989), $Bi_2Sr_2CaCu_2O_{8+\delta}$ (Kim, Yao, and Lieber, 1996), and $Tl_2Ba_2CaCu_2O_x$ (Vinnikov *et al.*, 1989). A hexagonal vortex lattice was also observed at higher fields in small-angle neutron-scattering measurements on $Bi_{2+x}Sr_{2-x}CaCu_2O_{8+\delta}$ (Cubitt *et al.*, 1993).

[1]The term "Bitter" refers to the conventional method of revealing domain boundaries in ferromagnets by decorating the surface with small ferromagnetic particles, which become attracted by the field inhomogeneity at the domain boundaries (Bitter, 1931). The Bitter pattern formed by the attraction of fine ferromagnetic particles to the vortices on the surface of a superconductor can be observed with an electron microscope.

On the other hand, until recently small-angle neutron-scattering measurements on large single crystals of $YBa_2Cu_3O_{7-\delta}$ have found that the vortex lattice has fourfold symmetry (Forgan *et al.*, 1990; Yethiraj *et al.*, 1993; Keimer *et al.*, 1994). A fourfold-symmetric vortex lattice was also observed at the surface of this material at $\mu_0 H = 6$ T using STS (Maggio-Aprile *et al.*, 1995). Although fourfold symmetry is expected from vortex lattice theories for a $d_{x^2-y^2}$-wave superconductor, all of these studies were performed on heavily twinned samples. The vortex lattice geometries observed in these experiments can be explained by a combination of an hexagonal lattice aligned with the twin boundaries, and distortions caused by the $\hat{a}$-$\hat{b}$ anisotropy (Walker and Timusk, 1995). In a more recent small-angle neutron scattering experiment on a detwinned single crystal of $YBa_2Cu_3O_{7-\delta}$, a well-ordered hexagonal vortex lattice distorted by the $\hat{a}$-$\hat{b}$ anisotropy was observed over the field range $0.2 < \mu_0 H < 4$ T (Johnson *et al.*, 1999). Hexagonal symmetry in this field range is consistent with recent theoretical calculations by Ichioka, Hasegawa, and Machida (1999b), which show that $d_{x^2-y^2}$-wave vortices prefer this arrangement at low fields. However, it is not known whether the vortex lattice that forms near T_c persists down to low T in field-cooled samples with strong pinning (vortex pinning is discussed in Sec. III.D.1). This is an important issue in determining the applicability of theories to imaging experiments.

Since high-quality single crystals have become available, the line shapes observed in μSR experiments on high-temperature cuprate superconductors at low temperatures and fields have predominantly been consistent with the theoretical field distribution for a hexagonal arrangement of vortices. Figure 10 shows a μSR line shape for $YBa_2Cu_3O_{7-\delta}$ compared to that for Sr_2RuO_4. Small-angle neutron-scattering measurements show that the vortex lattice in Sr_2RuO_4 has square symmetry (Riseman *et al.*, 1998). A square vortex lattice was inferred from earlier measurements of the μSR line shape in Sr_2RuO_4 single crystals (Aegerter, Lloyd, *et al.*, 1998). The difference between the minimum and saddle-point fields is larger in a square lattice than in a hexagonal lattice. Thus a large "shoulder" on the low-field side of the peak of the μSR line shape is a signature of a square vortex lattice. Strictly speaking, the difference between the μSR line shapes for hexagonal and square vortex lattices will depend on the values of λ, ξ, and the applied magnetic field. For example, with increasing λ or applied field, the line shapes for both geometries become more symmetric due to a reduction in the field inhomogeneity. For large λ or field, the line shapes in both cases are nearly symmetric and visually indistinguishable.

STS measurements on $YBa_2Cu_3O_{7-\delta}$ showed that the vortex cores at low temperature and moderate field are ellipsoidal in shape, with the ratio of the principle axes being essentially that of the $\hat{a}$-$\hat{b}$ plane anisotropy (Maggio-Aprile *et al.*, 1995). This implies that in the absence of anisotropy, the vortex cores are circular. More intriguing was the observation of a double-peak struc-

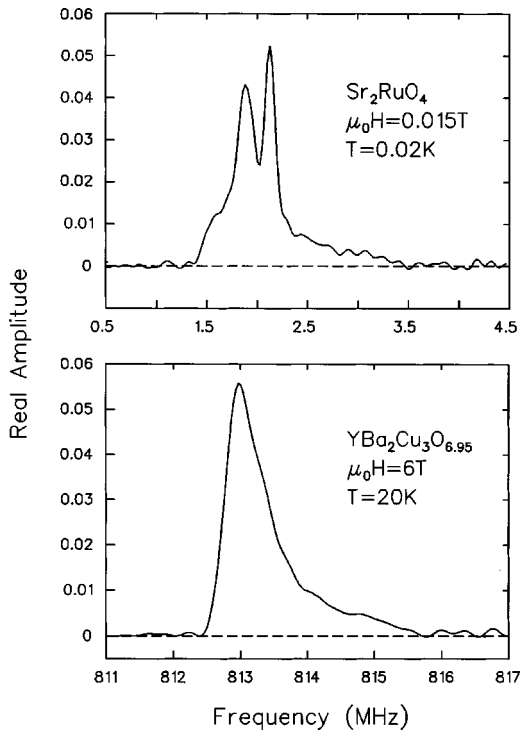

FIG. 10. Examples of a Fourier transform of the muon precession signal in Sr_2RuO_4 (Luke *et al.*, 1999) and detwinned $YBa_2Cu_3O_{6.95}$ (Sonier, Brewer, *et al.*, 1999). The sharp peak on the right-hand side, which is clearly visible for Sr_2RuO_4, is the background signal.

ture in the tunneling conductance within the vortex core near zero bias. The peaks were attributed to a couple of discrete bound quasiparticle states. However, this feature was not observed by Renner *et al.* (1998) in an STS study of the vortex cores in under- and overdoped $Bi_{2+x}Sr_{2-x}CaCu_2O_{8+\delta}$. Experiments of a different nature performed on $YBa_2Cu_3O_{7-\delta}$ (Karrai *et al.*, 1992) and $Nd_{1.85}Ce_{0.15}CuO_{4-\delta}$ (Jiang *et al.*, 1995) indicate that a few bound quasiparticle states may exist in the vortex cores of these materials.

It is still a matter of debate whether bound states exist in the vortex cores of a pure $d_{x^2-y^2}$-wave or high-temperature superconductor. Himeda *et al.* (1997) investigated the microscopic structure of a vortex core within the framework of the two-dimensional t-J model developed by Zhang and Rice (1988) for CuO_2 layered systems. For a wide range of hole dopings the order parameter has $d_{x^2-y^2}$-wave symmetry, and the local density of states at the core shows a single peak at zero bias. The latter finding is in agreement with the earlier lattice model calculation by Wang and MacDonald (1995) using the Bogoliubov–de Gennes formalism, which showed that the quasiparticle energy levels for a $d_{x^2-y^2}$-wave vortex form a continuum with a single peak in the local density of states at zero bias. On the other hand, Himeda *et al.* found that in the low-doping region an s-wave component is induced in the vicinity of the core, which blocks the propagation of quasiparticles along the nodal directions of the $d_{x^2-y^2}$-wave component. This results in a localization of quasiparticles near the core, splitting the zero-energy peak in two—as observed in the STS study of $YBa_2Cu_3O_{7-\delta}$. The model was later extended to include longer-range hopping terms, resulting in a slight enhancement of the peak splitting (Ogata *et al.*, 1998).

Franz and Tešanović (1998) attempted to explain the possible existence of bound states in the high-temperature superconductors in terms of a mixed $d_{x^2-y^2}+id_{xy}$ pairing state. For this symmetry there is a finite energy gap everywhere at the Fermi surface that permits localization of quasiparticles in the vortex core. Although the local density of states calculated for these bound quasiparticles was shown to resemble the vortex core spectrum observed in the STS experiment on $YBa_2Cu_3O_{7-\delta}$, the size of the d_{xy} component required to explain the STS experiment is inconsistent with other experiments that should be sensitive to a large imaginary component.

Yasui and Kita (1999) have put forth an alternative explanation for the double-peak structure observed in the STS experiment. They suggest that at high fields, where the intervortex spacing is reduced, there is an increased probability of low-energy quasiparticle hopping between $d_{x^2-y^2}$-wave vortex cores, which produces the double peak in the tunneling conductance. At low magnetic fields, the two peaks merge together to form the single broad peak at zero bias calculated earlier by others for a pure $d_{x^2-y^2}$-wave vortex (Wang and MacDonald, 1995; Himeda *et al.*, 1997; Franz and Tešanović, 1998). However, the double-peak structure calculated by Yasui and Kita occurs at fields above $0.3\,H_{c2}$, which is approximately five times larger than the magnetic field at which Maggio-Aprile *et al.* (1995) performed their measurements on $YBa_2Cu_3O_{7-\delta}$. We note that a detailed STS study of the field dependence of the differential tunneling conductance at the vortex core has not yet been done.

Given the anomalous normal-state properties of the high-temperature cuprate superconductors, it is reasonable to expect that the nature of the vortex cores in these materials is unconventional. One such novel prediction from $SO(5)$ theory is for the existence of an antiferromagnetic vortex core in underdoped compounds (Arovas *et al.*, 1997; Zhang, 1997). It was suggested that the μSR technique should be sensitive to such magnetic ordering in the vortex cores—either by observing steps in the high-field tail of the μSR line shape, or by observing muon spin relaxation in a longitudinal-field μSR experiment due to fluctuations of the antiferromagnetic moments. However, a μSR study of single-crystal underdoped $YBa_2Cu_3O_{6.57}$ (Sonier *et al.*, 1998) using both transverse and longitudinal fields, failed to provide any clear evidence for the existence of antiferromagnetic cores.

As mentioned earlier, the measurements on $Bi_{2+x}Sr_{2-x}CaCu_2O_{8+\delta}$ by Renner *et al.* (1998) showed no signature of bound quasiparticle states in the the low-temperature STS spectrum inside the vortex core, unlike similar measurments on $YBa_2Cu_3O_{7-\delta}$. More striking was the observation that the gaplike structure found in

the core strongly resembled the normal-state pseudogap measured above T_c in zero field. How to interpret the STS measurements on $YBa_2Cu_3O_{7-\delta}$ is still an open question. Since a pseudogap forms in the normal state of $YBa_2Cu_3O_{7-\delta}$ with the removal of oxygen, an STS study of the vortex cores in underdoped samples would be of great interest.

D. Pinning and thermal fluctuations

Only under ideal conditions will the vortices arrange themselves in a perfect periodic array that is static in time. In general, there will be some degree of disorder in the vortex lattice due to pinning. Furthermore, like to atoms in a crystal, the vortices are subject to thermal fluctuations and zero-point motion. In layered superconductors the vortices become highly two dimensional. Together, these phenomena can produce exotic vortex phases that can be investigated with the μSR technique.

1. Vortex pinning

When the magnetic field applied to a type-II superconductor exceeds H_{c1}, the total free energy of the system is lowered by allowing partial flux penetration in the form of vortices. Since the core of a vortex is essentially normal, there is a cost in energy equivalent to the condensation energy per unit length $(H_c^2/8\pi)\pi\xi^2$ for each vortex formed. This energy gain is more than compensated for by the decrease in magnetic energy per unit length $(H_c^2/8\pi)\pi\lambda^2$ due to the region around the vortex with nonzero magnetic field. However, the cost in energy due to the formation of the vortex core is lowered if the vortex overlaps with a defect where the superconducting order parameter is already suppressed. In this way spatial inhomogeneities in the superconducting order parameter arising from impurities, structural defects, chemical vacancies, grain boundaries, twin boundaries, etc., exert an attractive force on the vortex. The effective range r_p of the pinning force must be of the order of ξ to adequately pin a vortex, since this is the smallest length scale resolvable by the vortex core (Blatter, Feigl'man, *et al.*, 1994).

In magnetic fields where the repulsive interaction between vortex lines becomes significant, the pinning of vortices to fixed positions in the superconductor can deform the vortex lattice from its ideal configuration. Such deformations increase the elastic energy of the vortex lattice (Brandt, 1977a, 1977b, 1977c, 1977d; Brandt and Essmann, 1987). According to the collective-pinning theory of Larkin and Ovchinnikov (1979), the equilibrium configuration is achieved by minimizing the sum of the vortex line energy and the elastic energy of the vortex lattice. At low magnetic fields, the interaction energy between vortex lines is weak, so that random pinning centers will cause only a small increase in the elastic energy of the vortex lattice. This means that random pinning of the vortex lines will be most prominent at low fields. At high magnetic fields, weak pinning centers cannot compete with the increased strength of the vortex-vortex interactions. In this case, only strong pinning sites will hold individual vortex lines in place.

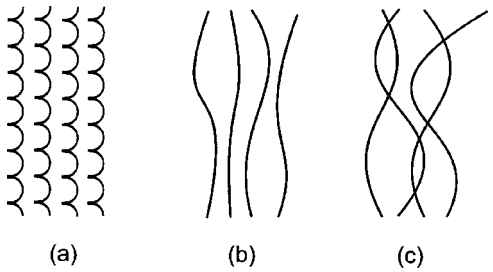

FIG. 11. Vortex lines: (a) twisted; (b) distorted; (c) entangled.

In the high-temperature cuprate superconductors, vortex lines are particularly susceptible to pinning because of the short coherence lengths and the weak coupling between the CuO_2 planes, which gives way to highly flexible vortices (Blatter, Feigel'man, *et al.*, 1994). Due to this flexibility, the vortices can become twisted, distorted, or entangled (Sudbø and Brandt, 1991a, 1991b) (see Fig. 11). According to Brandt (1991), randomly positioned stiff vortex lines will always broaden the μSR line shape, whereas the pinning of segments of highly flexible vortex lines will sharpen the measured magnetic-field distribution.

In the high-temperature cuprate superconductors, oxygen vacancies (Daeumling, Seuntjens, and Larbalestier, 1990) and twin boundaries (Kwok *et al.*, 1990) are the major sources of vortex pinning. The oxygen vacancies are weak, random pointlike pinning centers. As discussed in Sec. III.C.5, twin-boundary pinning can alter the orientation of the vortex lattice with respect to the underlying crystal lattice. If the spacing of twins is not commensurate with the equilibrium vortex lattice, the latter will become distorted near the twin boundaries or possibly throughout the sample, depending on the strength of the vortex-vortex interactions. If the vortex lines are rigid, pinning by rough surfaces can dominate the vortex lattice configuration in the bulk of thin films or powdered samples.

The strength of vortex pinning can be studied by determiming the sensitivity of the μSR line shape to small changes in magnetic field (Sonier *et al.*, 1994). Figure 12(a) shows the FFT of the muon spin precession signal in a *detwinned* crystal of $YBa_2Cu_3O_{6.95}$ after cooling to $T=5$ K in a magnetic field of $\mu_0 H=1.50$ T. When the field is decreased by 0.02 T, the residual background signal shifts down to the new applied field $\mu_0 H=1.48$ T [see Fig. 12(b)]. On the other hand, the signal originating from the sample does not shift in response to the small change in H. This indicates that the vortex lattice is firmly pinned by defects other than twin planes. The absence of any detectable background peak in the unshifted signal implies that there are no nonsuperconducting inclusions in the sample.

2. Thermal depinning and vortex lattice melting

At low temperatures, vortices are essentially frozen into a configuration. As the temperature is increased,

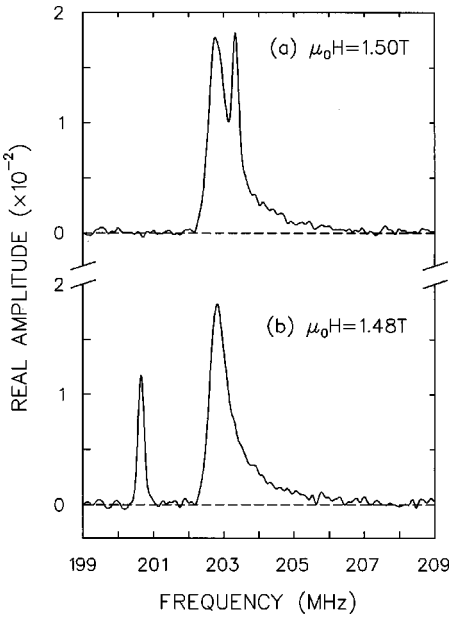

FIG. 12. Fourier transform of the muon spin precession signal in detwinned $YBa_2Cu_3O_{6.95}$: (a) after field cooling to $T=5$ K in a magnetic field $\mu_0 H=1.50$ T; (b) after field was lowered by 0.02 T with the sample temperature kept at $T=5$ K.

thermal fluctuation of the vortex positions becomes important. Thermal fluctutations in the high-temperature cuprate superconductors are considerably stronger than in conventional superconductors, due in part to smaller values of ξ, higher values of T_c, which allow for high thermal energies to be reached in the superconducting state, and the layered nature of these compounds.

Strong thermal fluctuations smooth out the effective pinning potential experienced by the vortex core, thus greatly reducing the pinning strength (Feigel'man and Vinokur, 1990). The depinning of vortices results in the so-called "irreversibility line" in the H-T phase diagram, such that above $H_{\rm irr}(T)$ the magnetic response of the sample becomes reversible. This also coincides with the region in which vortices are free to move in response to the Lorentz force created by a very small applied current. A consequence of the reversible region is that it removes the sharp resistive transition associated with the upper critical-field line $H_{c2}(T)$. In the high-temperature superconductors, $H_{\rm irr}(T)<H_{c2}(T)$, although the precise location of the irreversibility line is expected to depend on the nature and degree of pinning in the sample. By contrast, $H_{\rm irr}(T)\approx H_{c2}(T)$ in conventional superconductors.

The shape of the FFT of $YBa_2Cu_3O_{6.95}$ in Fig. 12(b) changes with increasing temperature due to the increase in the values of λ_{ab} and ξ_{ab}. However, the sample signal remains unshifted (see Fig. 13), which indicates that the vortices are still strongly pinned. Eventually, the temperature is large enough that thermal fluctutations depin some of the vortex lines. Raising the temperature further results in thermal depinning of the remaining vortices. By contrast, a μSR study of $NbSe_2$ showed that the pinning of vortices is weak in this material (Sonier *et al.*, 1997b). Even at low temperatures, a small shift in the applied field always resulted in a simultaneous frequency shift of the sample and background signals.

If the vortex fluctuations are sufficiently large, the vortex lattice may undergo a transition into a liquid phase above a characteristic phase line $H_m(T)$ (Brezin, Neslon, and Thiaville, 1985; Nelson, 1988; Houghton, Pelcovits, and Sudbø, 1989; Nelson and Seung, 1989). In the liquid phase, the vortices are not pinned and the interaction force between vortices is weak. As a result there is a loss of long-range spatial order. Experiments have now established that the transition from a liquid to

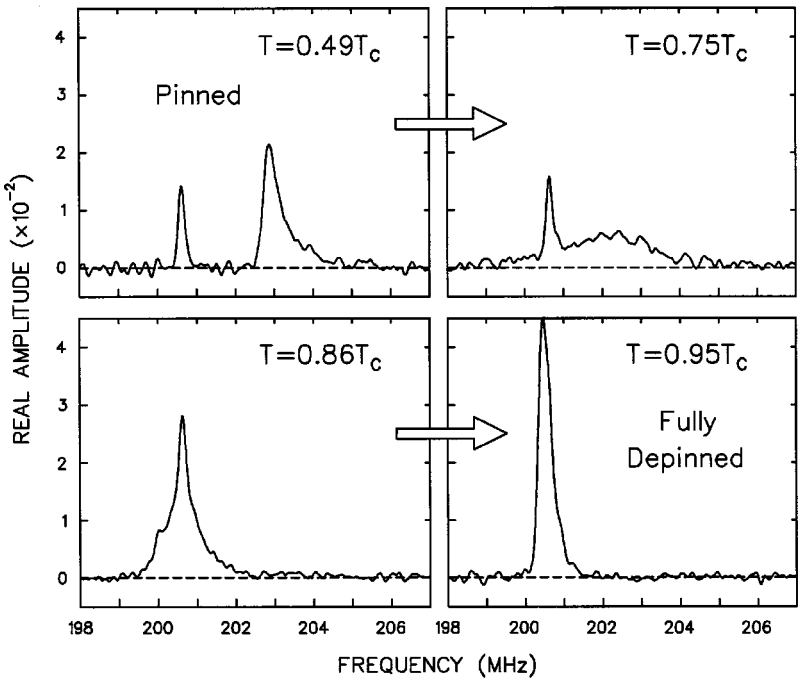

FIG. 13. The "field-shifted" μSR frequency spectrum from Fig. 12 after warming the sample to $T=0.49$, 0.75, 0.86, and $0.95T_c$.

solid vortex phase is first order in clean high-temperature cuprate superconductors (see, for example, Safar *et al.*, 1992; Kwok *et al.*, 1994; Fendrich *et al.*, 1996; Schilling *et al.*, 1996; Welp *et al.*, 1996). However, in the presence of *pinning-induced disorder*, the first-order transition from the liquid phase is modified—possibly to a "vortex-glass" phase (Feigel'man *et al.*, 1989; Fisher, 1989; Fisher, Fisher, and Huse, 1991) for weak, randomly distributed point defects, or to a "Bose glass" phase (Nelson and Vinokur, 1992) for correlated defects. The precise origin of vortex lattice melting is still open to question. The entanglement of vortex lines (see, for example, Nonomura, Xu, and Tachiki, 1999) and the proliferation of large vortex loops (Nguyen, Sudbø, and Hetzel, 1996) have been offered as possible mechanisms.

There are numerous theoretical predictions for the temperature dependence of H_m (see, for example, Brandt, 1989; Houghton, Pelcovits, and Sudbø, 1989; Nelson and Seung, 1989; Feigel'man and Vinokur, 1990; Vinokur *et al.*, 1990) which are based on the Lindemann criterion (Lindemann, 1910). In this picture the vortex lattice is expected to melt when the root-mean-square (RMS) thermal average of the vortex displacements from their equilibrium position $\langle u^2\rangle^{1/2}$ exceeds some small fraction c_L of the intervortex spacing L. Typically the Lindemann number c_L is of the order 0.1, although experimentally some variation in this number is expected, since the Lindemann criterion does not take into account the effects of vortex pinning in real superconductors.

In moderate magnetic fields, $H_{c1} \ll H \ll H_{c2}$, the melting transition in the H-T phase diagram is reasonably described by the power-law relation $H_m(T) \sim (T_c - T_m)^n$. Brandt (1989) and at the same time Houghton, Pelcovits, and Sudbø (1989), considered a nonlocal elastic theory for the vortex lattice and arrived at a power-law exponent $n=2$. Blatter and Ivlev (1993, 1994) later argued that this result is really only valid close to T_c. They performed a more rigorous calculation that took into account the suppression of the order parameter near $H_{c2}(T)$, as well as quantum fluctuations, to yield a melting line better described with a smaller value of n. This prediction is supported by several experiments on $YBa_2Cu_3O_{7-\delta}$, which report exponents with $n<1.45$ (Krusin-Elbaum *et al.*, 1991; Safar *et al.*, 1992; Schilling, Ott and Wolf, 1992; Safar *et al.*, 1993; Kwok *et al.*, 1994; Liang, Bonn, and Hardy, 1996; Welp *et al.*, 1996; Billon *et al.*, 1997). Some experiments have reported values of $n \approx 4/3$, the critical exponent expected within the 3D XY critical regime (Fisher, Fisher, and Huse, 1991).

3. Pancake vortices

Although $YBa_2Cu_3O_{7-\delta}$ is a layered material, near optimal doping the vortex lattice behaves essentially in a three-dimensional (3D) manner over a significant fraction of the H-T phase diagram. This is not the case for $Bi_{2+x}Sr_{2-x}CaCu_2O_{8+\delta}$ or underdoped $YBa_2Cu_3O_{7-\delta}$, where the coupling between planes is very weak even well below T_c. For these materials it is useful to think of a vortex line as being composed of a stack of aligned two-dimensional (2D) "pancake" vortices, where the pancakes are located within the CuO_2 superconducting layers (Clem, 1991) [see Fig. 14(a)]. The Lawrence-Doniach model (Lawrence and Doniach, 1971) provides a reasonable theoretical description of the situation. In this model, adjacent superconducting layers are separated by an insulating layer of thickness s. The vortex pancakes in adjacent layers are coupled by Josephson tunneling currents and electromagnetic interactions. The relevant parameter in the Lawrence-Doniach model is the ratio between the $\hat{c}$-axis coherence length ξ_c and s. When $\xi_c/s > \sqrt{2}$ there is no phase difference in the order parameter between adjacent superconducting layers, so that in the absence of pinning, the vortex lattice exhibits 3D behavior—equivalent to the anisotropic London and Ginzburg-Landau models. On the other hand, when $\xi_c/s < \sqrt{2}$ there is a phase difference and the Lawrence-Doniach theory describes a quasi-2D vortex structure. The Lawrence-Doniach model will not be an adequate description of a superconductor in which the material between the superconducting layers is metallic instead of insulating, since then the "proximity effect" will become important.

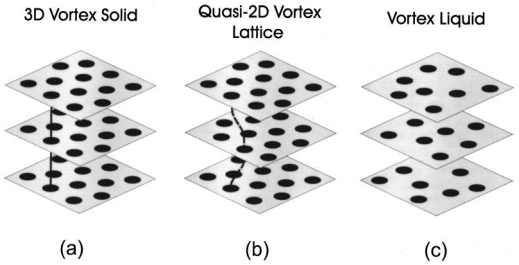

FIG. 14. Vortex lattice phases in layered superconductors: (a) vortex lattice composed of perfectly aligned pancake vortices; (b) pancake vortices ordered within the layers, but misaligned between layers; (c) melted vortex lattice where the pancake vortices are also decoupled between layers.

A μSR experiment performed by Kossler *et al.* (1998) has provided strong evidence for pancake vortices in $Bi_2Sr_2CaCu_2O_{8+\delta}$ single crystals. A magnetic field was applied at an angle of 45° to the $\hat{c}$ axis of the crystals while cooling to $T=2$ K, after which the field was turned off. Figure 15 shows FFT's of the muon spin precession signals recorded before and after turning off a field of $\mu_0 H = 0.01$ T. The positron detectors U-D measured the field component along the $\hat{c}$-axis direction, whereas the F-B detectors measured the field component in the $\hat{a}$-$\hat{b}$ plane. The loss of signal in the F-B detectors and the asymmetric line shape observed in the U-D detectors after turning off the field indicate that the muons are precessing around an internal magnetic field associated with pinned pancake vortices whose screening currents flow in the $\hat{a}$-$\hat{b}$ plane. When the same experiment was performed on a large single crystal of $YBa_2Cu_3O_{7-\delta}$, signals were observed in both pairs of detectors with the field turned off. This is exactly what one expects for 3D vortices pinned along the direction of the applied field.

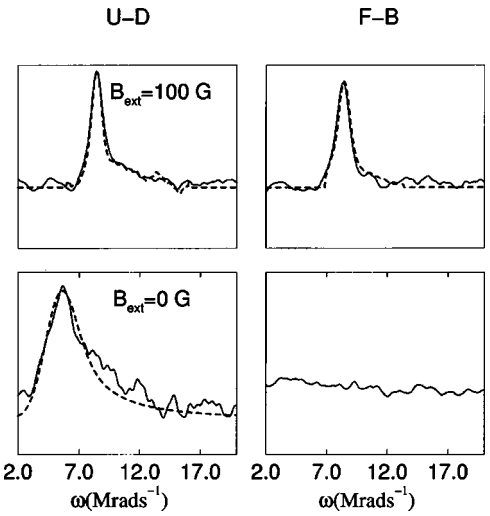

FIG. 15. Fourier transform of the muon spin precession signals recorded in the *U-D* and *F-B* positron detectors for $Bi_2Sr_2CaCu_2O_{8+\delta}$ single crystals: upper panels, cooled to $T=2$ K in a magnetic field $\mu_0 H=0.01$ T applied 45° to the crystallographic $\hat{c}$-axis direction; lower panels, with the field subsequently turned off. From Kossler *et al.*, 1998.

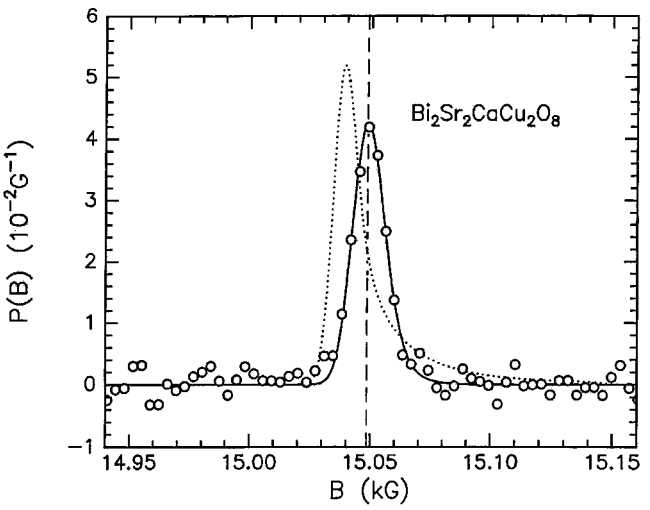

FIG. 16. Fourier transform of the muon spin precession signal in $Bi_2Sr_2CaCu_2O_{8+\delta}$ crystals after cooling in a field $\mu_0 H=1.5049$ T to $T=6$ K (open circles): dotted curve, the Fourier transform expected for a hexagonal arrangement of vortex lines; solid curve, a fit assuming random disorder of pancake vortices along the $\hat{c}$-axis direction. From Harshman *et al.*, 1993.

In a clean superconductor at low temperatures, pancake vortices in adjacent layers are aligned. However, in the presence of random inhomogeneities, pinning will displace some of the pancakes and cause a suppression of the phase coherence between layers (Koshelev, Glazman, and Larkin, 1996). The effects of random pinning-induced misalignment of pancake vortices on the measured μSR line shape have been the focus of several studies (Brandt, 1991; Harshman *et al.*, 1991, 1993; Lee *et al.*, 1993; Bernhard *et al.*, 1995; Koshelev, Glazman, and Larkin, 1996; Kossler *et al.*, 1997). These effects include truncation of the high-field tail and a reduction in both the linewidth and the line shape asymmetry. When the magnetic field is increased, the interaction between pancake vortices within a layer will eventually exceed the interlayer coupling strength of the pancake vortices. In this case, random pinning in the layers will lead to a misalignment of the pancake vortices between layers [see Fig. 14(b)]. Thus a dimensional crossover from a 3D to a 2D vortex structure at a field $H_{cr}(T)$ can be induced by random vortex pinning.

Below the melting transition, Harshman *et al.* (1993) observed a narrowing and a loss of asymmetry in the μSR line shape for $Bi_{2+x}Sr_{2-x}CaCu_2O_{8+\delta}$ after cooling the sample in a high magnetic field applied parallel to the $\hat{c}$ axis (see Fig. 16). Furthermore, the observed symmetric line shape was centered about the average internal field, which is inconsistent with a moderately disordered Abrikosov lattice. The μSR line shape could be fit to a model assuming pancake vortices disordered along the $\hat{c}$ axis by random pinning.

To quantify the observed changes in the shape of the measured field distribution, Lee *et al.* (1993) introduced the so-called *skewness parameter*,

$$\alpha=\langle(\Delta B)^3\rangle^{1/3}/\langle(\Delta B)^2\rangle^{1/2}, \tag{43}$$

where $\langle(\Delta B)^n\rangle=\langle(B-\langle B\rangle)^n\rangle$ are the nth moments of the μSR line shape. For a well-ordered vortex lattice, the value of α is typically close to unity. At low temperatures and high magnetic fields, a crossover from 3D to 2D was identified in $Bi_{2.15}Sr_{1.85}CaCu_2O_{8+\delta}$ by Lee *et al.* from a sharp drop in α (see Fig. 17) and a simultaneous reduction of the μSR linewidth. Transverse-field μSR and torque magnetometry measurements show that the crossover field depends upon the projection of the applied field along the $\hat{c}$-axis direction (Aegerter, Hofer, *et al.*, 1998),

$$H_{cr}(\theta)=H_{cr}(0)/\cos(\theta), \tag{44}$$

where θ is the angle between the applied field and the $\hat{c}$ axis. Transverse-field μSR measurements have also

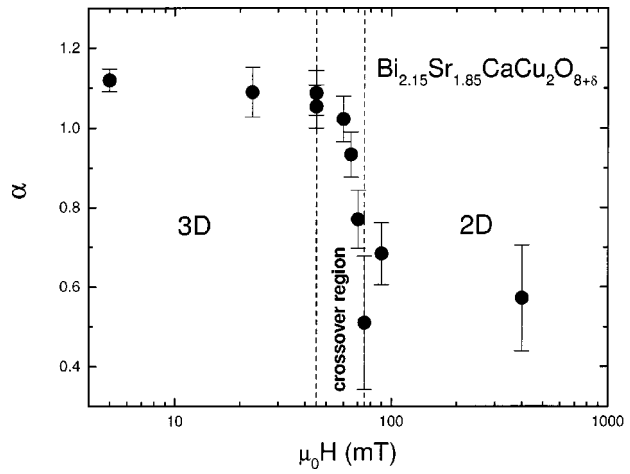

FIG. 17. Magnetic-field dependence of the skewness parameter α [defined in Eq. (43)] in single-crystal $Bi_{2.15}Sr_{1.85}CaCu_2O_{8+\delta}$ after field cooling to $T=5$ K. The sharp drop in α at $\mu_0 H\sim 50$ mT is attributed to a 3D to 2D crossover in the vortex lattice. From Lee *et al.*, 1993.

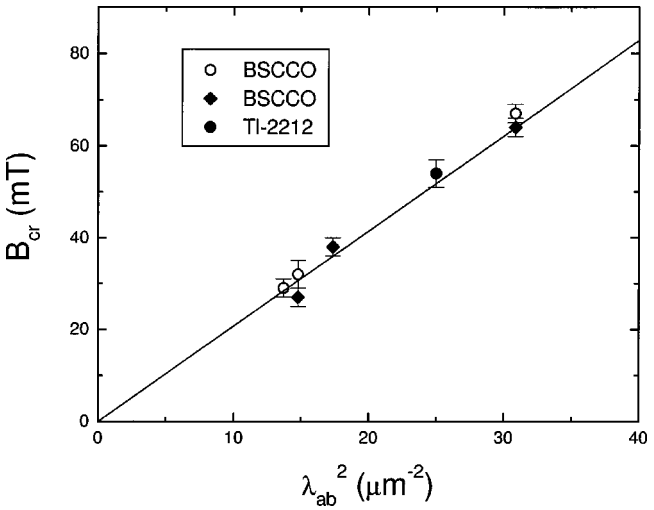

FIG. 18. The crossover field $B_{\rm cr}$ as a function of λ_{ab}^{-2}: ○, from μSR measurements in $Bi_{2.15}Sr_{1.85}CaCu_2O_{8+\delta}$ (BSCCO); ◆, from magnetization measurements in BSCCO; ●, from magnetization measurements in $Tl_2Sr_2CaCu_2O_{8+\delta}$ (Tl-2212). The solid line represents the relation $B_{\rm cr}=\Phi_0/\lambda_{ab}^2$. From Aegerter *et al.*, 1996.

shown that the crossover field $H_{\rm cr}$ shifts to higher fields in the presence of columnar defects formed by irradition with fast heavy ions (Lee *et al.*, 1998). The pinning introduced along the length of the columnar defects provides an additional mechanism to couple the pancake vortices from adjacent layers.

Although a ''dimensional crossover'' is a reasonable interpretation, there are other possible explanations for the observed changes of the μSR line shape in $Bi_{2+x}Sr_{2-x}CaCu_2O_{8+\delta}$ as the applied field is increased across $H_{\rm cr}$. For example, it has been proposed that the Abrikosov lattice transforms to a phase of entangled vortices at high field (Marchetti and Nelson, 1990). A pinning-induced transition from a weakly disordered Bragg glass phase (Giamarchi and Le Doussal, 1995) to a strongly disordered vortex glass (or pinned liquid) phase (Fisher, Fisher, and Huse, 1991) is another possible explanation. Recently, Menon, Dasgupta, and Ramakrishnan (1999) showed that the small μSR linewidths observed in $Bi_{2+x}Sr_{2-x}CaCu_2O_{8+\delta}$ at low temperatures and high fields are consistent with a glassy phase in which the short-range positional correlations of the vortices resemble those just above the melting transition.

A μSR study of $Bi_{2.15}Sr_{1.85}CaCu_2O_{8+\delta}$ single crystals with different oxygen stoichiometries showed that the crossover field obeys the relation (see Fig. 18, Aegerter *et al.*, 1996)

$$B_{\rm cr}=\Phi_0/\lambda_{ab}^2, \tag{45}$$

where $B_{\rm cr}$ was determined from the drop in α and λ_{ab} was determined from the London expression

$$B_0-B_{\rm sad}=\frac{2}{3}\frac{\Phi_0}{4\pi\lambda_{ab}^2}\ln(2), \tag{46}$$

where $B_0-B_{\rm sad}$ is the difference between the average

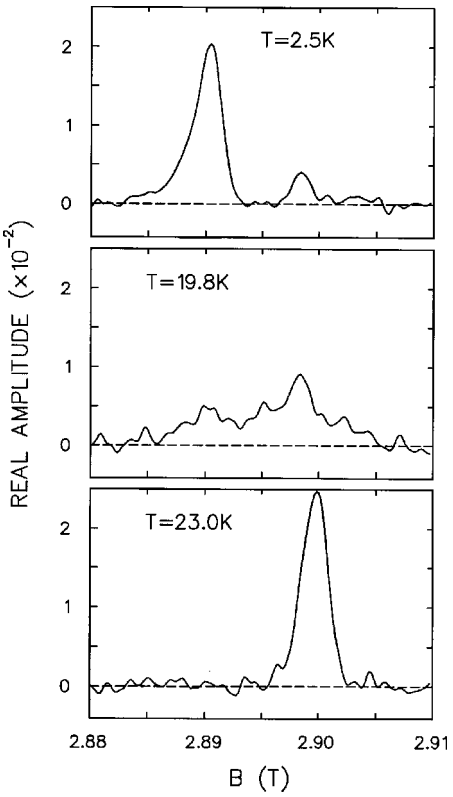

FIG. 19. Fourier transform of the muon precession signal in twinned $YBa_2Cu_3O_{6.60}$ after field cooling at $\mu_0H\approx 2.89$ T to $T=2.5$ K followed by an increase in the field to 2.90 T. The middle and bottom panels are the μSR line shapes upon warming the crystal to $T=19.8$ and 23.0 K, respectively (Sonier *et al.*, 2000).

internal field and the saddle-point field of an ideal vortex lattice. The results agree well with magnetization measurements, which are also shown in Fig. 18. Equation (45) is consistent with a vortex state in which the interlayer coupling of pancake vortices is dominated by electromagnetic interactions rather than Josephson coupling. Electromagnetic interactions are expected to dominate in highly anisotropic compounds in which $\gamma>\lambda_{ab}/s$, where s is the interlayer spacing and $\gamma=\lambda_c/\lambda_{ab}$. This is the case in the $Bi_{2+x}Sr_{2-x}CaCu_2O_{8+y}$ and $Tl_2Sr_2CaCu_2O_{8+\delta}$ systems, but not in the less anisotropic system $HgBa_2Ca_3Cu_4O_{10+\delta}$ (Aegerter *et al.*, 1996). In the latter compound the crossover field is better approximated by

$$B_{\rm cr}=\Phi_0/(\gamma s)^2, \tag{47}$$

as expected for a vortex system dominated by interlayer Josephson coupling.

A high-field crossover has also been observed in the μSR line shape of underdoped $YBa_2Cu_3O_{6.60}$ at low temperatures (Sonier *et al.*, 2000). Figure 19 shows the μSR line shape after cooling the sample in a field $\mu_0H\approx 2.89$ T to $T=2.5$ K, followed by an increase in the field $\mu_0\Delta H\approx 0.01$ T. The small background signal is positioned at the internal field $B=2.90$ T, whereas the signal originating from the sample looks as though the external field is still $\mu_0H=2.89$ T—indicating that the vortex lat-

tice is strongly pinned. However, the μSR line shape displays a *low-field tail* rather than the high-field tail associated with an ordered or moderately disordered 3D structure. Numerical calculations performed by Schneider, Schafroth, and Meier (1995), which account for the sample geometry (see Sec. II.B), show that such a line shape can originate from a system of 2D pancake vortices that are ordered within the CuO_2 layers, but disordered between adjacent layers. As in the case for $Bi_{2+x}Sr_{2-x}CaCu_2O_{8+\delta}$, there are several other disordered vortex lattice phases that may explain the observed changes of the μSR line shape in $YBa_2Cu_3O_{6.60}$ at low temperatures and high fields.

Misalignment of pancake vortices can also occur via thermal fluctuations [see Fig. 14(c)], which is opposed by Josephson and electromagnetic coupling between pancake vortices in adjacent superconducting layers. Because the strength of the intralayer vortex-vortex interactions increases with increasing magnetic field, the effect of thermal fluctuations on the vortex lattice in a highly anisotropic material is expected to be very different in the regions of weak and strong magnetic fields. The muon detects the field averaged over the fluctuations, since the typical time scale for thermal fluctuations of the vortices is $\sim 10^{-10}$ s (Song *et al.*, 1993), much shorter than the time range $2\pi/\gamma_\mu \delta B$, where γ_μ is the muon gyromagnetic ratio and δB is the range of the field fluctuation at the muon site. The rapid fluctutation of a vortex about its average position smears the magnetic field out over an effective radius $\langle u^2 \rangle^{1/2}$ (Brandt, 1991), thus increasing the size of the vortex cores measured with μSR. The smearing effect reduces the average value of the field in the vortex core, leading to a premature truncation of the high-field tail of the μSR line shape. A similar effect will result from the quantum-mechanical motion of vortices, which are expected to dominate fluctuations at extremely low temperatures.

Lee *et al.* (1993, 1995; Lee, Aegerter, *et al.*, 1997, 1998) have performed several μSR studies of thermal fluctuation effects on the vortex lattice in $Bi_{2+x}Sr_{2-x}CaCu_2O_{8+\delta}$. The melting transition was determined by observing simultaneous sharp reductions in α and the second moment $\langle \Delta B^2 \rangle^{1/2}$ of the field distribution as a function of temperature (see Fig. 20). The negative values of α above T_m result from the presence of a low-field tail in the μSR line shape associated with the sample geometry. Good agreement has been obtained between numerical calculations of the μSR line shape for a 2D vortex liquid in a platelike sample (Schneider, Schafroth, and Meier, 1995) and the line shapes measured by Lee *et al.* in the melted phase. The value of T_m is reduced with increasing applied magnetic field, because $\langle u^2 \rangle^{1/2}$ increases relative to the intervortex spacing. On the other hand, a μSR study by Lee, Aegerter, *et al.* (1998) showed that thermal fluctuations of the vortices are strongly suppressed by the addition of columnar defects, such that T_m is independent of the value of the applied field.

The phase line measured by Lee, Aegerter, *et al.* (1997) in $Bi_{2.15}Sr_{1.85}CaCu_2O_{8+\delta}$ is shown in Fig. 21. For

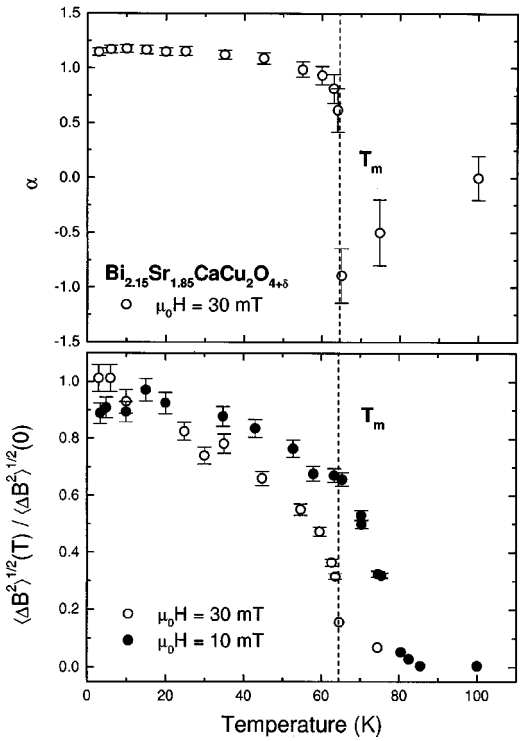

FIG. 20. Temperature dependence of the skewness parameter α (at $\mu_0 H = 30$ mT) and the line width $\langle (\Delta B)^2 \rangle$, at $\mu_0 H = 10$ and 30 mT, in $Bi_{2.15}Sr_{1.85}CaCu_2O_{8+\delta}$ crystals after field cooling. The simultaneous sharp drop in both parameters at T_m is evidence for a vortex lattice melting transition. From Lee, Aegerter, *et al.*, 1997.

$T < T^{em}$ the data suggest that electromagnetic coupling between the pancake vortices in adjacent superconducting layers controls the form of the melting line, as indicated by a fit to the theoretical prediction of Blatter

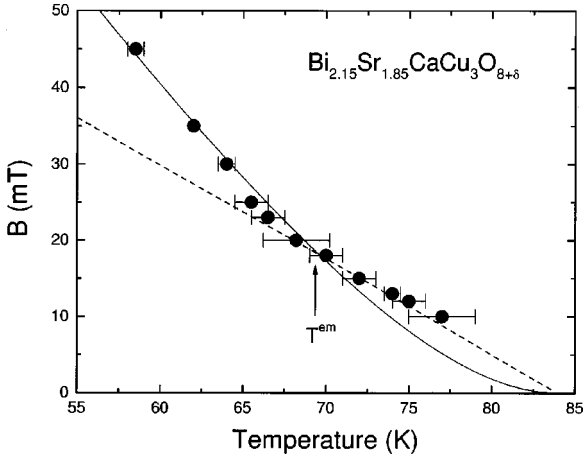

FIG. 21. Vortex B-T phase diagram for $Bi_{2.15}Sr_{1.85}CaCu_2O_{8+\delta}$ determined by Lee, Aegerter, *et al.* (1997): solid curve, a fit to the melting line predicted by Blatter *et al.* (1996) for the case in which the coupling between pancake vortices is predominantly electromagnetic; dashed curve, a fit to the predicted decoupling transition (Blatter *et al.*, 1996) in which the vortex lines break apart into 2D (pancake) vortices.

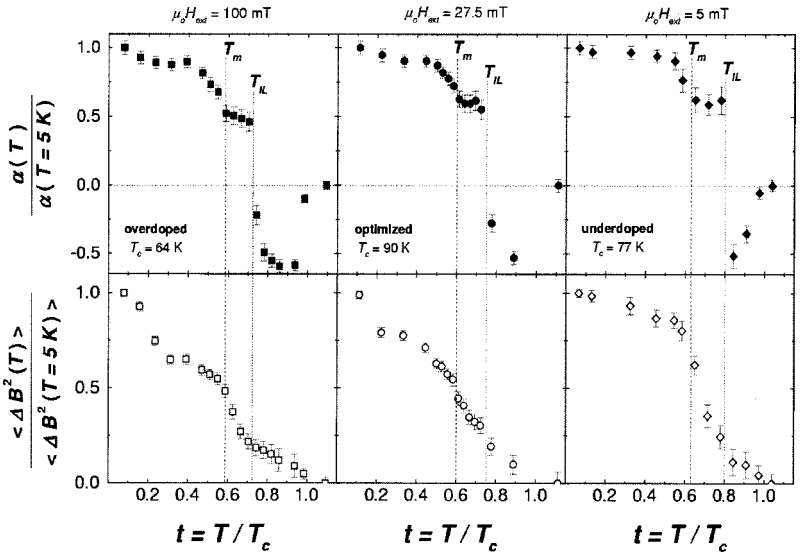

FIG. 22. Temperature dependence of the skewness parameter α and the second moment $\langle(\Delta B)^2\rangle$ in overdoped, optimally doped, and underdoped $Bi_2Sr_2CaCu_2O_{8+\delta}$ single crystals after cooling in fields of $\mu_0 H = 100$, 27.5, and 5 mT to $T = 5$ K. T_m and T_{IL} denote the temperatures of the intraplanar melting and the interplanar decoupling transitions, respectively. From Blasius *et al.*, 1999.

et al. (1996). On the other hand, for $T > T^{em}$ the data were better fit with the theoretical curve for decoupling of the pancake vortices in adjacent layers (Blatter *et al.*, 1996). Since the location of the phase line measured by μSR was close to where small-angle neutron-scattering experiments determined the loss of a vortex lattice to be, it was concluded that the intralayer melting and the interlayer decoupling transitions occurred either simultaneously or very close together. However, more recent μSR measurements by Blasius *et al.* (1999) on underdoped to overdoped $Bi_{2+x}Sr_{2-x}CaCu_2O_{8+\delta}$ have been interpreted as evidence for a two-stage melting transition in which the intralayer coupling is first overcome by thermal fluctuations, followed by interlayer decoupling (see Fig. 22). Furthermore, the intralayer melting transition is found to fall below the irreversibility line, whereas the interlayer decoupling of pancake vortices coincides with the irreversibility line.

The melted phase in underdoped $YBa_2Cu_3O_{6.60}$ has been observed with μSR in twinned and detwinned samples (Sonier *et al.*, 2000). Figure 23 shows the temperature dependence of α and λ_{ab}^{-2}. The latter was extracted assuming the field profile of Eq. (35) for an Abrikosov lattice. Below the melting temperature T_m, λ_{ab}^{-2} is roughly proportional to the μSR linewidth. However, above T_m the vortex lattice cannot be modeled with Eq. (35), as shown by the unphysical decrease in λ_{ab}^{-2} to zero. The failure of Eq. (35) to describe the measured field distribution above T_m and the sharp drop in the value of α provide strong evidence for a melting transition. Although there appears to be only a single transition signifying the onset of the melted phase, more data points in the vicinity of this transition are needed to confirm this. The results of this study are summarized in the phase diagram of Fig. 24. The low-field phase transition is best fit to a decoupling curve, as was the case for $Bi_{2+x}Sr_{2-x}CaCu_2O_{8+\delta}$ (Lee, Aegerter, *et al.*, 1997). Thus at low fields the melted phase of underdoped $YBa_2Cu_3O_{6.60}$ appears to consist of a liquid of 2D vortices, rather than a liquid of 3D vortex lines.

A μSR investigation of the organic superconductor κ-(BEDT-TTF)$_2$Cu(SCN)$_2$ was the first experiment to clearly identify the existence of an Abrikosov lattice in this material (Lee, Pratt, *et al.*, 1997). At low fields and temperatures the existence of this structure was evident from the μSR line shape, which showed the characteristic high-field tail. Upon increasing the field, a transition to a symmetric line shape was observed and identified as a dimensional crossover in the vortex structure at $\mu_0 H_{cr}(T) \approx 7$ mT. An additional crossover was observed

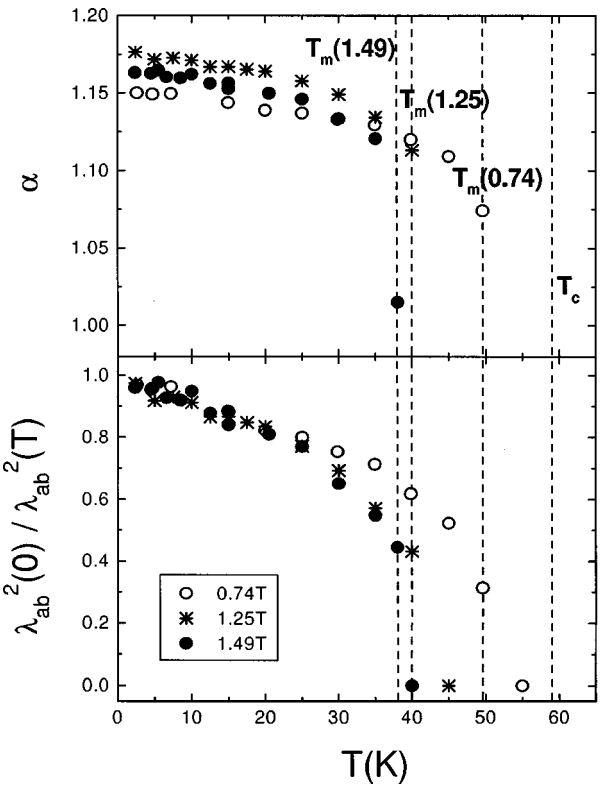

FIG. 23. Temperature dependence of α and λ_{ab}^{-2}: $*$, in detwinned $YBa_2Cu_3O_{6.60}$ single crystals after cooling in a field $\mu_0 H = 1.25$ T; ○, in twinned single crystals at $\mu_0 H = 0.74$ T; ●, twinned single crystals at $\mu_0 H = 1.49$ T. From Sonier, Brewer, *et al.*, 2000.

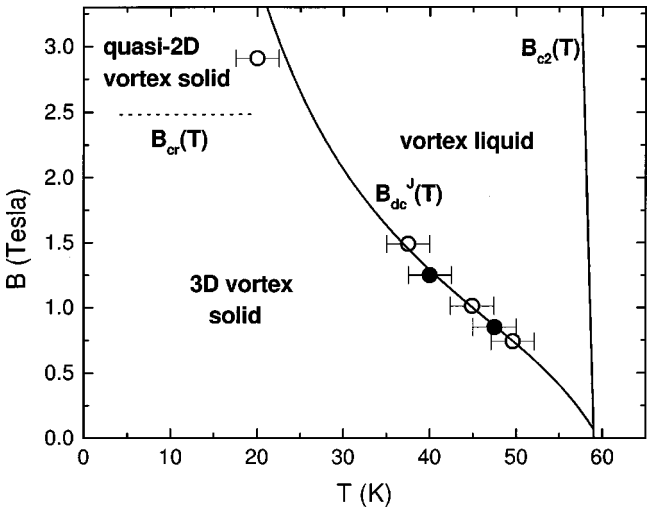

FIG. 24. The vortex B-T phase diagram for $YBa_2Cu_3O_{6.60}$: ●, detwinnned single crystals; ○, twinned single crystals; solid curve $B_{dc}^{J}(T)$, a fit to the theoretical decoupling transition predicted by Blatter *et al.* (1996) for $B<B_{cr}$. From Sonier, Brewer, *et al.*, 2000.

at low fields with increasing temperature. This transition was found to be consistent with Clem's (1991) prediction for the thermally induced breakup of vortex lines comprising weakly coupled pancake vortices.

4. The peak effect

In some low- and high-T_c superconductors, the magnetic-field dependence of the critical current density $J_c(H)$ approaches an anomalous maximum value at some intermediate field. The phenomenon known as the "peak effect" arises from an increase in pinning due to a decrease in the rigidity of the vortex lattice. In conventional low-T_c superconductors the peak effect is observed near the upper critical field H_{c2} and has been attributed to an elastic softening of the vortex lattice due to a reduction in the value of the order parameter as the normal state is approached (Crabtree and Nelson, 1997).

A μSR study of $NbSe_2$ (Rao *et al.*, 1998) showed that the peak effect in this material is accompanied by a sharp change in the internal magnetic-field distribution. In particular, a sudden drop of the skewness parameter α as a function of temperature was observed, indicating a sharp reduction in the spatial order of the vortex lattice. The temperature at which the transition occurred coincided with the onset of the peak-effect region observed in ac magnetic susceptibility measurements as a function of temperature. Similar findings were reported in a study of $CeRu_2$ (Yamashita *et al.*, 1997), in which the μSR line shape showed a sudden decrease in width at a field coinciding with the emergence of the peak effect.

IV. THE MAGNETIC PENETRATION DEPTH

A. Temperature dependence

1. Meissner state

The precise nature of the supercurrent response to an applied magnetic field depends on the relative sizes of the characteristic length scales λ and ξ and the angular dependence of the energy gap function $\Delta_{\hat{k}}$. As discussed in Sec. III.B.7, the supercurrent response is *local* when $\lambda>\xi$, in which case the supercurrent density J_s is essentially uniform on the scale of ξ. The supercurrent response is *linear* when J_s scales exactly with the superfluid velocity v_s, such that $J_s=-en_sv_s$.

In the conventional London model (London and London, 1935) the supercurrent response is both local and linear. For a static magnetic field $B(0)$ applied parallel to a planar vacuum-superconductor interface, the magnetic penetration depth may be defined as (Tinkham, 1996)

$$\lambda=\frac{1}{B(0)}\int_0^\infty B(r)dr, \tag{48}$$

where r is the distance into the superconductor measured from the surface, and $B(r)$ is a function describing the decay of the magnetic field into the superconducting region. In the London model $B(r)$ and $J_s(r)$ decay exponentially with distance inside the superconductor, such that at $T=0$ K

$$\frac{1}{\lambda_L^2}=\frac{4\pi n_s e^2}{m^*c^2}, \tag{49}$$

where λ_L is the London penetration depth, and n_s and m^* are the local density and effective mass of the superconducting carriers, respectively. Within this simple picture, λ_L is independent of magnetic field. As the temperature T is increased, quasiparticle excitations reduce n_s, so that the magnetic penetration depth increases with T such that $\lambda_L\to\infty$ as $T\to T_c$. In a pure s-wave superconductor in which there is an isotropic energy gap $\Delta(T)$ at the Fermi surface, the precise form of the temperature dependence at low T was predicted from BCS theory. In particular, for a clean superconductor in which $T\ll T_c$, the number of quasiparticles excited to energy states above the gap is exponentially activated, such that (Muhlschlegel, 1959)

$$\lambda(T)-\lambda(0)\simeq\sqrt{\pi\Delta(0)/2k_BT}\exp[-\Delta(0)/k_BT]. \tag{50}$$

On the other hand, if there are line or point nodes in the energy gap function $\Delta_{\hat{k}}$, a power-law dependence is expected, where $\lambda(T)-\lambda(0)\propto T^n$, $n=1$, 2, 3, or 4 (Gross *et al.*, 1964; Annett, Goldenfeld, and Renn, 1991). The nodes provide a conduit for extremely-low-energy quasiparticle excitations, so that significant pair breaking may occur at very low T.

Hirschfeld and Goldenfeld (1993) derived an approximate analytical expression for the magnetic penetration depth at low temperatures in a $d_{x^2-y^2}$-wave superconductor, namely,

$$\lambda(T)-\lambda(0)\simeq\lambda(0)C\frac{T}{\Delta(0)}, \tag{51}$$

where $C=\ln(2)$ for a circular Fermi surface. There is now considerable evidence for limiting T behavior for $\Delta\lambda(T)$ in hole-doped high-temperature superconduct-

ors. Following the first such finding by Hardy *et al.* (1993) from microwave measurements performed in the Meissner state of high-quality crystals of $YBa_2Cu_3O_{6.95}$, there have been reports of a strong linear-T term in clean single crystals of $YBa_2Cu_3O_{7-\delta}$ (Mao *et al.*, 1995; Srikanth *et al.*, 1997), $Bi_{2+x}Sr_{2-x}CaCu_2O_{8+\delta}$ (Jacobs *et al.*, 1995;Lee *et al.*, 1996; Shibauchi *et al.*, 1996; Waldmann *et al.*, 1996), $Tl_2Ba_2CuO_{6+\delta}$ (Broun *et al.*, 1997), and magnetically aligned powders of crystalline $HgBa_2Ca_2Cu_3O_{8+\delta}$ (Panagopoulos *et al.*, 1996). A linear variation of λ with temperature has also been reported in detwinned single crystals (Zhang *et al.*, 1994) and thin films (de Vaulchier *et al.*, 1996) of $YBa_2Cu_3O_{7-\delta}$.

Experiments on high-temperature cuprate superconductors that show T dependences other than linear are often explained in terms of extrinsic effects. A consequence of the nodes in the superconducting energy gap is that the physical properties of these materials are extremely sensitive to impurities and crystalline defects (Annett, Goldenfeld, and Leggett, 1996). A model of impurity scattering in a $d_{x^2-y^2}$-wave superconductor predicts a disorder-induced crossover of the low-temperature behavior of $\lambda(T)$ from T to T^2 dependence, due to the finite density of states at the Fermi level induced by the impurities (Annett, Goldenfeld, and Renn, 1991; Prohammer and Carbotte, 1991; Hirschfeld and Goldenfeld, 1993; Hirschfeld, 1995; Sun and Maki, 1995). The residual density of states accounts for the low-temperature penetration depth of experiments involving substitution of copper in the CuO_2 planes of $YBa_2Cu_3O_{6.95}$ with small quantities of the nonmagnetic impurity Zn and the magnetic impurity Ni (Bonn *et al.*, 1994)—assuming Ni is a much weaker scatterer than Zn (i.e., the Zn scattering is in the unitary limit, whereas the Ni scattering is in the Born limit). However, the model fails to describe the temperature dependence of microwave conductivity at low temperatures. Franz, Kallin *et al.* (1997) have pointed out that the suppression of the order parameter in the vicinity of the impurity sites must be taken into account in any theory. Recently, Hettler and Hirschfeld (1999) have developed a theory that includes the strong suppression of the order parameter around nonmagnetic impurity sites. The new model gives the correct low-temperature behavior of the microwave conductivity and predicts a larger enhancement of the low-temperature penetration depth. On the other hand, there is little change in the temperature dependence of the penetration depth compared to the dirty $d_{x^2-y^2}$-wave model, which neglects the suppression of the order parameter.

The penetration depth and T_c in the high-temperature superconductors are very sensitive to irradiation-induced point defects. In particular, defects introduced by the displacement of Cu or O atoms in the CuO_2 layers strongly suppress superconductivity (see, for example, Legris *et al.*, 1993). In general, samples with a high degree of chemical purity and homogeneity are needed to observe the intrinsic behavior of λ. The quality of the sample surface is also important for Meissner-state measurements, since the supercurrents flow within $\sim 10^3$ Å from the surface.

An exception in the high-temperature superconductor family appears to be the electron-doped compounds. For instance, measurements of $\lambda_{ab}(T)$ in $Nd_{1.85}Ce_{0.15}CuO_4$ single crystals are consistent with s-wave BCS theory and show no evidence of a linear-T term (Wu *et al.*, 1993; Anlage *et al.*, 1994). Furthermore, in contrast to the hole-doped systems, Zn substitution of Cu has little effect, whereas Ni substitution drastically suppresses superconductivity (see, for example, Felner *et al.*, 1990). Recently, Maki and Puchkaryov (1998) have proposed that the strong effect of Ni substitution can be described by the Abrikosov-Gor'kov theory of magnetic impurities in an s-wave superconductor (Abrikosov and Gor'kov, 1961).

Nevertheless, Cooper (1996) has shown that the measured low-T penetration depth can be greatly affected by the strong Nd moments in $Nd_{1.85}Ce_{0.15}CuO_4$. Furthermore, impurities and chemical inhomogeneity may play a significant role in many of the experiments performed on electron-doped superconductors. It is known that a small amount of excess oxygen is detrimental for superconductivity in these systems (Fortune *et al.*, 1991; Zhu and Manthiram, 1994) and removal of oxygen via a high-temperature reduction process usually results in evaporation of Cu from the surface (Brinkmann *et al.*, 1996). To properly address whether or not the electron-doped compounds are $d_{x^2-y^2}$-wave superconductors will require samples with a high degree of oxygen homogeneity and an experimental technique that probes the bulk, such as μSR.

2. Vortex state

Measurements of the temperature dependence of λ with μSR are unique in that the magnetic penetration depth is determined in the vortex state. This is in contrast to excluded-volume techniques such as microwave cavity perturbation, inductive methods, and far-infrared reflectivity, which measure $\lambda(T)$ [or $\Delta\lambda(T)$] in the Meissner state. With μSR one measures the length scale λ associated with decay of the field from the normal vortex core into the surrounding superconducting medium—rather than decay of the field from vacuum into the surface of the superconductor. A natural consequence is that λ measured by μSR is a length scale characteristic of the bulk material. We note that μSR cannot directly measure λ along a single crystallographic direction. Thus measurements are limited to mixed quantities, such as $\lambda_{ab}=(\lambda_a\lambda_b)^{1/2}$. However, a simple scaling argument can be used to show that the μSR line shape is unaffected by anisotropy unless defect pinning is also involved (Sonier, Kiefl, *et al.*, 1997a).

Recent advancements in the development of ultralow-energy (<30 keV) muon beams (Morenzoni *et al.*, 1994) has made it possible to implant muons near the surface of a sample. Niedermayer *et al.* (1999) have observed changes in the μSR line shape across the surface of a

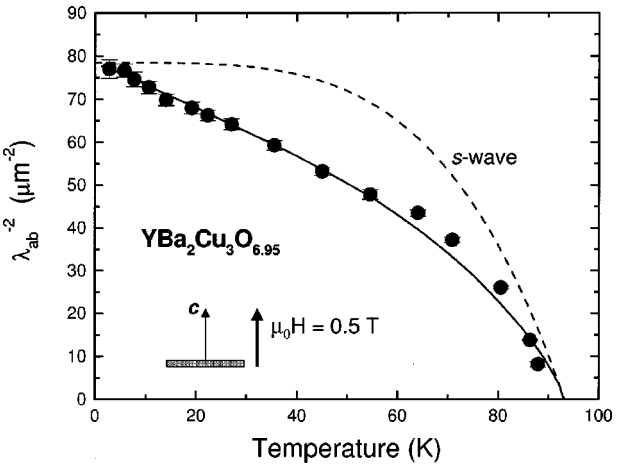

FIG. 25. Temperature dependence of λ_{ab}^{-2} in single-crystal $YBa_2Cu_3O_{6.95}$ at $\mu_0 H = 0.5$ T (solid circles): solid curve, the microwave measurements of $\Delta\lambda_{ab}$ by Hardy *et al.* (1993) converted to λ_{ab}^{-2} using the μSR value of $\lambda_{ab}(0)$; dashed curve, the variation with temperature expected for a conventional *s*-wave superconductor.

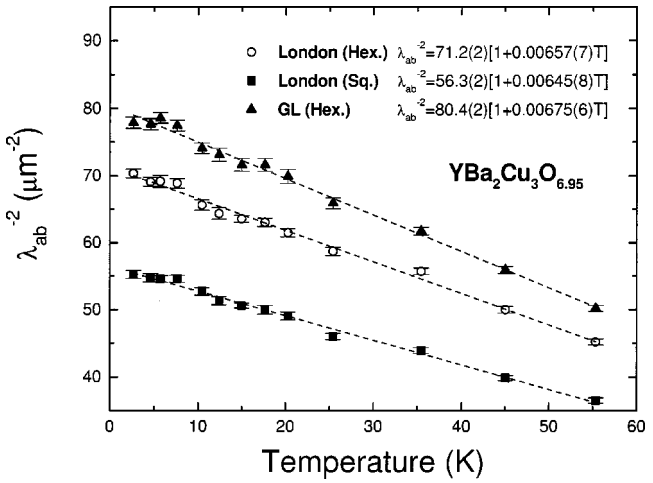

FIG. 26. Temperature dependence of λ_{ab}^{-2} in single-crystal $YBa_2Cu_3O_{6.95}$ at $\mu_0 H = 0.19$ T determined from fits to the modified London model [Eq. (30)] and the Ginzburg-Landau (GL) model [Eq. (35)] for the field profile $B(r)$. Fits to the modified London model are shown assuming a hexagonal (Hex.) and square (Sq.) geometry for the vortex lattice. The linear fits are discussed in the text.

$YBa_2Cu_3O_{7-\delta}$ thin film, which are consistent with theoretical calculations based on the London model for the emergence of vortex lines through the surface. The value of λ_{ab} extracted from the data was found to agree with that determined from other techniques. Ultralow-energy muons have also been used to measure λ_{ab} in the Meissner state. Measurements on a $YBa_2Cu_3O_{7-\delta}$ thin film (Jackson *et al.*, 2000) show that the field exponentially decays inward from the sample surface, as predicted by London theory. Increasing the intensity of the low-energy muon beam is the next technical obstacle to overcome before performing a full study of λ_{ab} at the surface. We restrict further discussion in this review article to "conventional" μSR measurements performed in the bulk.

The limiting T behavior of $\lambda(T)$ that is expected for a $d_{x^2-y^2}$-wave superconductor with nodes in the energy gap has been observed with μSR in the high-temperature cuprate superconductors. The first unambiguous report was a μSR study on high-quality twinned single crystals of $YBa_2Cu_3O_{6.95}$ (Sonier *et al.*, 1994). In this study, the modified London model [see Eq. (30)] and hexagonal symmetry were assumed for the field profile $B(r)$ of the vortex lattice. Although this result clearly showed that λ_{ab} changed linearly as a function of temperature at low T, it was later realized that the chosen sum over reciprocal-lattice vectors in Eq. (30) was too small. Figure 25 shows the temperature dependence of λ_{ab}^{-2} obtained by refitting the μSR time spectra at $\mu_0 H = 0.5$ T from Sonier *et al.* (1994) with the analytical Ginzburg-Landau model [see Eq. (35)]. The solid curve in Fig. 25 represents the zero-field microwave measurements of $\Delta\lambda_{ab}(T) = \lambda_{ab}(T) - \lambda_{ab}(1.35\text{ K})$ performed by Hardy *et al.* (1993) on similar high-quality twinned $YBa_2Cu_3O_{6.95}$ crystals. To plot $\lambda_{ab}^{-2}(T)$ for the microwave data, the extrapolated value of $\lambda_{ab}(1.35\text{ K})$ from the μSR experiment was used. The excellent agreement between the measurements in the vortex state and those in the Meissner state indicate that the variation of the superfluid denisty n_s as a function of temperature is identical in both phases. It also suggests that thermal fluctuations of the vortices play a minor role in the temperature dependence of λ_{ab}^{-2} measured with μSR. This is not surprising given the strong pinning at low T in this material.

Despite the good agreement with the microwave measurements, it is perhaps necessary to address the following questions: How sensitive are the μSR measurements of $\lambda_{ab}(T)$ to (i) the assumed model for $B(r)$, (ii) the assumed geometry of the vortex lattice, and (iii) the presence of twin boundaries in the crystal? Figure 26 shows the temperature dependence of λ_{ab}^{-2} in $YBa_2Cu_3O_{6.95}$ determined from fits to the modified London and Ginzburg-Landau models for $B(r)$, assuming a hexagonal arrangement of vortices. Although the quality of the fits is comparable for the two models, the absolute value of λ_{ab} is significantly different. Fitting the data in Fig. 26 to a linear relation gives $\lambda_{ab}(0) \approx 1185(17)$ Å and 1115(15) Å for the modified London and Ginzburg-Landau models, respectively. Despite this difference, the coefficient of the term linear in T is comparable for the two models. Thus $d\lambda_{ab}/dT$ can be determined with reasonable accuracy, independent of the model for $B(r)$.

Figure 26 also shows the temperature dependence of λ_{ab}^{-2} for fits to the modified London model, assuming a square vortex lattice. The quality of the fits to the μSR time spectra was found to be slightly worse than for the hexagonal case. A fit to a linear relation gives $\lambda_{ab}(0) \approx 1185(17)$ Å and 1333(24) Å for the hexagonal and square vortex lattice geometries, respectively. On the other hand, the coefficient of the term linear in T agrees for the two geometries. This result is consistent with the theoretical work by Affleck, Franz, and Amin (1996), who showed that including additional terms in the free

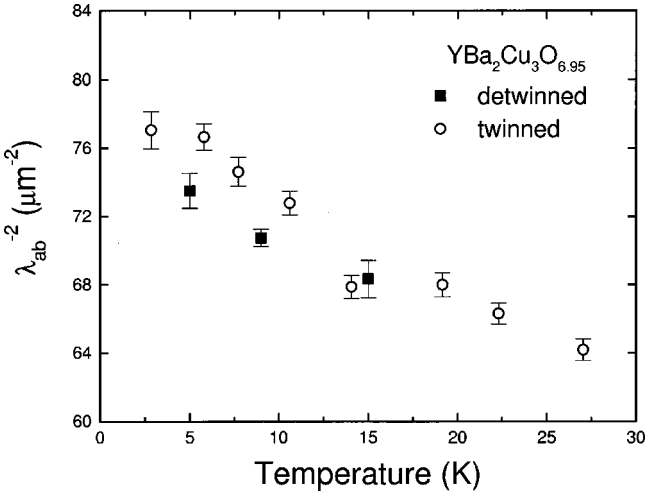

FIG. 27. Temperature dependence of λ_{ab}^{-2} in a single crystal of $YBa_2Cu_3O_{6.95}$ at $\mu_0 H = 0.5$ T: ○, twinned; ■, detwinned.

energy of the vortex state produces only minor changes in the internal field distribution. Thus reliable information concerning $\lambda(T)$ and $\xi(T)$ can still be obtained in a μSR experiment even when the vortex lattice geometry is unknown.

Figure 27 shows the temperature dependence of λ_{ab}^{-2} in a twinned and detwinned crystal of $YBa_2Cu_3O_{6.95}$ at $\mu_0 H = 0.5$ T. The presence of the twins does not seem to affect the qualitative behavior of $\lambda_{ab}(T)$. There are however, differences in the absolute value of λ_{ab} between the twinned and detwinned crystal. This is likely due to distortions of the vortex lattice caused by the combination of the $\hat{a}$-$\hat{b}$ anisotropy and the twin-boundary pinning. As before, differences in the assumed and actual geometry of the vortex lattice lead to larger uncertainty in the absolute value of λ_{ab}, but do not greatly affect the determined value of $d\lambda_{ab}/dT$.

Since λ_{ab}^{-2} is not the only quantity that contributes to the width of the μSR line shape, we mention here the behavior of the additional broadening parameter σ_f presented in Eq. (14). The temperature dependence of this quantity in $YBa_2Cu_3O_{6.95}$ at two different magnetic fields is shown in Fig. 28(a). The behavior of σ_f as a function of T is similar to that of λ_{ab}^{-2}. To determine the degree of disorder in the vortex lattice, one can subtract in quadrature the contribution of the nuclear moments to the muon depolarization rate,

$$\sigma_{\rm dis}^2 = \sigma_f^2 - \sigma_{\rm dip}^2 . \tag{52}$$

The contribution from the nuclear dipolar moments $\sigma_{\rm dip}$ is approximately the muon depolarization rate in the normal state. An upper limit for the root-mean-square displacement $\langle s^2 \rangle^{1/2}$ of the vortices from their ideal positions in the vortex lattice due to random pinning can be obtained from $\sigma_{\rm dis}$ through the relation (Riseman *et al.*, 1995)

$$\langle s^2 \rangle^{1/2} \approx \frac{\sigma_{\rm dis}}{B_0}\sqrt{2}\left(\sum_{\mathbf{K}} \frac{K^2}{[1+K^2\lambda_{ab}^2/(1-b)]^2} \right)^{-1/2} . \tag{53}$$

Figure 28(b) shows the temperature dependence of

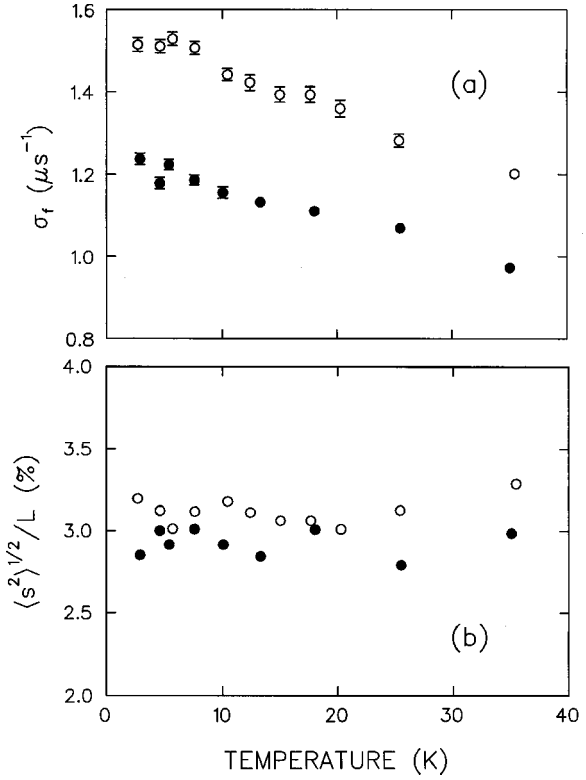

FIG. 28. Temperature dependence of (a) the additional broadening parameter σ_f and (b) the RMS displacement $\langle s^2 \rangle^{1/2}$ of the vortices from their ideal positions expressed as a percentage of the intervortex spacing L, in $YBa_2Cu_3O_{6.95}$: ○, at $\mu_0 H = 0.2$ T; ●, at $\mu_0 H = 1.5$ T.

$\langle s^2 \rangle^{1/2}$ in $YBa_2Cu_3O_{6.95}$ plotted as a percentage of the intervortex spacing $L = (2\phi_0/\sqrt{3}B_0)^{1/2}$ in a "disorder-free" hexagonal Abrikosov vortex lattice. The small disorder in the vortex lattice is essentially temperature independent and, as expected, larger at $\mu_0 H = 0.2$ T than at $\mu_0 H = 1.5$ T. Moreover, the agreement as a percentage of L suggests that the disorder scales with the nearest-neighbor distance between vortex lines. This result is inconsistent with a dramatic change in the vortex lattice geometry over this narrow field range. Similar results are found in $NbSe_2$.

A limiting T behavior has been observed for λ_{ab}^{-2} in μSR studies on other high-temperature superconductors. In particular, Luke *et al.* (1997) found that λ_{ab}^{-2} varied as a linear function of T at low temperature in $La_{1.85}Sr_{0.15}CuO_4$ single crystals (see Fig. 29). A linear T dependence has also been reported for the muon depolarization rate σ in unoriented polycrystalline samples of Ca- and La-doped $YBa_2Cu_4O_8$ (Shengelaya *et al.*, 1998; see Fig. 30) and more recently by Panagopoulos *et al.* (1999) in polycrystalline samples of $La_{2-x}Sr_xCuO_4$ and $HgBa_2CuO_{4+\delta}$. In the polycrystalline studies, a Gaussian distribution of local fields was assumed in the analysis of the μSR spectra. Although one can assume that a Gaussian approximation in a clean polycrystalline sample roughly gives $\sigma(T) \propto \lambda^{-2}(T)$, we shall show in the next section that $\sigma(H)$ cannot be considered a measure of $\lambda^{-2}(H)$.

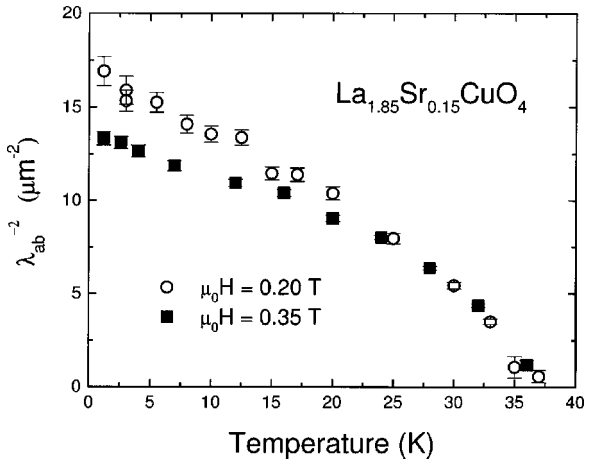

FIG. 29. Temperature dependence of λ_{ab}^{-2} in $La_{1.85}Sr_{0.15}CuO_4$ single crystals: ○, at $\mu_0 H = 0.20$ T; ■, at $\mu_0 H = 0.35$ T. From Luke *et al.*, 1997.

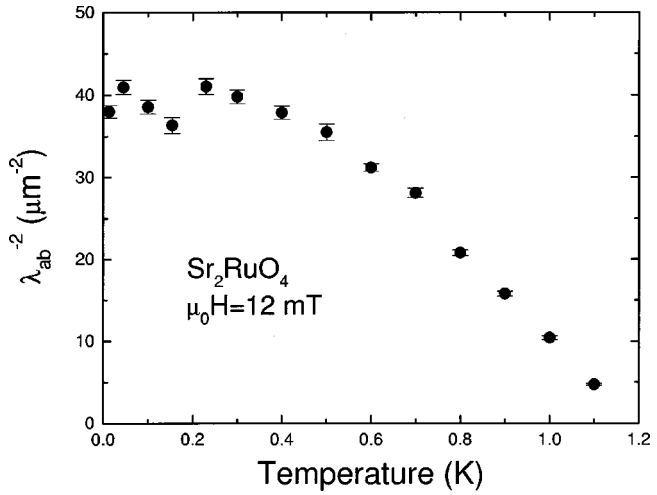

FIG. 31. Temperature dependence of λ_{ab}^{-2} in Sr_2RuO_4 single crystals at $\mu_0 H = 12$ mT. From Luke *et al.*, 1999.

It is still an open question why a linear T dependence of σ was not clearly observed in previous μSR studies on polycrystalline samples. It is likely that some of the early attempts at measuring $\sigma(T)$ resulted in misleading conclusions, partly because of problems with sample quality. On the other hand, many of the early studies clearly suffered from a lack of sufficient data points at low temperature. For example, Ansaldo *et al.* (1991) observed a clear departure of $\sigma(T)$ from conventional BCS behavior in $YBa_2Cu_4O_8$, which they attributed to the existence of two energy gaps corresponding to electronic states in the double chains and in the CuO_2 layers. However, no measurements were taken below 10 K, where the effect of the nodes in the superconducting energy gap on the temperature dependence of the superfluid density is most distinguishable from conventional behavior.

Aegerter, Lloyd, *et al.* (1998) estimated the temperature dependence of λ_{ab} in single-crystal Sr_2RuO_4 from the second moment $\langle \Delta B^2 \rangle^{1/2}$ of the measured field distribution. The temperature dependence of λ_{ab}^{-2} at low T could be represented by a linear function, indicating the presence of nodes in the energy gap function. However, the scatter of the data was such that results were also consistent with a saturation of λ_{ab} at low T, as expected in the absence of nodes.

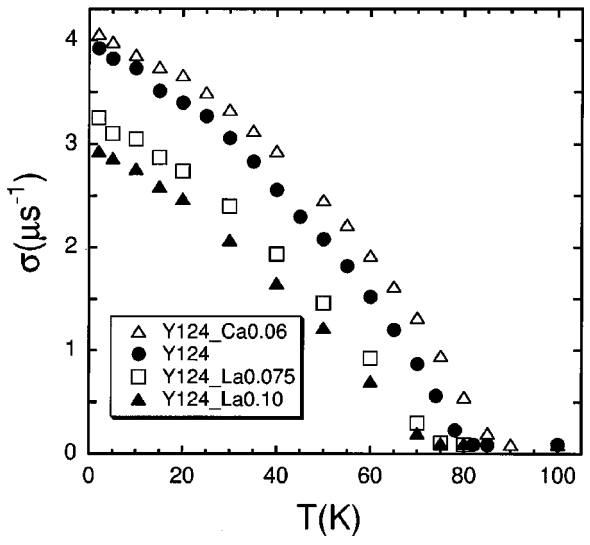

FIG. 30. Temperature dependence of the muon depolarization rate σ in polycrystalline samples of pure, Ca-doped, and La-doped $YBa_2Cu_4O_8$. From Shengelaya *et al.*, 1998.

It is interesting to note that Uemura *et al.* (1988) observed a clearly linear T dependence of σ in powdered samples of $YBa_2Cu_3O_{6.95}$ and $YBa_2Cu_3O_{6.66}$. Unfortunately, the authors concluded that the increase of λ (calculated from σ) with increasing temperature at low T was not fast enough to arise from nodes at the Fermi surface in the energy gap.

Very recently, Luke *et al.* (1999) determined $\lambda_{ab}(T)$ in Sr_2RuO_4 single crystals from fits to the measured muon spin precession signal, which assumed the field distribution of the orbital Ginzburg-Landau superconductivity model described in Sec. III.B.7 (Agterberg, 1998; Heeb and Agterberg, 1999). As shown in Fig. 31, λ_{ab}^{-2} was found to be nearly independent of T at low temperatures. This result is consistent with a superconducting energy gap with no nodes, as expected for a p-wave (odd-parity) E_{2u} state. This state, which breaks time-reversal symmetry and has only one superconducting transition, was inferred from an earlier zero-field μSR study (Luke *et al.*, 1998).

B. Magnetic-field dependence

1. Nonlinear effects

In general, the response of a superconductor to an applied magnetic field is nonlinear. Bardeen (1954) first considered a nonlinear supercurrent response for a conventional s-wave superconductor, arising from the thermal population of quasiparticles. The superflow $\mathbf{v_s}$ induced by the magnetic field results in a semiclassical Doppler shift of the quasiparticle energy levels by an amount proportional to $\mathbf{v_s} \cdot \mathbf{v_f}$, where $\mathbf{v_f}$ is the Fermi ve-

locity. The quasiparticle levels with velocity $\mathbf{v_f}$ in opposite direction to $\mathbf{v_s}$ are shifted to lower energies. These quasiparticle excitations form a backward-flowing current, which produces a "nonlinear" relationship between $\mathbf{J_s}$ and $\mathbf{v_s}$. This weakening of the supercurrent response results in an increased penetration of the field, i.e., a field dependence for λ. In particular, at low temperatures in the Meissner state, λ is predicted to change quadratically with H,

$$\frac{\lambda(H,T)}{\lambda(0,T)} = 1 + \beta_1(T)\left[\frac{H}{H_0(T)}\right]^2, \tag{54}$$

where $H_0(T)$ is a characteristic field on the order of the thermodynamic critical field $H_c(T)$, and $\beta_1(T)$ is a thermally activated prefactor that decreases as $\exp(-\Delta/T)$ for $T \to 0$ K. The nonlinear effects are relevant at fields above $H_0(T)$ and below a characteristic crossover temperature $T^*(H)$. The field dependence is typically weak in an s-wave superconductor because the finite gap prevents the shifted levels from being occupied at low T.

Yip and Sauls (1992) proposed that the field dependence of λ in the Meissner state could be used to determine the angular position of nodes in the energy gap. The excited quasiparticle levels near the nodes with $\mathbf{v_f}$ in the opposite direction to $\mathbf{v_s}$ are shifted by the field to energies below the Fermi level E_F, resulting in a strong field dependence of λ. In a $d_{x^2-y^2}$-wave superconductor at $T = 0$ K, λ is predicted to change linearly with H at low T (Yip and Sauls, 1992; Stojković and Valls, 1995; Xu, Yip, and Sauls, 1995),

$$\frac{\lambda(H,T)}{\lambda(0,T)} = 1 + \beta_2(T)\left[\frac{H}{H_0(T)}\right], \tag{55}$$

where $\beta_2(T)$ is a temperature-dependent coefficient that remains finite at $T = 0$ K due to the nodes in the gap. The absolute value of $\beta_2(T)$ depends on the direction of the field relative to the nodes, with the strongest field dependence occurring for $\mathbf{v_s}$ flowing along the direction of the nodes. According to this theory, $\lambda(H,T)$ is a linear function of H and a quadratic function of T below $T^*(H)$, and a quadratic function of H and a linear function of I above $T^*(H)$.

Maeda *et al.* (1995) observed a linear H dependence of λ_{ab} in $Bi_2Sr_2CaCu_2O_8$ thin films, but at relatively high temperatures where the Yip and Sauls theory predicts an H^2 behavior. Similar findings were reported in $YBa_2Cu_3O_{7-\delta}$ and $Tl_2Ba_2CaCu_2O_y$ (Maeda *et al.*, 1996). The nonlinear effects observed in these studies have since been attributed to extrinsic effects. More recent measurements by Bidinosti *et al.* (1999) using a novel ac susceptometer show that $\Delta\lambda(H)$ in $YBa_2Cu_3O_{6.95}$ does not exhibit the temperature dependence or directional field dependence predicted by Yip and Sauls. Recently, Li, Hirschfeld, and Wölfe (1998) have shown that the expected linear H dependence can be modified by nonlocal effects not considered in the original Yip and Sauls theory.

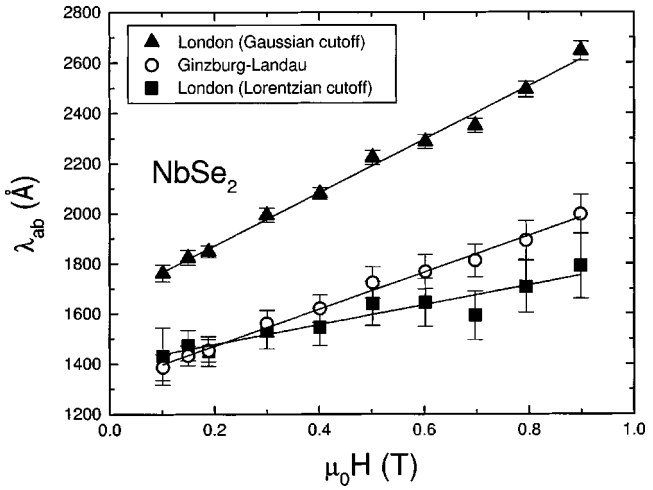

FIG. 32. Magnetic-field dependence of λ_{ab} in $NbSe_2$ at $T = 2.3$ K, determined from fits to three different models for the field profile $B(r)$ of the vortex lattice, i.e., the London model [Eq. (30)], with Gaussian and Lorentzian cutoff factors, and the analytical Ginzburg-Landau model [Eq. (35)]. The solid lines are fits to $\lambda_{ab}(H) = \lambda_{ab}(0)[1 + \beta h]$ where $\lambda_{ab}(0)$, β are ▲, 1659(16) Å, 1.85(7); ○, 1323(11) Å, 1.62(6); ■, 1398(24) Å, 0.8(1).

2. Nonlocal effects

Nonlocal effects were discussed in Sec. III.B.7 and Sec. III.C.4. In a $d_{x^2-y^2}$-wave superconductor, nonlocal effects are most important at low temperatures, where the quasiparticles predominantly occupy regions near the gap nodes. Kosztin and Legget (1997) determined that, in the Meissner state, this small fraction of the Fermi surface governed by nonlocal electrodynamics results in a crossover from T to T^2 dependence for λ at extremely low T. Thus either nonlinear or nonlocal effects modify the linear T dependence of λ to a quadratic T dependence below a characteristic temperature T^*. To observe this experimentally, one must distinguish these effects from the T^2 dependence that can arise from sample impurities.

The presence of nonlocal effects at low T also modifies the linear H dependence of λ expected solely from nonlinear effects—since the supercurrent response is weakened by the nonlocal electrodynamics of quasiparticle excitations near the nodes in the superconducting energy gap.

3. Extension to the vortex state

Observing nonlinear and nonlocal effects in the vortex state is complicated by the fact that the relative spacing between vortices is reduced when the applied field is increased. Thus the measured field dependence of λ will be strongly influenced by the nature of the vortex-vortex interactions. The associated change in the spatial variation of field between neighboring vortices means that μSR measurements of $\lambda(H)$ are more sensitive to the model used for $B(r)$ than measurements of $\lambda(T)$.

To illustrate this point, Fig. 32 shows the field depen-

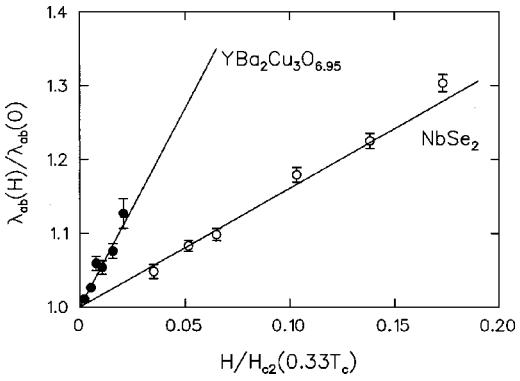

FIG. 33. Magnetic-field dependence of $\lambda_{ab}(H/H_{c2})/\lambda_{ab}(0)$ at $T=0.33T_c$: ●, in $YBa_2Cu_3O_{6.95}$ where $H_{c2}(0.33T_c)=95$ T; ○, in $NbSe_2$ where $H_{c2}(0.33T_c)=2.9$ T.

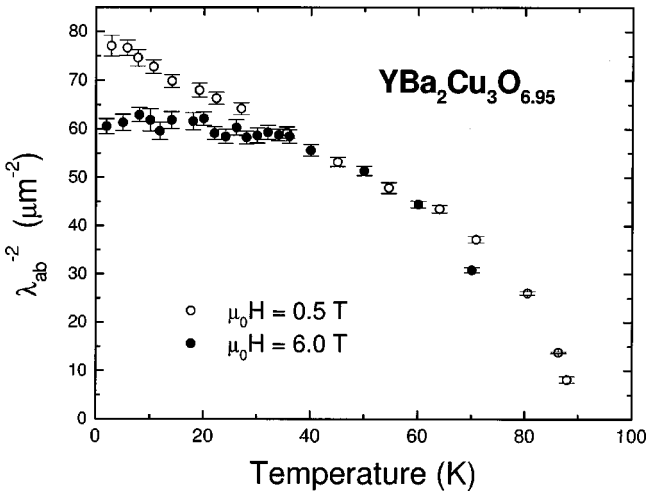

FIG. 34. Temperature dependence of λ_{ab}^{-2} in detwinned single crystals of $YBa_2Cu_3O_{6.95}$ at $\mu_0H=0.5$ T and 6.0 T. At intermediate temperatures the two data sets agree. The difference between these sets at $T\approx 65$ K is attributed to vortex lattice melting at $\mu_0H=6.0$ T. The low-T behavior is attributed to nonlocal and nonlinear effects as discussed in the text. From Sonier, Brewer, *et al.*, 1999.

dence of λ_{ab} in $NbSe_2$ at $T=2.3$ K over the range $0.03<H/H_{c2}<0.31$, obtained by fitting the μSR time spectra with a polarization function assuming one of three different models for $B(r)$. A linear H dependence for $\lambda_{ab}(H)$ is clearly observed in all three cases; however, both the absolute value of λ_{ab} and the slope $d\lambda_{ab}/dH$ are different. This suggests that $\lambda_{ab}(H)$ partially reflects the uncertainty of the theoretical model used for $B(r)$. At low fields there is good agreement between the modified London model using a Lorentzian cutoff factor and the Ginzburg-Landau model. This is reasonable since the Lorentzian cutoff is strictly valid only at low reduced fields $b=B/B_{c2}$. On the other hand, the modified London model using a Gaussian cutoff gives a significantly higher value for λ_{ab} and a stronger field dependence. The Gaussian cutoff, however, is derived from the solution of the Ginzburg-Landau equations near H_{c2} and is thus not really appropriate for measurements at low b. Apart from this model dependence, λ_{ab} appears to have a residual field dependence of intrinsic origin—possibly associated with nonlinear effects.

The field dependence of λ_{ab} in $YBa_2Cu_3O_{6.95}$ was investigated by Sonier, Kiefl *et al.* (1997a) using the modified London model for $B(r)$. Here we have reanalyzed the experimental data using the more appropriate Ginzburg-Landau model [see Eq. (35)], which properly accounts for the finite size of the vortex cores. Figure 33 shows a comparison of the normalized field dependence of λ_{ab} in $YBa_2Cu_3O_{6.95}$ to that in $NbSe_2$ (Sonier, Kiefl, *et al.*, 1997b), at $T=0.33\,T_c$. As expected, the field dependence of λ_{ab} is considerably stronger in $YBa_2Cu_3O_{6.95}$ due to the nonlinear and nonlocal electrodynamics of the quasiparticle excitations near the gap nodes. A field dependence for λ_{ab}^{-2} at low T was also observed by Luke *et al.* (1997) in a μSR experiment on single crystals of $La_{1.85}Sr_{0.15}CuO_4$ (see Fig. 29).

Recently, a new experiment was performed by Sonier, Brewer, *et al.* (1999) on $YBa_2Cu_3O_{6.95}$ to precisely determine the behavior of λ_{ab} as a function of H. A novel high-magnetic-field spectrometer was developed to extend the measurements well above $\mu_0H=2$ T. At $\mu_0H=4$ T and 6 T, $\lambda_{ab}^{-2}(T)$ was found to be nearly independent of temperature at low T [see Fig. 34]. The well-established linear T dependence of λ_{ab} is expected to be observed only at temperatures above the energy scale of the nonlinear and nonlocal effects. Amin, Affleck, and Franz (1998) numerically calculated the influence of these effects on the vortex state of a $d_{x^2-y^2}$-wave superconductor. They found that the nonlocal response to the applied field alters the spatial dependence of the local magnetic field by suppressing the local maximum of $B(r)$ at the vortex center. The effect on the magnetic-field distribution is enhanced at higher fields due to the increased vortex density. With increasing field there is greater overlap of the regions in the vicinity of the vortex cores modified by the nonlocal effects. Because nonlocal effects are not incorporated into the analysis of the μSR experiment, deviations from the fitted model for $B(r)$ (which assumes λ_{ab} is independent of H) result in a field dependence for the extracted λ_{ab} This does not imply a change of the superconducting carrier density. There is also an additional, but smaller, contribution to $\lambda_{ab}(H)$ from nonlinear effects. Amin, Affleck, and Franz (1998) calculated the field dependence of the *effective* penetration depth in almost the same way it was determined from the μSR experiment. Their results for the combined calculation of both nonlinear and nonlocal effects are shown in Fig. 35, compared to the measured field dependence of λ_{ab} in $YBa_2Cu_3O_{6.95}$ extrapolated to $T=0$ K (Sonier, Brewer, *et al.*, 1999). The agreement is remarkable and offers strong support for the present theoretical picture of how the magnetic field influences the low-lying quasiparticle excitations in the vortex state of a high-temperature cuprate superconductor. More recently, the temperature dependence of λ_{ab} has been calculated from this model taking into account only the nonlocal corrections (Amin, Franz, and Affleck, 2000). Although good agreement with the μSR measurements is obtained at high magnetic fields, the theoretical result

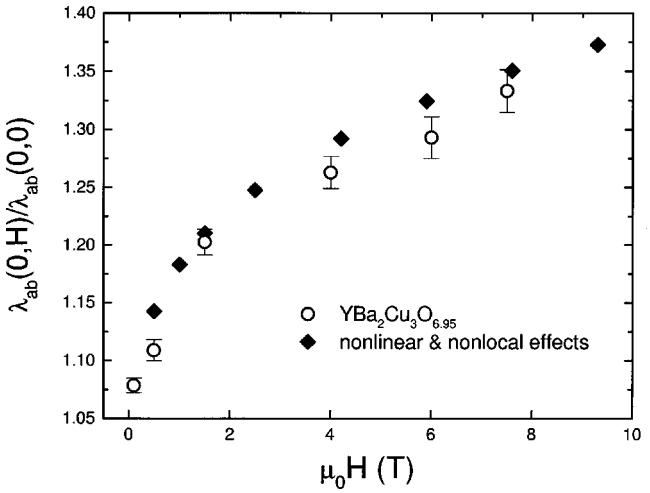

FIG. 35. Magnetic-field dependence of $\lambda_{ab}(0,H)/\lambda_{ab}(0,0)$ in detwinned single crystals of $YBa_2Cu_3O_{6.95}$: ○, extrapolated to $T=0$ K; ◆, predicted behavior (Amin, Affleck, and Franz, 1998) for the combination of nonlinear and nonlocal effects in the vortex state of a $d_{x^2-y^2}$-wave superconductor. From Sonier, Brewer, *et al.*, 1999.

does not exhibit the limiting T behavior observed at low fields.

Recently, Wang and MacDonald (1999) performed a microscopic calculation of the field dependence of the penetration depth in the vortex state of s- and $d_{x^2-y^2}$-wave superconductors. They found that the effective penetration depth measured in a μSR experiment increases with increasing magnetic field for both types of superconductors. However, consistent with the work of Amin, Affleck, and Franz (1998), they found a stronger field dependence in the $d_{x^2-y^2}$-wave case due to the nonlinear and nonlocal supercurrent response. Furthermore, the linear T dependence of λ at low temperature (which is a signature of $d_{x^2-y^2}$-wave superconductivity) was predicted to cross over to a T^2 dependence at $k_B T^* \sim (H/H_{c2})^{1/2}\Delta_0$, where Δ_0 is the maximum of the superconducting energy gap in the Meissner state. Agreement with the data in Fig. 34 can be obtained assuming reasonable values of the upper critical field H_{c2} and Δ_0.

The effective $\lambda_{ab}(H)$ measured with μSR can of course also be influenced by changes in the vortex lattice geometry, since this also alters the functional form of $B(r)$. The neutron experiment by Johnson *et al.* (1999) on detwinned $YBa_2Cu_3O_{6.95}$ appears to rule out any change in vortex lattice geometry over the field range considered in the μSR experiment. As discussed in Sec. III.C.2, this does not necessarily imply that the symmetry of the individual vortices is unchanged—since the vortex lattice will reflect the symmetry of the individual vortices only at higher fields, where the vortices strongly interact.

Finally, it should be clear that the correct field dependence of λ_{ab} cannot be obtained in a μSR experiment by assuming a Gaussian distribution of local fields. Even in the absence of nonlinear and nonlocal effects, the shape of the field distribution $n(B)$ changes with increasing field due to the changing vortex density. We emphasize the shortcomings of the simple Gaussian analysis by noting that the experimental data of Sonier, Brewer, *et al.* (1999) showed only a small dip in the Gaussian depolarization rate σ at high field and low temperature, but no crossover to a nearly T-independent region as found in the full analysis of the μSR line shape.

4. Charge and impurity doping

There have been numerous transverse-field μSR studies of the dependence of λ on charge or impurity doping in high-temperature cuprate superconductors. The majority of these experiments were performed on polycrystalline samples, assuming a Gaussian distribution of muon precession frequencies and that the depolarization rate from the fitted Gaussian relaxation function $\exp(-\sigma^2 t^2/2)$ obeys the simple relationship $\sigma \propto \lambda^{-2} \propto n_s/m^*$. Generally speaking, this a reasonable approximation at low temperatures and magnetic fields in clean polycrystalline samples, where "clean" means free of impurities. Nevertheless, the reader should be aware that, in unoriented polycrystalline samples, σ contains contributions from λ_a, λ_b, and λ_c, and thus partially reflects changes in coupling strength between superconducting layers.

In a series of μSR experiments on samples with different charge-carrier concentrations, Uemura *et al.* (1988, 1989, 1991, 1993) established universal behavior for the variation of T_c with $\sigma(0)$, where $\sigma(0)$ is the muon depolarization rate extrapolated to $T=0$ K. In the high-temperature superconductors the slope of T_c vs $\sigma(0)$ was found to increase in the underdoped regime, saturate for optimal doping, and then decrease in the overdoped regime (see Fig. 36). Organic $(BEDT\text{-}TTF)_2Cu(SCN)_2$, alkali-doped C_{60}, and some other superconductors were found to fall on the same universal curve. Studies of overdoped $Tl_2Ba_2CuO_{6+\delta}$ showed that $\sigma(0)$ tends toward zero and T_c is strongly suppressed with increased hole doping (Niedermayer *et al.*, 1993; Uemura *et al.*, 1993). Assuming that $\sigma(0) \propto \lambda(0)^{-2} \propto n_s/m^*$, Uemura (1995a, 1995b, 1997) proposed that the universal correlation between T_c and n_s/m^* in high-temperature cuprate superconductors arises from an evolution from Bose-Einstein to BCS condensation with increasing carrier concentration n_s. For low values of n_s, singlet pairs form above T_c at the so-called pseudogap temperature T^* and then upon cooling undergo Bose-Einstein condensation at T_c. On the other hand, with increasing n_s, T_c increases whereas T^* decreases. At optimal doping, the value of T_c is equivalent to T^*, so that pair formation and condensation occur simultaneously (i.e., BCS condensation).

It has been pointed out that not all of the high-temperature superconductors follow the "Uemura line." Tallon *et al.* (1995) showed that $\sigma(0)$ in polycrystalline samples of $YBa_2Cu_3O_{7-\delta}$, $Y_2Ba_4Cu_7O_{15-\delta}$, and $YBa_2Cu_4O_8$ is enhanced above the Uemura line when $\delta \to 0$ (see Fig. 37). These compounds differ from the other high-temperature superconductors in that they

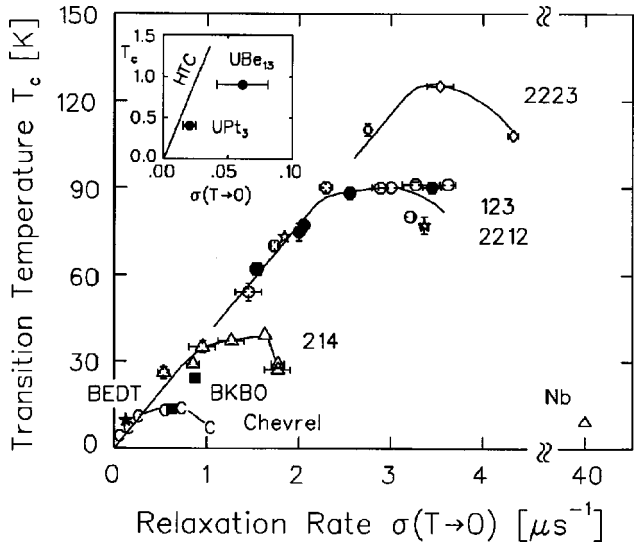

FIG. 36. T_c vs muon depolarization rate $\sigma(0)$ in (i) the high-temperature superconductors: $YBa_2Cu_3O_{7-\delta}$ (123), $La_{2-x}Sr_xCuO_4$ (214), $Bi_2Sr_2CaCu_2O_8$, and $Tl_{0.5}Pb_{0.5}Sr_2CaCu_2O_7$ (2212), and $Bi_{2-x}Pb_xSr_2Ca_2Cu_3O_{10}$, $Tl_2Ba_2Ca_2Cu_3O_{10}$, and $Tl_{0.5}Pb_{0.5}Sr_2Ca_2Cu_3O_9$ (2223) [note: hole doping increases with increasing $\sigma(0)$]; (ii) $Ba_{1-x}K_xBiO_3$ (BKBO); (iii) the Chevrel-phase systems $LaMo_6Se_8$, $LaMo_6S_8$, and $PbMo_6S_8$; (iv) the organic superconductor $(BEDT\text{-}TTF)_2Cu(SCN)_2$; (v) the conventional superconductor Nb; and (vi) the heavy-fermion superconductors UPt_3 and UBe_{13}. From Uemura *et al.*, 1991.

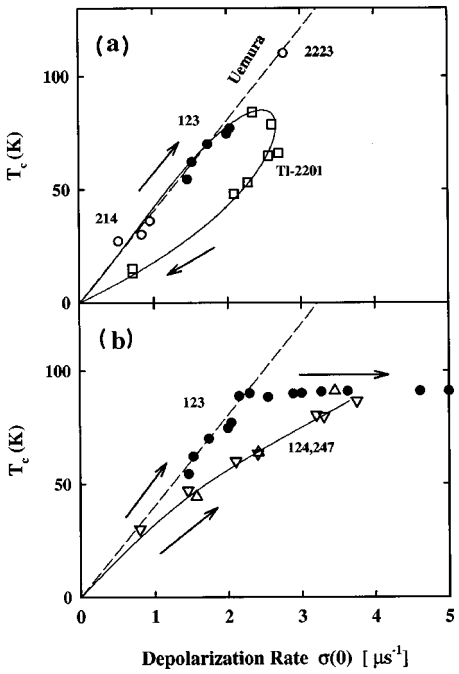

FIG. 37. T_c vs the zero-temperature muon depolarization rate $\sigma(0)$. (a) "Universal" behavior of underdoped La-214 (open circles), Y-123 (solid circles), and Bi-2223 (open circle) systems (Uemura *et al.*, 1991), and behavior of the overdoped Tl-2201 (open squares) system (Niedermayer *et al.*, 1993; Uemura *et al.*, 1993). (b) Complete oxygen doping range for ●, Y-123 (Pümpin *et al.*, 1990b; Uemura *et al.*, 1991); △, Y-247; ▽, (Y,Ca/La)-124 and $YBa_2(Cu,Zn)O_8$. From Tallon *et al.*, 1995.

contain CuO chains in addition to the CuO_2 planes. As $\delta\rightarrow 0$, the chains become free of disorder, so it was concluded that the enhanced values of $\sigma(0)$ are due to an additional contribution to n_s from carriers on the chains participating in superconductivity.

The temperature dependence of λ_{ab}^{-2} determined from μSR measurements on single-crystal $YBa_2Cu_3O_{6.60}$ (Sonier, Brewer, *et al.*, 1997, 2000) is shown in Fig. 23(b). Above the vortex lattice melting transition $T_m(H)$ it is not straightforward to extract λ_{ab}. The observed rapid reduction of λ_{ab}^{-2} above $T_m(H)$ is an artifact of the modeling procedure (which assumes a regular Abrikosov vortex lattice) and arises from a sudden loss of asymmetry in the μSR line shape in the melted region. At low temperatures, where λ_{ab}^{-2} is observed to vary as a linear function of T, the slope $d[\lambda_{ab}/\lambda_{ab}(0)]/d(T/T_c)$ is weaker than in the optimally doped compound. These measurements show excellent agreement with microwave cavity measurements (Bonn *et al.*, 1996) of $\Delta\lambda_{ab}(T)=\lambda_{ab}(T)-\lambda_{ab}(1.25\,\mathrm{K})$ in zero dc magnetic field (see Sonier, Brewer, *et al.*, 1997). The microwave measurements show that the strength of the term linear in T/T_c changes substantially as a function of oxygen doping only in the $\hat{b}$ direction, i.e., the direction of the CuO chains. One possible interpretation of this result is that disorder in the CuO chains causes pair breaking (Atkinson, 1999).

The substitution of Zn for planar Cu in the high-temperature superconductors has attracted considerable attention. Small concentrations of Zn drastically reduce T_c and alter the temperature dependence of λ at low T (Bonn *et al.*, 1994). In the normal state, Zn induces a weak magnetic moment, which affects the magnetism associated with neighboring Cu atoms (Alloul *et al.*, 1991; Mahajan *et al.*, 1994). However, in the superconducting state these moments may be screened by quasiparticles, so their role in the superconducting state is still under investigation.

Bernhard, Tallon, *et al.* (1996) measured the decrease of $\sigma(0)$ due to Zn substitution in polycrystalline samples of $Y_{0.8}Ca_{0.2}Ba_2(Cu_{1-y}Zn_y)_3O_{7-\delta}$ and overdoped $La_{0.79}Sr_{0.21}Cu_{1-y}Zn_yO_4$. They observed a reduction of $\sigma(0)$ with increasing Zn concentration, which they attributed to pair breaking in a $d_{x^2-y^2}$-wave superconductor due to unitary scattering by the Zn impurities (see Sec. IV.A.1).

A similar μSR study by Nachumi *et al.* (1996) on $La_{2-x}Sr_x(Cu_{1-y}Zn_y)O_4$ and $YBa_2(Cu_{1-y}Zn_y)_3O_{6.63}$ yielded qualitatively similar data, but was interpreted in the context of their so-called "swiss cheese" model—whereby the suppression of the superconducting order parameter in the region of the Zn impurity leads to the exclusion of superconducting charge carriers within an area $\pi\xi_{ab}$ around the Zn atom. Spontaneous phase separation into charged regions, similar to the swiss cheese model, was offered as a possible explanation for the observed decrease in T_c vs $\sigma(0)$ in the overdoped regime of the Uemura plot. Currently, there is growing

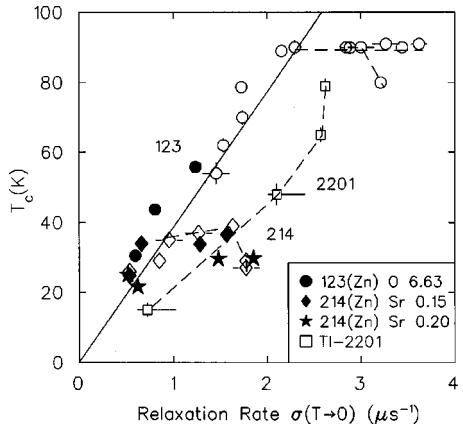

FIG. 38. T_c vs muon depolarization rate $\sigma(0)$ in La-214 and Y-123 systems, and the overdoped Tl-2201 system: solid symbols: Zn-substituted; open symbols, pure. The solid line is the universal behavior found in the underdoped cuprate superconductors. The Zn-substituted systems show the same behavior as the oxygen-doped pure systems. From Nachumi *et al.*, 1996.

evidence that all high-temperature cuprate superconductors possess either static or dynamic phase separation into charge-rich and antiferromagnetic charge-poor regions—also known as stripes.

An interesting finding in the study by Nachumi *et al.* was that the Zn-impurity-doped samples fell on the same universal curve as the pure samples with various hole dopings (different oxygen concentrations), as shown in Fig. 38. This implies that the relationship between T_c and the ratio n_s/m^* does not depend on the nature of doping—in particular, whether the materials are charge or impurity doped. However, Bernhard *et al.* (1998) pointed out that their own measurements on *heavily* Zn-substituted $Y_{0.8}Ca_2(Cu_{1-y}Zn_y)_3O_{7-\delta}$ lie predominantly to the left of the universal line in Fig. 38, consistent with the model for impurity scattering in a $d_{x^2-y^2}$-wave superconductor. Nachumi *et al.* (1998) responded to this comment by suggesting that large concentrations of Zn could result in semimacroscopic phase separation in which a large fraction of the sample volume is not superconducting. Furthermore, they argued that in dirty samples (i.e., large Zn concentration) where the mean free path becomes comparable to the size of the superconducting coherence length, σ is no longer approximately proportional to λ^{-2} (or n_s). Either of these factors could explain why the data for heavily Zn-doped samples fall to the left of the universal T_c vs $\sigma(0)$ plot.

Another point of contention in these studies is the suppression of T_c with increasing disorder. That is, the $d_{x^2-y^2}$-wave impurity model overestimates the suppression of T_c with increasing Zn concentration. However, as shown previously by Franz, Kallin, *et al.* (1997) and discussed in Sec. IV.A.1, the problem is alleviated by taking into account the suppression of the $d_{x^2-y^2}$-wave order parameter in the vicinity of the Zn impurities. The swiss cheese model is conceptually the same as this latter picture.

V. THE VORTEX CORE SIZE

Recently, μSR has been used to determine the size of the vortex cores in single-crystal superconductors (Sonier *et al.*, 1997b; Sonier, Brewer, *et al.*, 1997, 1999; Sonier, Kiefl, *et al.*, 1999). The μSR technique has several distinct advantages over STS, which has also been used to measure the size of vortex cores (Hartmann, Drechsler, and Heiden, 1993; Volodin, Golubov, and Aarts, 1997). First, since μSR is a bulk technique, it is insensitive to most effects the sample surface has on the vortices. For instance, calculations by Kirtley *et al.* (1999) show that the apparent size of a vortex can increase by as much as 30% at the sample surface. Recent measurements of the μSR line shape across the surface of a $YBa_2Cu_3O_{7-\delta}$ thin film using ultralow-energy muons has confirmed this effect (Niedermayer *et al.*, 1999; see Sec. IV.A.2). The enhanced pinning effects at the sample surface can disorder the vortex lattice, changing the nature of the vortex-vortex interactions, which certainly play some role in the core size. Only for the case of rigid vortex lines will pinning at the surface influence the vortex structure in the bulk. Second, μSR measurements can be performed deep in the superconducting state at low temperatures (using a dilution refrigerator) and at low magnetic fields. On the other hand, STS measurements are typically performed at higher fields where the vortices are easy to locate. STS is also technically difficult to perform at temperatures well below $T\approx 2$ K. To date, μSR is the only technique that has been able to measure the effective core size deep in the superconducting state of a high-temperature superconductor.

The definition of the vortex core size is not well established, since there exists no discontinuity in the spatial dependence of theoretical quantities between the core and the surrounding superconducting medium. A commonly used definition comes from Ginzburg-Landau theory, where the core radius r_0 is defined as the distance from the vortex axis to where the superconducting order parameter rises to $1/\sqrt{2}$ of its maximum value. This is essentially where the supercurrent density $|J_s(r)|$ reaches its maximum value (see Fig. 1). In a μSR experiment, the supercurrent density $J_s(r)$ is obtained from the *fitted* field profile $B(r)$ using the Maxwell relation $\mathbf{J}(\mathbf{r})=(c/4\pi)\nabla\times\mathbf{B}(\mathbf{r})$. The core size r_0 is then the distance from $r=0$ (i.e., the core center) to the value of r where $|J_s(r)|$ reaches its maximum value. As discussed in Sec. III.B.3, the behavior of r_0 is similar to ξ_1, which is related to the slope of the order parameter at the vortex core center. Thus a change in the value of r_0 reflects a change in the length scale for spatial variations of the supercurrent density near the center of the vortex. Outside the vortex core (i.e., $r>r_0$), $J_s(r)$ decays algebraically as $1/r$, and at distances beyond $r>\lambda$, $J_s(r)$ decays exponentially with increasing radial distance r.

Because μSR measures an ensemble-averaged polarization function, r_0 represents the average size of the vortex cores in the sample, whereas STS probes individual vortices. The accuracy of the measurement hinges

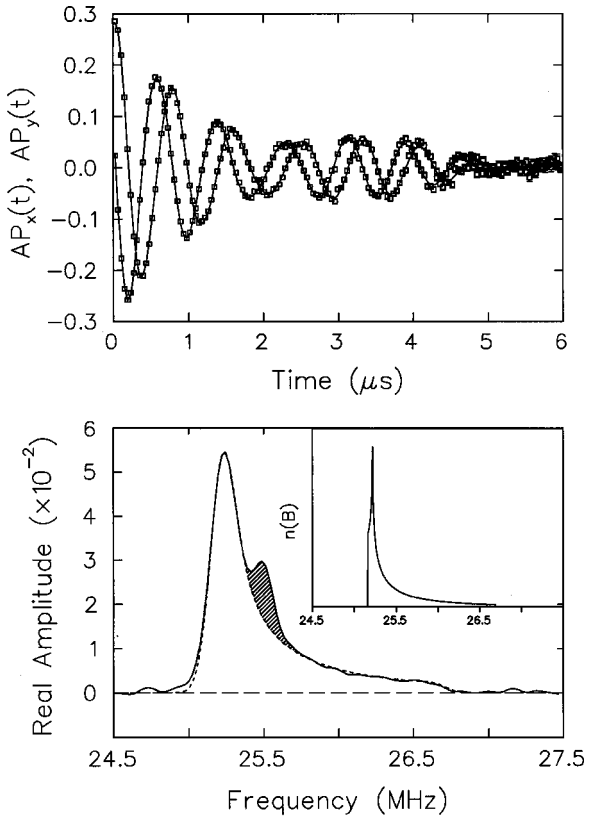

FIG. 39. Transverse-field μSR measurement in the vortex state. Upper panel, muon spin precession signal in $NbSe_2$ after cooling in a field $\mu_0 H = 0.19$ T to $T = 2.3$ K. The solid curve is a fit assuming Eq. (35) for the field profile $B(r)$ of the vortex lattice. Lower panel: solid curve, Fourier transform of the measured muon spin precession signal; and the Fourier transform of the fit to the muon spin precession signal. The shaded region is the background signal. Inset: Theoretical field distribution $n(B)$ corresponding to the function $B(r)$ used to fit the time spectrum.

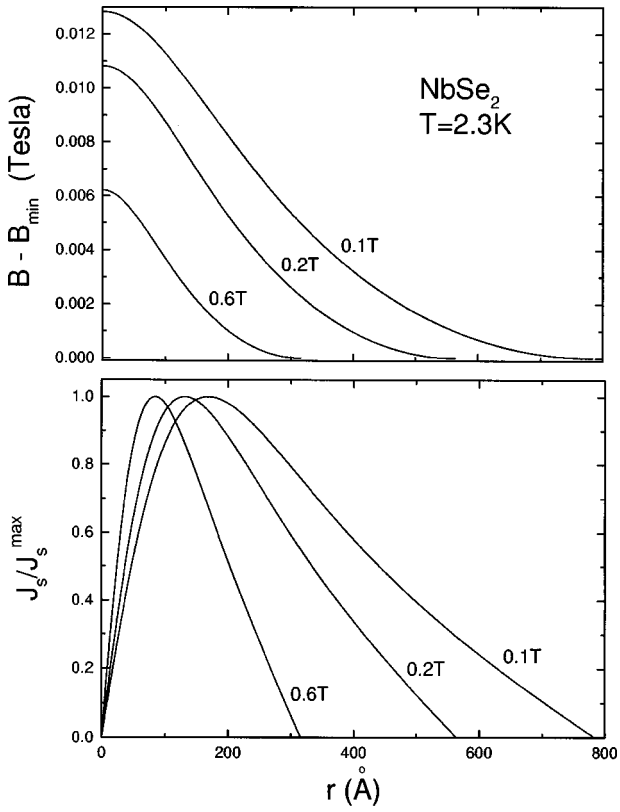

FIG. 40. The magnetic field and supercurrent density as a function of radial distance from the vortex center in $NbSe_2$ for applied fields $\mu_0 H = 0.1$, 0.2, and 0.6 T. The magnetic field is plotted as the difference between B and the minimum field $B_{\min}$. The supercurrent density is normalized to its maximum value.

upon the following important detail: *The correct $J_s(r)$ profile only requires that a good fit to the data is obtained, independent of the theoretical model used for $B(r)$*. This is because the curl of any function $\mathbf{B}(\mathbf{r})$ that fits the data well gives the same $J_s(r)$ profile. In practice, the finite number of counts in the core region, coupled with the fact that a "perfect" fit of the measured field distribution is never achieved, leads to some uncertainty in the value of r_0.

A. Magnetic-field dependence

The dependence of r_0 on magnetic field has been measured with μSR in single-crystal $NbSe_2$ (Sonier *et al.*, 1997b), which has a well-ordered hexagonal Abrikosov vortex lattice at fields above ~ 25 G (Hess *et al.*, 1989; Hess, Murray, and Waszczak, 1992; Gammel *et al.*, 1994; Volodin *et al.*, 1998). An example of a fit to the measured muon spin precession signal taken from this study is shown in Fig. 39. The theoretical polarization function was generated assuming that the field profile $B(r)$ is given by the analytical Ginzburg-Landau model [see Eq. (35)]. The magnetic-field distribution $n(B)$ corresponding to the fit function $B(r)$ is shown in the inset, and the FFT's of the measured muon spin precession signal and the fitted theoretical muon polarization function are shown in the lower panel. The broadening effects associated with the FFT (see Sec. II.E) are apparent in a comparison of $n(B)$ with the FFT of the fitted polarization function. The deviation of the fit on the low-field side of the μSR line shape is attributed to the sample geometry effect discussed in Sec. III.D.3. As described in Sec. V, r_0 is extracted from the peak of the supercurrent density profile corresponding to the fitted $B(r)$ (see Fig. 40). Figure 41 shows the magnetic-field dependence of r_0 in $NbSe_2$ and its sensitivity to the model of $B(r)$ used to generate the $J_s(r)$ profile. There is only a weak model dependence, indicating that all of the models fit the vortex core reasonably well. The results obtained using the Ginzburg-Landau model are believed to be the most accurate, since this model self-consistently accounts for the finite size of the vortex cores.

The field dependence of the fitted value of the Ginzburg-Landau coherence length ξ_{ab} [from Eq. (35)] is shown in Fig. 42. At high field the value of ξ_{ab} is comparable to r_0. The length scale ξ_{ab} characterizes the spatial variation of the order parameter within the vor-

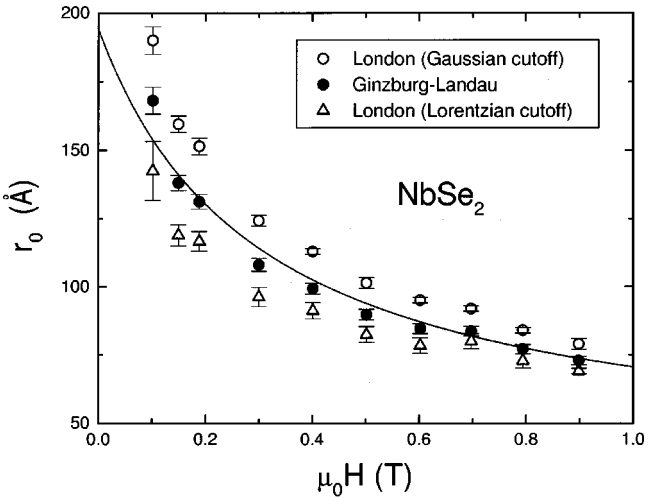

FIG. 41. Magnetic-field dependence of the core radius r_0 in $NbSe_2$ at $T=2.3$ K obtained from the $J_s(r)$ profiles generated from fits to three different models for $B(r)$: solid curve, a fit to the results for the Ginzburg-Landau model (solid circles) which depends only on the intervortex spacing. From Sonier, Kiefl, *et al.*, 1997b.

tex core. This is different from the BCS coherence length ξ_0, which characterizes the spatial extent of the Cooper pair wave function in the pure superconducting medium and is directly related to the energy-gap function [see Eq. (42)]. In a μSR experiment, the extracted value of ξ_{ab} will depend on the model assumed for $B(r)$. On the other hand, as discussed in Sec. V and shown in Fig. 41, r_0 is fairly robust with respect to the model for $B(r)$.

A strong magnetic-field dependence of r_0 (and ξ_{ab}) has also been measured in detwinned single crystals of optimally-doped $YBa_2Cu_3O_{6.95}$ (Sonier, Kiefl, *et al.*, 1999; Sonier, Brewer, *et al.*, 1999) and underdoped $YBa_2Cu_3O_{6.60}$ (Sonier, Brewer, *et al.*, 1997). Figure 43 shows the measurements in the optimally doped crystals.

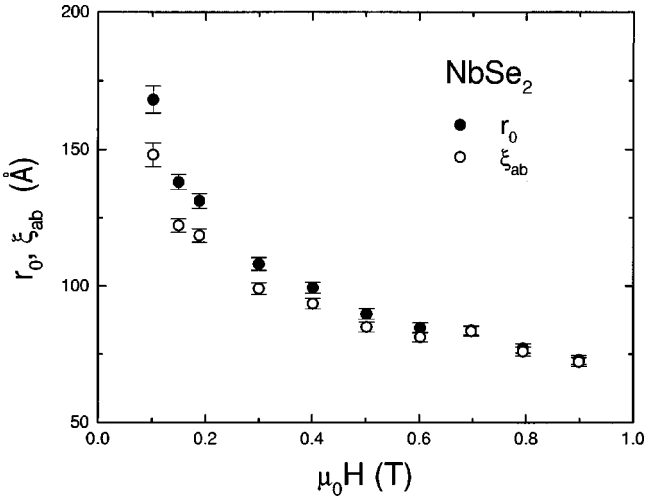

FIG. 42. Magnetic-field dependence in $NbSe_2$ at $T=2.3$ K: ○, of the Ginzburg-Landau coherence length ξ_{ab}; ●, of the vortex core radius r_0.

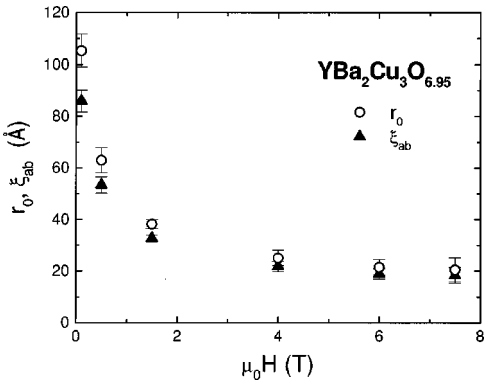

FIG. 43. Magnetic-field dependence ξ_{ab} in detwinned single crystals of $YBa_2Cu_3O_{6.95}$ extrapolated to $T=0$ K: ▲, of the Ginzburg-Landau coherence length ξ_{ab}; ○, of the vortex core radius r_0. From Sonier, Brewer, *et al.*, 1999.

At high field the size of the vortex cores saturates at $\xi_{ab}\approx 18.5$ Å, implying a value of $H_{c2}(0)=96.3$ T for the upper critical field at $T=0$ K. These values agree quantitatively with estimates from other experimental techniques. However, μSR is the only technique that has directly measured ξ_{ab} deep in the superconducting state.

Several theoretical studies predict that r_0 shrinks with increasing magnetic field (Golubov and Hartmann, 1994; Ichioka, Hasegawa, and Machida, 1999a, 1999b; see Sec. III.B.4 and Sec. III.C.2). In these studies r_0 was obtained from the self-consistent supercurrent density distribution of the Eilenberger (or Usadel) equations. The variation of r_0 with magnetic field is found to be similar to the field dependence of the length scale ξ_1, defined from the initial slope of the order parameter at the vortex center [see Eq. (32)]. The reduction of the superconducting order parameter within a vortex costs *condensation energy*. This energy cost increases with increasing magnetic field, because the density of vortices in the sample increases, i.e., $n_f=B_0/\Phi_0$. A consequence of the

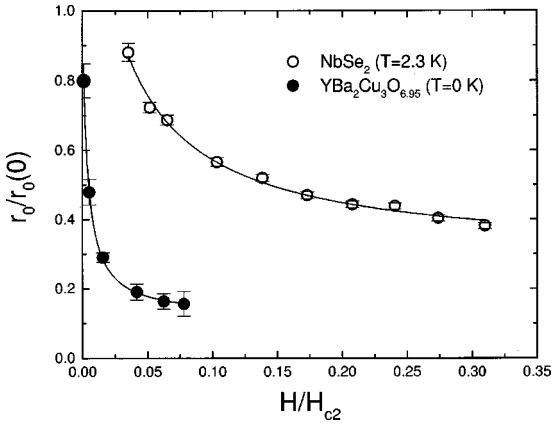

FIG. 44. Magnetic-field dependence of the core size r_0 normalized to the extrapolated value $r_0(\mu_0 H=0)$: ○, for single-crystal $NbSe_2$ at $T=2.3$ K; ●, for $YBa_2Cu_3O_{6.95}$ extrapolated to $T=0$ K.

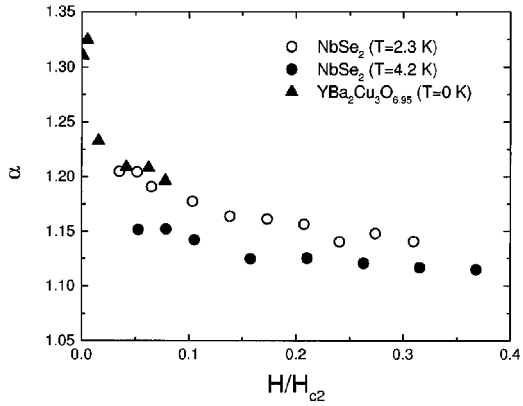

FIG. 45. Magnetic-field dependence of the skewness parameter α: ○, in $NbSe_2$ at $T=2.3$ K; ●, at 4.2 K; ▲, in $YBa_2Cu_3O_{6.95}$ extrapolated to $T=0$ K.

shrinking vortex cores with increasing magnetic field is that some of the energy lost due to the formation of additional vortices is saved.

The strength of the field dependence of the core size in $NbSe_2$ is compared with that in $YBa_2Cu_3O_{6.95}$ in Fig. 44. At low field, the value of r_0 in $YBa_2Cu_3O_{6.95}$ decreases more rapidly with increasing magnetic field than in $NbSe_2$. The theoretical calculations of Ichioka, Hasegawa, and Machida (1999b) predict precisely this difference between an s-wave and $d_{x^2-y^2}$-wave superconductor.

It might be argued that the field dependence of r_0 measured by μSR could have some other origin, unrelated to an actual change in the slope of the supercurrent density (or order parameter) within the vortex core. A possible explanation is that, in the layered systems studied, the weak interactions between vortices at low fields allow for strong random pinning of individual pancake vortices. For this case, the muons detect an enlarged effective core size associated with the random wandering of the vortex lines. This effect decreases the length of the high-field tail of the μSR line shape. Furthermore, the field distribution becomes symmetric at an external field that is substantially smaller than the decoupling field at which the vortex lines are completely destroyed by pinning (Koshelev, Glazman, and Larkin, 1996). However, the field dependence of the skewness parameter α (see Fig. 45) measured in $NbSe_2$ and $YBa_2Cu_3O_{7-\delta}$ at low temperatures agrees well with the quasiclassical predictions for an ideal vortex lattice in an s-wave and $d_{x^2-y^2}$-wave superconductor, respectively (Ichioka, Hasegawa, and Machida, 1999b). In particular, the value of α is greater than unity at all fields considered, as expected for an ideal lattice of straight vortex lines.

An alternative explanation for the field dependence of r_0 may be that the muons detect the field averaged over the zero-point motion of the vortices at low magnetic fields. However, a sizable contribution from this effect would also reduce the asymmetry of the μSR line shape.

Hartmann, Drechsler, and Heiden (1993) measured the spatial variation of the tunneling current across individual vortices at the surface of $NbSe_2$ with an STS probe. The tunneling current profile, which reflects the local density of states at the sample surface, is roughly Gaussian-shaped due to the spatial variation of the localized quasiparticle core states. The half-width of the tunneling current profile was found to increase with decreasing field, implying an increase of the vortex core radius. STS does not probe deep enough into the surface to be sensitive to vortex line wandering. On the other hand, because the STS tip scans across the vortices at a rate considerably slower than vortex fluctuations, the STS measurements (like μSR) are sensitive to zero-point motion of the vortices.

Although there may be several possible origins for the field dependence of the core size reported in the μSR and STS experiments, many of these ideas are incompatible with a recent specific-heat study that has established a direct link between the quasiparticle excitation spectrum of the vortex cores and the μSR measurements (Sonier, Hundley, *et al.*, 1999). In an s-wave superconductor, there is a contribution to the linear-T term of the electronic specific heat $C(H)$ that is proportional to the density of localized quasiparticle states in the vortex core. Since the density of vortices increases linearly as a function of magnetic field, this term is expected to be proportional to H. However, the magnetic-field dependence of $C(H)/T$ in $NbSe_2$ was observed to have a curvature at low fields. It was shown that this low-field curvature is precisely accounted for by the expansion of the vortex cores measured with μSR and the field dependence of the magnetic induction B above H_{c1}. The increased size of the vortices at low fields produces a corresponding increase in the density of bound quasiparticle states in the vortex cores, which in turn results in the observed low-field curvature of $C(H)/T$. Since neither vortex fluctuations nor random wandering of the vortex lines should change the electronic structure of the vortex cores in this way, this study strongly suggests that μSR is sensitive to intrinsic changes in vortex core size. As discussed by Sonier, Hundley, *et al.* (1999), there have been many reports of similar curvature of $C(H)/T$ at low magnetic fields in other s-wave superconductors. In some of these studies the variation with field was found to be hysteretic—presumably due to disorder of the vortex lattice. This suggests that the field dependence of the core size is somehow related to the nature of the vortex-vortex interactions.

Recently, Nohara *et al.* (1999) measured the magnetic-field dependence of the specific heat in pure and alloyed $Y(Ni_{1-x}Pt_x)_2B_2C$ and $Nb_{1-x}Ta_xSe_2$ single crystals. They observed a low-field curvature of $C(H)/T$ in the pure $(x=0)$ samples. However, in the alloyed $(x=0.2)$ samples $C(H)/T$ was found to be proportional to H. The authors attribute the low-field curvature in the pure sample to the shrinking of the vortex cores with increasing magnetic field. They speculate that the core shrinking arises from a repulsive vortex-vortex interaction mediated by a coherent transfer of quasiparticles between the cores. Impurity scattering would disrupt the coherent motion of these quasiparticles, thus eliminating

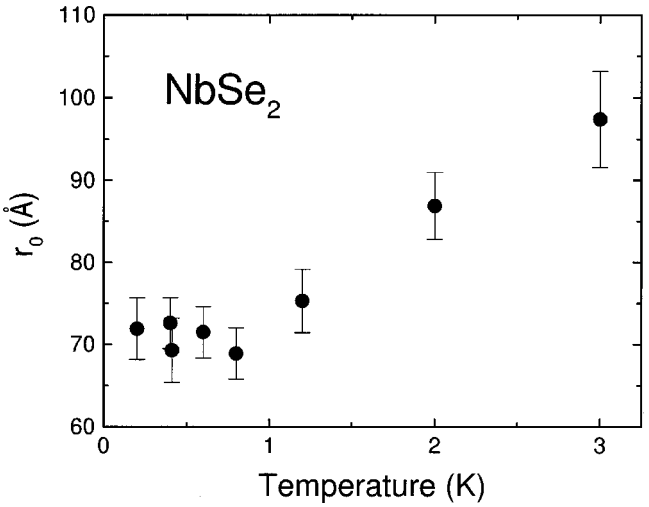

FIG. 46. Temperature dependence of the vortex core size r_0 in $NbSe_2$ at $\mu_0 H = 0.5$ T. From Miller *et al.*, 1999.

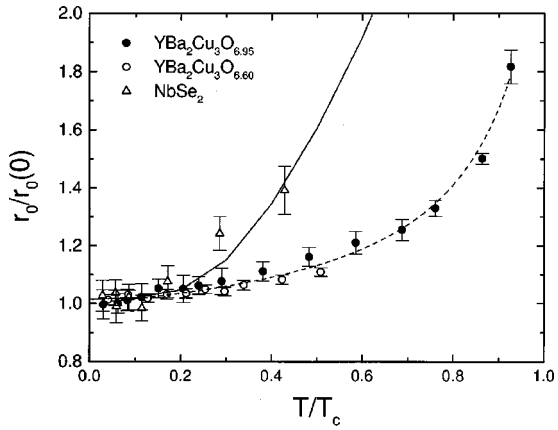

FIG. 47. Temperature dependence of the core size $r_0(T)/r_0(0)$ in $NbSe_2$, $T_c = 7$ K (Miller *et al.*, 1999), $YBa_2Cu_3O_{6.95}$, $T_c = 93.2$ K (Sonier, Kiefl, *et al.*, 1999), and $YBa_2Cu_3O_{6.60}$, $T_c = 59$ K (Sonier, Brewer, *et al.*, 1997) at $\mu_0 H = 0.5$ T.

the field dependence of the core size in dirty superconductors. In the same study Nohara *et al.* show that the temperature dependence of the upper critical field H_{c2} shows positive curvature near T_c only in the pure samples. Using the relation $H_{c2} = \Phi_0/2\pi\xi^2$ they remark that the positive curvature is evidence that the core size shrinks with increasing field, since this enhances H_{c2}.

In summary, although results to date are highly suggestive of an intrinsic mechanism responsible for the field dependence of the effective core size measured with μSR, it is unclear as to how far the vortex lattice at low fields deviates from the ideal Abrikosov lattice. Certainly, both flux-lattice disorder and the wandering of vortex lines play some role in these measurements. Studies of isotropic (i.e., nonlayered) systems and direct measurements with other experimental techniques comprise future endeavors needed to resolve this issue.

B. Temperature dependence

As explained in Sec. III.D.3, thermal fluctuations of the vortices can increase the effective core size measured with μSR. This must be taken into account when interpreting measurements of the temperature dependence of r_0. Despite this complication, a number of important trends have been established.

For $NbSe_2$, μSR studies of single crystals show that the value of r_0 decreases with decreasing temperature and becomes independent of temperature at $T \lesssim 1$ K (Sonier, Brewer, *et al.*, 1997; Miller *et al.*, 1999; see Fig. 46). Both of these features of the μSR data are predicted for the Kramer-Pesch effect, discussed in Sec. III.B.3. However, the strength of the temperature dependence of r_0 is weaker than predicted. This cannot be due to thermal fluctuations of the vortices, since fluctuations increase the effective core size measured with μSR. Thus the data shown in Fig. 46 represent an upper limit for the strength of the temperature dependence of r_0.

Another important discrepancy is that the saturation of r_0 occurs at a temperature higher than expected from theory. For example, Hayashi *et al.* (1998) predict that the reduction of the core size in $NbSe_2$ should saturate below 100 mK. There are several possible origins for the quantitative differences between the μSR results and the theoretical calculations of the Kramer-Pesch effect for $NbSe_2$. For instance, existing theories do not include the effect of vortex-vortex interactions. Naively, one expects the Kramer-Pesch effect to have a strong field dependence, if the core size varies with field. A complete μSR study of the magnetic-field dependence of the Kramer-Pesch effect has not yet been carried out. It is also possible that zero-point motion of the vortices may limit the low-temperature value of r_0. The importance of zero-point motion of vortices in real materials is at present unknown.

Scanning tunneling spectroscopy measurements carried out on $NbSe_2$ over the temperature range $1.8 \lesssim T \lesssim 6$ K clearly show that the size of the vortex cores (estimated from the spatial dependence of the tunneling current) is reduced with decreasing temperature (Volodin, Golubov, and Aarts, 1997). Furthermore, this same study shows that the size of the vortex cores at low T also depends on the value of the bias voltage. Volodin, Golubov, and Aarts (1997) attributed the energy dependence to the BCS coherence factors for an s-wave superconductor.

The temperature dependence of r_0 measured with μSR in single crystals of $YBa_2Cu_3O_{7-\delta}$ (Sonier, Kiefl, *et al.*, 1997b, 1999) is found to be considerably weaker than in $NbSe_2$ (see Fig. 47). Thermal fluctuations are expected to be larger in the high-temperature superconductors, so the actual temperature dependence of r_0 in $YBa_2Cu_3O_{7-\delta}$ is likely to be even weaker than that shown in Fig. 47. Hayashi, *et al.* (1998) have argued that the quantum-limit temperature in $YBa_2Cu_3O_{7-\delta}$ is much higher than in $NbSe_2$, resulting in a weak Kramer-Pesch effect. To date, the Kramer-Pesch effect for a $d_{x^2-y^2}$-wave superconductor has not been calculated in the quantum limit.

The μSR measurements on $YBa_2Cu_3O_{6.95}$ ($T_c = 93.2$ K) are in agreement with microwave power absorption measurements in the vortex state of $T_c = 90$ K, $YBa_2Cu_3O_{7-\delta}$ single crystals (Matsuda *et al.*, 1994), which show no evidence for the Kramer-Pesch effect. However, in this microwave study the derivative of the field with respect to the surface resistance in $T_c = 60$ K single crystals is found to be proportional to $\ln(T_c/T)$. This temperature dependence is predicted from the Kramer-Pesch effect (Doettinger, Huebener, and Kittelberger, 1997). This result contradicts the μSR measurements on $YBa_2Cu_3O_{6.60}$ ($T_c = 59$ K) single crystals (Sonier, Brewer, *et al.*, 1997), which show a weak temperature dependence for r_0, comparable to that measured in $YBa_2Cu_3O_{6.95}$ (see Fig. 47). The difference is an important one, since there is still some debate as to whether the vortex cores of the high-temperature superconductors contain bound quasiparticle states and thus whether a Kramer-Pesch effect exists in these materials.

Finally, we note that flux-flow resistance measurements performed on thin films of the electron-doped compound $Nd_{1.85}Ce_{0.15}CuO_{4-\delta}$ (Doettinger, Huebener, and Kittelberger, 1997) indirectly show evidence for a Kramer-Pesch effect, in a logarithmic dependence of voltage on current. The Kramer-Pesch effect in this case arises from the excitation of quasiparticle core states due to the current-induced electric field, rather than from thermal excitations as in the case of a static vortex. On the other hand, no logarithmic dependence was found in the I-V characteristics of thin films of the hole-doped compound $La_{1.85}Sr_{0.15}CuO_{4-\delta}$. The pairing symmetries in the electron- and hole-doped high-temperature cuprate superconductors are generally believed to be those of s waves and $d_{x^2-y^2}$-waves, respectively. The absence of a Kramer-Pesch effect in the hole-doped compound may be due to the delocalized quasiparticles associated with the cores, which dominate the energy dissipation for a moving vortex. Depopulation of these quasiparticle states has therefore little effect on the vortex core size.

VI. SUMMARY

In this review, we have shown that transverse-field μSR measurements of the magnetic-field distribution in the vortex state of a type-II superconductor provide a unique way of obtaining reliable information about the behavior of the characteristic length scales deep in the superconducting state. Although it is certainly desirable to have prior knowledge of the vortex structure, it is not an absolute requirement for employing the μSR technique. In the high-temperature cuprate superconductors and other unconventional systems, for which a consensus concerning the structure of the vortex lattice is not well established, μSR has found clear differences from conventional low-T_c superconductors in the behavior of λ and the effective vortex core size r_0. We have demonstrated through a number of examples that μSR is also a powerful tool for investigating exotic vortex phases.

We have argued that the temperature dependence of the magnetic penetration depth λ can be measured accurately with μSR—as borne out by the good agreement with microwave cavity perturbation measurements on similar crystals. At low magnetic fields, μSR has established that the supercurrent response in the bulk of a superconductor is similar to that at the sample's surface. When the measured field distribution is inaccurately modeled, however, the absolute value of λ becomes uncertain. Thus one must be cautious when using absolute values of λ reported from a μSR experiment.

We have pointed out that measurements of the magnetic-field dependence of λ are generally more difficult in the vortex state, because the positions of the vortices change with field. In this case, both the variation and the absolute value of λ as a function of magnetic field depend strongly on the manner in which the measured field distribution is modeled. Nevertheless, upper and lower limits on the strength of the field dependence can usually be established. In the present review article we have shown that there is some intrinsic field dependence of λ in both conventional and high-temperature superconductors. The considerably stronger field dependence in the latter is undoubtedly related to the nodes in the superconducting energy gap.

We have shown that the variation of the effective vortex core size with temperature and magnetic field in the bulk of a sample can be measured with μSR. The results of μSR studies of the core size exhibit the general trends predicted by theory. However, there are important quantitative discrepancies between experiment and theory, which at present are only partially understood.

Finally, we remark that despite the tremendous advancements in μSR measurements of the vortex state in recent years, future efforts will undoubtedly lead to exciting new findings. In particular, the development of new spectrometers capable of greatly enhancing the counting rates (thus increasing the sensistivity to the vortex core region), advancements in modeling μSR spectra, improvements in the general understanding of the vortex structure through other techniques, and the further development of ultralow-energy muon beams will make possible future endeavours that will certainly lead to a deeper understanding of the vortex state.

ACKNOWLEDGMENTS

We would like to thank our many long-term experimental collaborators who continue to provide valuable assistance in our ongoing projects. We have benefited from discussions and exchange of ideas with K. Machida, I. Affleck, D. F. Agterberg, M. H. S. Amin, A. J. Berlinsky, and M. Franz. We thank those members of the μSR community who graciously provided both figures and further insight into their work. The writing of this review article was supported by the Natural Sciences and Engineering Research Council of Canada, the Canadian Institute for Advanced Research, and at Los Alamos National Laboratory by the U.S. Department of Energy.

REFERENCES

Abragam, A., 1970, *The Principles of Nuclear Magnetism* (Oxford, Clarendon).

Abrikosov, A. A., 1957, Sov. Phys. JETP **5**, 1174.

Abrikosov, A. A., and L. P. Gor'kov, 1961, Sov. Phys. JETP **12**, 1243.

Aegerter, C. M., J. Hofer, I. M. Savíc, H. Keller, S. L. Lee, C. Ager, S. H. Lloyd, and E. M. Forgan, 1998, Phys. Rev. B **57**, 1253.

Aegerter, C. M., S. L. Lee, H. Keller, E. M. Forgan, and S. H. Lloyd, 1996, Phys. Rev. B **54**, R15 661.

Aegerter, C. M., S. H. Lloyd, C. Ager, S. L. Lee, S. Romer, H. Keller, and E. M. Forgan, 1998, J. Phys.: Condens. Matter **10**, 7445.

Aeppli, G., R. J. Cava, E. J. Ansaldo, J. H. Brewer, S. R. Kreitzman, G. M. Luke, D. R. Noakes, and R. F. Kiefl, 1987, Phys. Rev. B **35**, 7129.

Affleck, I., M. Franz, and M. H. Amin, 1996, Phys. Rev. B **55**, R704.

Agterberg, D. F., 1998, Phys. Rev. B **58**, 14 484.

Alloul, H., P. Mendels, H. Casalta, J. F. Marucco, and J. Arabski, 1991, Phys. Rev. Lett. **67**, 3140.

Amato, A., 1997, Rev. Mod. Phys. **69**, 1119.

Amin, M. H. S., I. Affleck, and M. Franz, 1998, Phys. Rev. B **58**, 5848.

Amin, M. H. S., M. Franz, and I. Affleck, 2000, Phys. Rev. Lett. **84**, 5864.

Anlage Steven, M., Dong Ho Wu, Jian Mao, S. N. Mao, X. X. Xi, T. Venkatesan, J. L. Peng, and R. L. Greene, 1994, Phys. Rev. B **50**, 523.

Annett, J. F., N. D. Goldenfeld, and A. J. Leggett, 1996, in *Physical Properties of High-Temperature Superconductors V*, edited by D. M. Ginsberg (World Scientific, Singapore), p. 375.

Annett, J. F., N. D. Goldenfeld, and S. R. Renn, 1991, Phys. Rev. B **43**, 2778.

Ansaldo, E. J., Ch. Niedermayer, J. L. Tallon, D. M. Pooke, J. H. Brewer, and G. D. Morris, 1991, Phys. Lett. A **158**, 479.

Arovas, D. P., A. J. Berlinsky, C. Kallin, and Shou-Cheng Zhang, 1997, Phys. Rev. Lett. **79**, 2867.

Atkinson, W. A., 1999, Phys. Rev. B **59**, 3377.

Bardeen, J., 1954, Phys. Rev. **94**, 554.

Bardeen, J., L. N. Cooper, and J. R. Schrieffer, 1957, Phys. Rev. **108**, 1175.

Bardeen, J., and M. J. Stephen, 1965, Phys. Rev. **140**, A1197.

Berlinsky, A. J., A. L. Fetter, M. Franz, C. Kallin, and P. I. Soininen, 1995, Phys. Rev. Lett. **75**, 2200.

Bernhard, C., Ch. Niedermayer, *et al.*, 1995, Phys. Rev. B **52**, R7050.

Bernhard, C., Ch. Niedermayer, *et al.*, 1996, Phys. Rev. B **53**, 8790.

Bernhard, C., J. L. Tallon, C. Bucci, R. De Renzi, G. Guidi, G. V. M. Williams, and Ch. Niedermayer, 1996, Phys. Rev. Lett. **77**, 2304.

Bernhard, C., J. L. Tallon, C. Bucci, R. De Renzi, G. Guidi, G. V. M. Williams, and Ch. Niedermayer, 1998, Phys. Rev. Lett. **80**, 205.

Beveridge, J. L., J. Doornbos, D. M. Garner, D. J. Arseneau, I. D. Reid, and M. Senba, 1985, Nucl. Instrum. Methods Phys. Res. A **240**, 316.

Bidinosti, C. P., W. N. Hardy, D. A. Bonn, and Ruixing Liang, 1999, Phys. Rev. Lett. **83**, 3277.

Billon, B., M. Charalambous, J. Chaussy, R. Koch, and R. Liang, 1997, Phys. Rev. B **55**, R14 753.

Bitter, F., 1931, Phys. Rev. **38**, 1903.

Blasius, T., Ch. Niedermayer, J. L. Tallon, D. M. Pooke, A. Golnik, and C. Bernhard, 1999, Phys. Rev. Lett. **82**, 4926.

Blatter, G., M. V. Feigel'man, V. B. Geshkenbein, A. I. Larkin, and V. M. Vinokur, 1994, Rev. Mod. Phys. **66**, 1125.

Blatter, G., V. Geshkebein, A. Larkin, and H. Nordberg, 1996, Phys. Rev. B **54**, 72.

Blatter, G., and B. I. Ivlev, 1993, Phys. Rev. Lett. **70**, 2621.

Blatter, G., and B. I. Ivlev, 1994, Phys. Rev. B **50**, 10 272.

Bonn, D. A., S. Kamal, A. Bonakdarpour, Ruixing Liang, W. N. Hardy, C. C. Homes, D. N. Basov, and T. Timusk, 1996, Czech. J. Phys. **46**, 3195.

Bonn, D. A., S. Kamal, K. Zhang, R. Liang, D. J. Barr, E. Klein, and W. N. Hardy, 1994, Phys. Rev. B **50**, 4051.

Brandt, E. H., 1972, Phys. Status Solidi B **51**, 345.

Brandt, E. H., 1977a, J. Low Temp. Phys. **26**, 709.

Brandt, E. H., 1977b, J. Low Temp. Phys. **26**, 735.

Brandt, E. H., 1977c, J. Low Temp. Phys. **28**, 263.

Brandt, E. H., 1977d, J. Low Temp. Phys. **28**, 291.

Brandt, E. H., 1988a, J. Low Temp. Phys. **73**, 355.

Brandt, E. H., 1988b, Phys. Rev. B **37**, 2349.

Brandt, E. H., 1989, Phys. Rev. Lett. **63**, 1106.

Brandt, E. H., 1991, Phys. Rev. Lett. **66**, 3213.

Brandt, E. H., 1997, Phys. Rev. Lett. **78**, 2208.

Brandt, E. H., and A. Seeger, 1986, Adv. Phys. **35**, 189.

Brandt, E. H., and U. Essmann, 1987, Phys. Status Solidi B **144**, 13.

Brewer, J. H., 1994, in *Encyclopedia of Applied Physics*, edited by G. L. Trigg (VCH, New York), Vol. 11, p. 23.

Brewer, J. H., E. J. Ansaldo, *et al.*, 1988, Phys. Rev. Lett. **60**, 1073.

Brewer, J. H., R. F. Kiefl, *et al.*, 1990, Hyperfine Interact. **63**, 177.

Brezin, E., D. R. Nelson, and A. Thiaville, 1985, Phys. Rev. B **31**, 7124.

Brinkmann, M., T. Rex., H. Bach, and K. Westerholt, 1996, J. Cryst. Growth **163**, 369.

Broun, D. M., D. C. Morgan, R. J. Ormeno, S. F. Lee, A. W. Tyler, A. P. Mackenzie, and J. R. Waldram, 1997, Phys. Rev. B **56**, R11 443.

Budnick, J. I., B. Chamberland, D. P. Yang, C. Niedermayer, A. Golnik, E. Recknagel, M. Rossmanith, and A. Weidinger, 1988, Europhys. Lett. **5**, 651.

Campbell, L. J., M. M. Doria, and V. G. Kogan, 1988, Phys. Rev. B **38**, 2439.

Caroli, C., P. G. de Gennes, and J. Matricon, 1964, Phys. Lett. **9**, 307.

Clem, J. R., 1975, J. Low Temp. Phys. **18**, 427.

Clem, J. R., 1991, Phys. Rev. B **43**, 7837.

Cooley, J. W., and J. W. Tukey, 1965, Math. Comput. **19**, 297.

Cooper, J. R., 1996, Phys. Rev. B **54**, R3753.

Cox, S. F. J., 1987, J. Phys. C **20**, 3107.

Crabtree, D. W., and D. Nelson, 1997, Phys. Today **50** (4), 38.

Cubitt, R., *et al.*, 1993, Nature (London) **365**, 407.

Daemen, L. L., L. J. Campbell, and V. G. Kogan, 1992, Phys. Rev. B **46**, 3631.

Daeumling, M., J. M. Seuntjens, and D. C. Larbalestier, 1990, Nature (London) **346**, 6282.

de Vaulchier, L. A., J. P. Vieren, Y. Guldner, N. Bontemps, R. Combescot, Y. Lemaitre, and J. C. Mage, 1996, Europhys. Lett. **33**, 153.

de Wilde, Y., M. Iavarone, U. Welp, V. Metlushko, A. E. Koshelev, I. Aranson, G. W. Crabtree, and P. C. Canfield, 1997, Phys. Rev. Lett. **78**, 4273.
Doettinger, S. G., R. P. Huebener, and S. Kittelberger, 1997, Phys. Rev. B **55**, 6044.
Dolan, G. J., F. Holtzberg, C. Feild, and T. R. Dinger, 1989, Phys. Rev. Lett. **62**, 218.
Drulis, H., Z. G. Xu, J. W. Brill, L. E. De Long, and J. C. Hou, 1991, Phys. Rev. B **44**, 4731.
Eilenberger, G., 1968, Z. Phys. **214**, 195.
Eskildsen, M. R., *et al.*, 1997, Phys. Rev. Lett. **78**, 1968.
Feigel'man, M. V., V. B. Geshkenbein, A. I. Larkin, and V. M. Vinokur, 1989, Phys. Rev. Lett. **63**, 2303.
Feigel'man, M. V., and V. M. Vinokur, 1990, Phys. Rev. B **41**, 8986.
Felner, I., D. Hechel, and U. Yaron, 1990, Physica C **165**, 247.
Fendrich, J. A., U. Welp, W. K. Kwok, A. E. Koshelev, G. W. Crabtree, and B. W. Veal, 1996, Phys. Rev. Lett. **77**, 2073.
Fesenko, V., V. Gorbunov, A. Sidorenko, and V. Smilga, 1993, Physica C **211**, 343.
Fisher, D. S., M. P. A. Fisher, and D. A. Huse, 1991, Phys. Rev. B **43**, 130.
Fisher, M. P. A., 1989, Phys. Rev. Lett. **62**, 1415.
Forgan, E. M., and S. L. Lee, 1995, Phys. Rev. Lett. **75**, 1422.
Forgan, E. M., D. M. Paul, H. A. Mook, P. A. Timmins, H. Keller, S. Sutton, and J. S. Abell, 1990, Nature (London) **343**, 735.
Forgan, E. M., M. T. Wylie, S. Lloyd, M. P. Nutley, S. L. Lee, R. Cubitt, C. Aegerter, H. Keller, and T. W. Li, 1997, Hyperfine Interact. **105**, 61.
Fortune, N. A., K. Murata, M. Ishibashi, Y. Yokoyama, and Y. Nishihara, 1991, Phys. Rev. B **43**, 12 930.
Franz, M., I. Affleck, and M. H. S. Amin, 1997, Phys. Rev. Lett. **79**, 1555.
Franz, M., C. Kallin, A. J. Berlinsky, and M. L. Salkola, 1997, Phys. Rev. B **56**, 7882.
Franz, M., C. Kallin, P. I. Soininen, A. J. Berlinsky, and A. L. Fetter, 1996, Phys. Rev. B **53**, 5795.
Franz, M., and Z. Tešanović, 1998, Phys. Rev. Lett. **80**, 4763.
Gammel, P. L., D. J. Bishop, G. J. Dolan, J. R. Kwo, C. A. Murray, L. F. Schneemeyer, and J. V. Waszczak, 1987, Phys. Rev. Lett. **59**, 2592.
Gammel, P. L., D. A. Huse, R. N. Kleiman, B. Batlogg, C. S. Oglesby, E. Bucher, D. J. Bishop, T. E. Mason, and K. Mortensen, 1994, Phys. Rev. Lett. **72**, 278.
Giamarchi, T., and P. Le Doussal, 1995, Phys. Rev. B **52**, 1242.
Ginzburg, V. L., and L. D. Landau, 1950, Zh. Éksp. Teor. Fiz. **20**, 1064 [Sov. Phys. JETP **20**, 1964 (1950)].
Golubov, A. A., and U. Hartmann, 1994, Phys. Rev. Lett. **72**, 3602.
Gor'kov, L. P., 1958, Sov. Phys. JETP **7**, 505.
Gor'kov, L. P., 1959, Sov. Phys. JETP **9**, 1364.
Gross, F., *et al.*, 1964, Z. Phys. **64**, 175.
Gygi, F., and M. Schlüter, 1990, Phys. Rev. B **41**, 822.
Gygi, F., and M. Schlüter, 1991, Phys. Rev. B **43**, 7609.
Hao, Z., J. R. Clem, M. W. McElfresh, L. Civale, A. P. Malozemoff, and F. Holtzberg, 1991, Phys. Rev. B **43**, 2844.
Hardy, W. N., D. A. Bonn, D. C. Morgan, Ruixing Liang, and Kuan Zhang, 1993, Phys. Rev. Lett. **70**, 3999.
Harshmann, D. R., G. Aeppli, *et al.*, 1987, Phys. Rev. B **36**, 2386.
Harshman, D. R., E. H. Brandt, A. T. Fiory, M. Inui, D. B. Mitzi, L. F. Schneemeyer, and J. V. Waszczak, 1993, Phys. Rev. B **47**, 2905.
Harshman, D. R., R. N. Kleiman, M. Inui, G. P. Espinosa, D. B. Mitzi, A. Kapitulnik, T. Pfiz, and D. Ll. Williams, 1991, Phys. Rev. Lett. **67**, 3152.
Harshmann, D. R., L. F. Schneemeyer, *et al.*, 1989, Phys. Rev. B **39**, 851.
Hartmann, U., T. Drechsler, and C. Heiden, 1993, Proc. SPIE **1855**, 140.
Hayashi, N., M. Ichioka, and K. Machida, 1996, Phys. Rev. Lett. **77**, 4074.
Hayashi, N., M. Ichioka, and K. Machida, 1997, Phys. Rev. B **56**, 9052.
Hayashi, N., T. Isoshima, M. Ichioka, and K. Machida, 1998, Phys. Rev. Lett. **80**, 2921.
Heeb, R., and D. F. Agterberg, 1999, Phys. Rev. B **59**, 7076.
Heeb, R., A. van Otterlo, M. Sigrist, and G. Blatter, 1996, Phys. Rev. B **54**, 9385.
Heffner, R. H., *et al.*, 1990, Phys. Rev. Lett. **65**, 2816.
Herlach, D., *et al.*, 1990, Hyperfine Interact. **63**, 41.
Hess, H. F., 1991, Physica C **185-189**, 259.
Hess, H. F., C. A. Murray, and J. V. Waszczak, 1992, Phys. Rev. Lett. **69**, 2138.
Hess, H. F., R. B. Robinson, R. C. Dynes, J. M. Valles, Jr., and J. V. Waszczak, 1989, Phys. Rev. Lett. **62**, 214.
Hess, H. F., R. B. Robinson, and J. V. Waszczak, 1990, Phys. Rev. Lett. **64**, 2711.
Hettler, M. H., and P. J. Hirschfeld, 1999, Phys. Rev. B **59**, 9606.
Himeda, A., M. Ogata, Y. Tanaka, and S. Kashiwaya, 1997, J. Phys. Soc. Jpn. **66**, 3367.
Hirshfeld, P. J., 1995, J. Phys. Chem. Solids **56**, 1605.
Hirshfeld, P. J., and N. Goldenfeld, 1993, Phys. Rev. B **48**, 4219.
Houghton, A., R. A. Pelcovits, and A. A. Sudbø, 1989, Phys. Rev. B **40**, 6763.
Huse, D. A., 1992, Phys. Rev. B **46**, 8621.
Ichioka, M., N. Enomoto, N. Hayashi, and K. Machida, 1996a, Phys. Rev. B **53**, 2233.
Ichioka, M., N. Enomoto, and K. Machida, 1997, J. Phys. Soc. Jpn. **66**, 3928.
Ichioka, M., A. Hasegawa, and K. Machida, 1999a, Phys. Rev. B **59**, 184.
Ichioka, M., A. Hasegawa, and K. Machida, 1999b, Phys. Rev. B **59**, 8902.
Ichioka, M., N. Hayashi, N. Enomoto, and K. Machida, 1996b, Phys. Rev. B **53**, 15 316.
Ichioka, M., N. Hayashi, and K. Machida, 1997, Phys. Rev. B **55**, 6565.
Indenbom, M. V., H. Kronmüller, T. W. Li, P. H. Kes, and A. A. Menovsky, 1994, Physica C **222**, 203.
Jackson, T. J., T. M. Riseman, E. M. Forgan, H. Glückler, T. Prokscha, E. Morenzoni, M. Pleines, Ch. Niedermayer, G. Shatz, H. Luetkens, and J. Litterst, 2000, Phys. Rev. Lett. **84**, 4958.
Jacobs, T., S. Sridhar, Qiang Li, G. D. Gu, and N. Koshizuka, 1995, Phys. Rev. Lett. **75**, 4516.
Jiang, X., Wu Jiang, S. N. Mao, R. L. Greene, T. Venkatesan, and C. J. Lobb, 1995, Physica C **254**, 175.
Johnson, S. T., *et al.*, 1999, Phys. Rev. Lett. **82**, 2792.

Karrai, K., E. J. Choi, F. Dunmore, S. Liu, H. D. Drew, Qi Li, D. B. Fenner, Y. D. Zhu, and Fu-Chun Zhang, 1992, Phys. Rev. Lett. **69**, 152.
Keimer, B., W. Y. Shih, R. W. Erwin, J. W. Lynn, F. Dogan, and I. A. Aksay, 1994, Phys. Rev. Lett. **73**, 3459.
Kiefl, R. F., J. H. Brewer, *et al.*, 1990, Phys. Rev. Lett. **64**, 2082.
Kiefl, R. F., W. A. MacFarlane, *et al.*, 1993, Phys. Rev. Lett. **70**, 3987.
Kiefl, R. F., T. M. Riseman, *et al.*, 1988, Physica C **153-155**, 757.
Kim, P., Z. Yao, and C. M. Lieber, 1996, Phys. Rev. Lett. **77**, 5118.
Kirtley, J. R., V. G. Kogan, J. R. Clem, and K. A. Moler, 1999, Phys. Rev. B **59**, 4343.
Klein, U., 1990, Phys. Rev. B **41**, 4819.
Kleiner, W. H., L. M. Roth, and S. H. Autler, 1964, Phys. Rev. **133**, A1226.
Kogan, V. G., M. Bullock, B. Harmon, P. Miranović, Lj. Dobrosavljević-Grujić, P. L. Gammel, and D. J. Bishop, 1997, Phys. Rev. B **55**, R8693.
Kogan, V. G., P. Miranović, Lj. Dobrosavljević-Grujić, W. E. Pickett, and D. K. Christen, 1997, Phys. Rev. Lett. **79**, 741.
Koshelev, A. E., L. I. Glazman, and A. I. Larkin, 1996, Phys. Rev. B **53**, 2786.
Kossler, W. J., Y. Dai, K. G. Petzinger, A. J. Greer, D. Ll. Williams, E. Koster, D. R. Harshman, and D. B. Mitzi, 1998, Phys. Rev. Lett. **80**, 592.
Kossler, W. J., A. D. Goonewardene, A. J. Greer, D. Li. Williams, E. Koster, D. R. Harshman, J. Z. Liu, and R. N. Shelton, 1997, Phys. Rev. B **56**, 2376.
Kosztin, I., and A. J. Legget, 1997, Phys. Rev. Lett. **79**, 135.
Kramer, L., and W. Pesch, 1974, Z. Phys. **269**, 59.
Kramer, L., W. Pesch, and R. J. Watts-Tobin, 1974, J. Low Temp. Phys. **14**, 29.
Krusin-Elbaum, L., L. Civale, F. Holtzberg, A. P. Malozemoff, and C. Field, 1991, Phys. Rev. Lett. **67**, 3156.
Kwok, W. K., J. Fendrich, U. Welp, S. Fleshler, J. Downey, and G. W. Crabtree, 1994, Phys. Rev. Lett. **72**, 1108.
Kwok, W. K., U. Welp, G. W. Crabtree, K. G. Vandervoort, R. Hulscher, and J. Z. Liu, 1990, Phys. Rev. Lett. **64**, 966.
Larkin, A. I., and Yu. V. Ovchinnikov, 1979, J. Low Temp. Phys. **34**, 409.
Lawrence, W. E., and S. Doniach, 1971, in *Proceedings of the Twelfth International Conference on Low-Temperature Physics*, edited by E. Kanda (Academic Press of Japan, Kyoto), p. 361.
Lee, Shih-Fu, D. C. Morgan, R. J. Ormeno, D. M. Broun, R. A. Doyle, J. R. Waldram, and K. Kadowaki, 1996, Phys. Rev. Lett. **77**, 735.
Lee, S. L., C. M. Aegerter, *et al.*, 1997, Phys. Rev. B **55**, 5666.
Lee, S. L., C. M. Aegerter, S. H. Lloyd, *et al.*, 1998, Phys. Rev. Lett. **81**, 5209.
Lee, S. L., F. L. Pratt, S. J. Blundell, C. M. Aegerter, P. A. Pattenden, K. H. Chow, E. M. Forgan, T. Sasaki, W. Hayes, and H. Keller, 1997, Phys. Rev. Lett. **79**, 1563.
Lee, S. L., M. Warden, *et al.*, 1995, Phys. Rev. Lett. **75**, 922.
Lee, S. L., P. Zimmermann, *et al.*, 1993, Phys. Rev. Lett. **71**, 3862.
Legris, A., F. Rullier-Albenque, E. Radeva, and P. Lejay, 1993, J. Phys. I **3**, 1605.
Li, M.-R., P. J. Hirschfeld, and P. Wölfe, 1998, Phys. Rev. Lett. **81**, 5640.
Liang, R., D. A. Bonn, and W. N. Hardy, 1996, Phys. Rev. Lett. **76**, 835.
Lindemann, F., 1910, Phys. Z. **11**, 69.
London, F., and H. London, 1935, Proc. R. Soc. London, Ser. A **149**, 71.
Luke, G. M., Y. Fudamoto, *et al.*, 1997, Physica C **282-287**, 1465.
Luke, G. M., Y. Fudamoto, *et al.*, 1998, Nature (London) **394**, 558.
Luke, G. M., Y. Fudamoto, *et al.*, 1999, unpublished.
Luke, G. M., A. Keren, L. P. Le, W. D. Wu, Y. J. Uemura, D. A. Bonn, L. Taillefer, and J. D. Garrett, 1993, Phys. Rev. Lett. **71**, 1466.
Maeda, A., *et al.*, 1996, J. Phys. Soc. Jpn. **65**, 3638.
Maeda, A., Y. Iino, T. Hanaguri, N. Motohira, K. Kishio, and T. Fukase, 1995, Phys. Rev. Lett. **74**, 1202.
Maggio-Aprile, I., Ch. Renner, A. Erb, E. Walker, and Ø. Fischer, 1995, Phys. Rev. Lett. **75**, 2754.
Mahajan, A. V., H. Alloul, G. Collin, and J. F. Marucco, 1994, Phys. Rev. Lett. **72**, 3100.
Maki, K., and E. Puchkaryov, 1998, Europhys. Lett. **42**, 209.
Mao, Jian, D. H. Wu, J. L. Peng, R. L. Greene, and Steven M. Anlage, 1995, Phys. Rev. B **51**, R3316.
Marchetti, M. C., and D. R. Nelson, 1990, Phys. Rev. B **41**, 1910.
Matsuda, Y., N. P. Ong, Y. F. Yan, J. M. Harris, and J. B. Peterson, 1994, Phys. Rev. B **49**, 4380.
Meissner, W., and R. Ochsenfeld, 1933, Naturwissenschaften **21**, 787.
Menon, G. I., C. Dasgupta, and T. V. Ramakrishnan, 1999, Phys. Rev. B **60**, 7607.
Miller, R., R. F. Kiefl, J. H. Brewer, J. Chakhalian, S. Dunsiger, G. D. Morris, J. E. Sonier, and W. A. MacFarlane, 2000, Phys. Rev. Lett. (in press).
Morenzoni, E., F. Kottmann, D. Maden, B. Matthias, M. Meyberg, Th. Prokscha, Th. Wutzke, and U. Zimmermann, 1994, Phys. Rev. Lett. **72**, 2793.
Muhlschlegel, B., 1959, Z. Phys. **155**, 313.
Nachumi, B., *et al.*, 1996, Phys. Rev. Lett. **77**, 5421.
Nachumi, B., *et al.*, 1998, Phys. Rev. Lett. **80**, 206.
Nelson, D. R., 1988, Phys. Rev. Lett. **60**, 1973.
Nelson, D. R., and H. S. Seung, 1989, Phys. Rev. B **39**, 9153.
Nelson, D. R., and V. M. Vinokur, 1992, Phys. Rev. Lett. **68**, 2398.
Niedermayer, Ch., C. Bernhard, U. Binninger, H. Glückler, J. L. Tallon, E. J. Ansaldo, and J. I. Budnick, 1993, Phys. Rev. Lett. **71**, 1764.
Niedermayer, Ch., E. M. Forgan, *et al.*, 1999, Phys. Rev. Lett. **83**, 3932.
Nishida, N., and H. Miyatake, 1990, Hyperfine Interact. **63**, 183.
Nishida, N., H. Miyatake, *et al.*, 1987, Jpn. J. Appl. Phys., Part 1 **26**, 1856.
Nguyen, A. K., A. Sudbø, and R. E. Hetzel, 1996, Phys. Rev. Lett. **77**, 1592.
Nohara, M., M. Isshiki, F. Sakai, and H. Takagi, 1999, J. Phys. Soc. Jpn. **68**, 1078.
Nonomura, Y., X. Hu, and M. Tachiki, 1999, Phys. Rev. B **59**, R11 657.
Ogata, M., A. Himeda, Y. Tanaka, and S. Kashiwaya, 1998, J. Phys. Chem. Solids **59**, 1849.

Panagopoulos, C., J. R. Cooper, G. B. Peacock, I. Gameson, P. P. Edwards, W. Schmidbauer, and J. W. Hodby, 1996, Phys. Rev. B **53**, R2999.
Panagopoulos, C., B. D. Rainford, J. R. Cooper, W. Lo, J. L. Tallon, J. W. Loram, J. Betouras, Y. S. Wang, and C. W. Chu, 1999, Phys. Rev. B **60**, 14 617.
Paul, D. M., C. V. Tomy, C. M. Aegerter, R. Cubitt, S. H. Lloyd, E. M. Forgan, S. L. Lee, and M. Yethiraj, 1998, Phys. Rev. Lett. **80**, 1517.
Pesch, W., and L. Kramer, 1974, J. Low Temp. Phys. **15**, 367.
Pippard, A. B., 1950, Proc. R. Soc. London, Ser. A **203**, 210.
Prohammer, M., and J. P. Carbotte, 1991, Phys. Rev. B **43**, 5370.
Pümpin, B., *et al.*, 1990a, Phys. Rev. B **42**, 8019.
Pümpin, B., H. Keller, W. Kündig, I. M. Savíc, J. W. Schneider, H. Simmler, P. Zimmerman, E. Kaldis, and C. Rossel, 1990b, Hyperfine Interact. **63**, 25.
Rainer, D., J. A. Sauls, and D. Waxman, 1996, Phys. Rev. B **54**, 10 094.
Rainford, B. D., and G. J. Daniell, 1994, Hyperfine Interact. **87**, 1129.
Rao, T. V. Chandrasekhar, *et al.*, 1998, Physica C **299**, 267.
Ren, Y., J. H. Xu, and C. S. Ting, 1995, Phys. Rev. Lett. **74**, 3680.
Renner, Ch., B. Revaz, K. Kadowaki, I. Maggio-Aprile, and Ø. Fischer, 1998, Phys. Rev. Lett. **80**, 3606.
Riseman, T. M., 1993, Ph.D. thesis (University of British Columbia).
Riseman, T. M., *et al.*, 1995, Phys. Rev. B **52**, 10 569.
Riseman, T. M., *et al.*, 1998, Nature (London) **396**, 242.
Rosov, N., J. W. Lynn, and T. E. Grigereit, 1994, J. Appl. Phys. **76**, 6772.
Safar, H., P. L. Gammel, D. A. Huse, D. J. Bishop, W. C. Lee, J. Giapintzakis, and D. M. Ginsberg, 1993, Phys. Rev. Lett. **70**, 3800.
Safar, H., P. L. Gammel, D. A. Huse, D. J. Bishop, J. P. Rice, and D. M. Ginsberg, 1992, Phys. Rev. Lett. **69**, 824.
Schenck, A., 1985, *Muon Spin Rotation Spectroscopy: Principles and Applications in Solid State Physics* (Adam Hilger, Bristol, England).
Schilling, A., R. A. Fisher, N. E. Phillips, U. Welp, D. Dasgupta, W. K. Kwok, and G. W. Crabtree, 1996, Nature (London) **382**, 791.
Schilling, A., H. R. Ott, and Th. Wolf, 1992, Phys. Rev. B **46**, 14 253.
Schneider, J. W., R. F. Kiefl, *et al.*, 1993, Phys. Rev. Lett. **71**, 557.
Schneider, J. W., S. Schafroth, and P. F. Meier, 1995, Phys. Rev. B **52**, 3790.
Schopohl, N., and K. Maki, 1995, Phys. Rev. B **52**, 490.
Schwarz, W., E. H. Brandt, K.-P. Döring, U. Essmann, K. Fürderer, M. Gladisch, D. Herlach, G. Majer, H.-J. Mundinger, H. Orth, A. Seeger, and M. Schmolz, 1986, Hyperfine Interact. **31**, 247.
Serene, J. W., and D. Rainer, 1983, Phys. Rep. **101**, 221.
Shengelaya, A., C. M. Aegerter, S. Romer, H. Keller, P. W. Klamut, R. Dybzinski, B. Dabrowski, I. M. Savić, and J. Klamut, 1998, Phys. Rev. B **58**, 3457.
Shibauchi, T., N. Katase, T. Tamegai, and K. Uchinokura, 1996, Physica C **264**, 227.
Shore, J. D., M. Huang, A. T. Dorsey, and J. P. Sethna, 1989, Phys. Rev. Lett. **62**, 3089.
Soininen, P. I., C. Kallin, and A. J. Berlinsky, 1994, Phys. Rev. B **50**, 13 883.
Song, Y. Q., W. P. Halperin, L. Tonge, T. J. Marks, M. Ledvij, V. G. Kogan, and L. N. Bulaevskii, 1993, Phys. Rev. Lett. **70**, 3127.
Sonier, J. E., J. H. Brewer, *et al.*, 1997, Phys. Rev. Lett. **79**, 2875.
Sonier, J. E., J. H. Brewer, *et al.*, 1998, unpublished.
Sonier, J. E., J. H. Brewer, *et al.*, 2000, Phys. Rev. B **61**, R890.
Sonier, J. E., J. H. Brewer, R. F. Kiefl, G. D. Morris, R. I. Miller, D. A. Bonn, J. Chakhalian, R. H. Heffner, W. N. Hardy, and R. Liang, 1999, Phys. Rev. Lett. **83**, 4156.
Sonier, J. E., M. F. Hundley, J. D. Thompson, and J. W. Brill, 1999, Phys. Rev. Lett. **82**, 4914.
Sonier, J. E., R. F. Kiefl, J. H. Brewer, D. A. Bonn, S. R. Dunsiger, W. N. Hardy, Ruixing Liang, R. I. Miller, D. R. Noakes, and C. E. Stronach, 1999, Phys. Rev. B **59**, R729.
Sonier, J. E., R. F. Kiefl, *et al.*, 1994, Phys. Rev. Lett. **72**, 744.
Sonier, J. E., R. F. Kiefl, *et al.*, 1997a, Phys. Rev. B **55**, 11 789.
Sonier, J. E., R. F. Kiefl, J. H. Brewer, J. Chakhalian, S. R. Dunsiger, W. A. MacFarlane, R. I. Miller, A. Wong, G. M. Luke, and J. W. Brill, 1997b, Phys. Rev. Lett. **79**, 1742.
Srikanth, H., B. A. Willemsen, T. Jacobs, S. Sridhar, A. Erb, E. Walker, and R. Flükiger, 1997, Phys. Rev. B **55**, R14 733.
Stojković, B. P., and O. T. Valls, 1995, Phys. Rev. B **51**, 6049.
Sudbø, A., and E. H. Brandt, 1991a, Phys. Rev. Lett. **67**, 3176.
Sudbø, A., and E. H. Brandt, 1991b, Phys. Rev. B **43**, 10 482.
Sun, Y., and K. Maki, 1995, Phys. Rev. B **51**, 6059.
Tallon, J. L., C. Bernhard, U. Binninger, A. Hofer, G. V. M. Williams, E. J. Ansaldo, J. I. Budnick, and Ch. Niedermayer, 1995, Phys. Rev. Lett. **74**, 1008.
Thiemann, S. L., Z. Radović, and V. G. Kogan, 1989, Phys. Rev. B **39**, 11 406.
Tinkham, M., 1996, *Introduction to Superconductivity: Second Edition* (McGraw-Hill, New York), pp. 167–168.
Uemura, Y. J., 1995a, in *Polarons and Bipolarons in High-T_c Superconductors and Related Materials*, edited by E. K. H. Salje, A. S. Alexandrov, and W. Y. Liang (Cambridge University, Cambridge, England), p. 453.
Uemura, Y. J., 1995b, in *Proceedings of the CCAST Symposium on High-T_c Superconductivity and the C_{60} Family*, Beijing, 1994, edited by S. Feng and H. C. Ren (Gordon & Breach, New York), p. 113.
Uemura, Y. J., 1997, Physica C **282-283**, 194.
Uemura, Y. J., V. J. Emery, *et al.*, 1988, Phys. Rev. B **38**, 909.
Uemura, Y. J., A. Keren, *et al.*, 1993, Nature (London) **364**, 605.
Uemura, Y. J., L. P. Le, *et al.*, 1991, Phys. Rev. Lett. **66**, 2665.
Uemura, Y. J., G. M. Luke, *et al.*, 1989, Phys. Rev. Lett. **62**, 2317.
Ullah, S., A. T. Dorsey, and L. J. Buchholtz, 1990, Phys. Rev. B **42**, 9950.
Usadel, K. D., 1970, Phys. Rev. Lett. **25**, 507.
Usadel, K. D., 1971, Phys. Rev. B **4**, 99.
Vinnikov, L. Ya., L. A. Gurevich, G. A. Emelchenko, G. A. Kazaryan, N. N. Kolesnikov, M. P. Kulakov, D. Ya. Lenchinenko, and Yu. A. Ossipyan, 1989, Solid State Commun. **70**, 1145.
Vinokur, V. M., M. V. Feigel'man, V. B. Geschkenbein, and A. I. Larkin, 1990, Phys. Rev. Lett. **65**, 259.
Volodin, A. P., A. A. Golubov, and J. Aarts, 1997, Z. Phys. B: Condens. Matter **102**, 317.

Volodin, A., K. Temst, C. Van Haesendonck, and Y. Bruynseraede, 1998, Appl. Phys. Lett. **73**, 1134.
Volovik, G. E., 1993, Pis'ma Zh. Eksp. Teor. Fiz. **58**, 455.
Waldmann, O., F. Steinmeyer, P. Müller, J. J. Neumeier, F. X. Régi, H. Savary, and J. Schneck, 1996, Phys. Rev. B **53**, 11 825.
Walker, M. B., and T. Timusk, 1995, Phys. Rev. B **52**, 97.
Wang, Yong, and A. H. MacDonald, 1995, Phys. Rev. B **52**, R3876.
Wang, Yong, and A. H. MacDonald, 1999, Solid State Commun. **109**, 289.
Welp, U., J. A. Fendrich, W. K. Kwok, G. W. Crabtree, and B. W. Veal, 1996, Phys. Rev. Lett. **76**, 4809.
Wu, , Dong Ho, Jian Mao, S. N. Mao, J. L. Peng, X. X. Xi, T. Venkatesan, R. L. Greene, and Steven M. Anlage, 1993, Phys. Rev. Lett. **70**, 85.
Xu, D., S. K. Yip, and J. A. Sauls, 1995, Phys. Rev. B **51**, 16 233.
Xu, J. H., Y. Ren, and C. S. Ting, 1995, Phys. Rev. B **52**, 7663.
Xu, J. H., Y. Ren, and C. S. Ting, 1996, Int. J. Mod. Phys. B **10**, 2699.
Yamashita, A., K. Ishii, T. Yokoo, J. Akimitsu, M. Hedo, Y. Inada, Y. Onuki, E. Yamamoto, Y. Haga, and R. Kadono, 1997, Phys. Rev. Lett. **79**, 3771.
Yaouanc, A., P. Dalmas de Réotier, and E. H. Brandt, 1997, Phys. Rev. B **55**, 11 107.
Yasui, K., and T. Kita, 1999, Phys. Rev. Lett. **83**, 4168.
Yethiraj, M., D. K. Christen, D. McK. Paul, P. Miranovic, and J. R. Thompson, 1999, Phys. Rev. Lett. **82**, 5112.
Yethiraj, M., H. A. Mook, G. D. Wignall, R. Cubbitt, E. M. Forgan, D. M. Paul, and T. Armstrong, 1993, Phys. Rev. Lett. **70**, 857.
Yip, S. K., and J. A. Sauls, 1992, Phys. Rev. Lett. **69**, 2264.
Zhang, F. C., and T. M. Rice, 1988, Phys. Rev. B **37**, 3759.
Zhang, K., D. A. Bonn, S. Kamal, R. Liang, D. J. Barr, W. N. Hardy, D. Basov, and T. Timusk, 1994, Phys. Rev. Lett. **73**, 2484.
Zhang, S. C., 1997, Science **275**, 1089.
Zhu, Y. T., and A. Manthiram, 1994, Physica C **224**, 256.